

UNIVERSITAT POLITÈCNICA DE CATALUNYA

DOCTORAL THESIS

**Anomalous diffusion,
from life to machines**

Author:
Gorka MUÑOZ-GIL

Supervisor:
Dr. M. LEWENSTEIN

Co-supervisor:
Dr. M. A.
GARCIA-MARCH

*Thesis conducted in the Quantum Optics Theory group at ICFO, between
2016 and 2020.*



UNIVERSITAT POLITÈCNICA
DE CATALUNYA
BARCELONATECH

List of Publications

This thesis is based on the following publications:

1. *Nonergodic subdiffusion from transient interactions with heterogeneous partners*
C. Charalambous, G. Muñoz-Gil, A. Celi, M.F. García-Parajo, M. Lewenstein, C. Manzo, M. A. García-March, Phys. Rev. E **95**, 032403 (2017).
2. *Transient subdiffusion from an Ising environment*
G. Muñoz-Gil, C. Charalambous, M. A. García-March, M. F. García-Parajo, C. Manzo, M. Lewenstein, and A. Celi, Phys. Rev. E **96**, 052140 (2017).
3. *Diffusion through a network of compartments separated by partially-transmitting boundaries*
G. Muñoz-Gil, M. A. García-March, C. Manzo, A. Celi and M. Lewenstein, Front. Phys. **7**, 31 (2019).
4. *Efficient training of energy-based models via spin-glass control*
A. Pozas-Kerstjens*, G. Muñoz-Gil*, M. A. García-March, A. Acín, M. Lewenstein and P. R. Grzybowski, arXiv:1910.01592 (2019). (* equal contribution)
5. *Single trajectory characterization via machine learning*
G. Muñoz-Gil, M. A. García-March, C. Manzo, J. D. Martín-Guerrero and M. Lewenstein, New J. Phys., **22** (1), 013010 (2020).
6. *AnDi: The Anomalous Diffusion Challenge*
G. Muñoz-Gil, G. Volpe, M. A. Garcia-March, R. Metzler, M. Lewenstein, C. Manzo, arXiv:2003.12036 and www.andi-challenge.org (2020).
7. *Phase separation of tunable biomolecular condensates predicted by an interacting particle model*
G. Muñoz-Gil, C. Romero, Nicolás Mateos, Lara Isabel De Llobet Cucalon, Guillaum Filion, M. Beato, M. Lewenstein and M. F. García-Parajo, J. Torreno-Pina, <https://doi.org/10.1101/2020.09.09.289876> (2020).

Other works of the author not included in this thesis:

1. *Control of anomalous diffusion of a Bose polaron*
C. Charalambous, M. A. García-March, G. Muñoz-Gil, P. R. Grzybowski and M. Lewenstein, Quantum **4**, 232 (2020)

Abstract

Diffusion refers to numerous phenomena, by which particles and bodies of all kinds move throughout any kind of material, has emerged as one of the most prominent subjects in the study of complex systems. Motivated by the recent developments in experimental techniques, the field had an important burst in theoretical research, particularly in the study of the motion of particles in biological environments. Just with the information retrieved from the trajectories of particles we are now able to characterize many properties of the system with astonishing accuracy. For instance, when Einstein introduced the diffusion theory back in 1905, he used the motion of microscopic particles to calculate the size of the atoms of the liquid these were suspended. Initially, most of the experimental evidence showed that such systems follow Brownian-like dynamics, i.e. the homogeneous interaction between the particles and the environment led to its stochastic, but uncorrelated motion. However, we know now that such a simple explanation lacks crucial phenomena that have been shown to arise in a plethora of physical systems. The divergence from Brownian dynamics led to the theory of anomalous diffusion, in which the particles are affected in a way or another by their interactions with the environment such that their diffusion changes drastically. For instance features such as ergodicity, Gaussianity, or ageing are now crucial for in the understanding of diffusion processes, well beyond Brownian motion.

In theoretical terms, anomalous diffusion has a well-developed framework, able to explain most of the current experimental observations. However, it has been usually focused in describing the systems in terms of its macroscopic behaviour. This means that the processes are described by means of general models, able to predict the average or collective features. Even though such an approach leads to a correct description of the system and hints on the actual underlying phenomena, it lacks the understanding of the particular microscopic interactions leading to anomalous diffusion.

The work presented in this Thesis has two main goals. First, we will explore how one may use microscopical (or phenomenological) models to understand anomalous diffusion. By microscopical model we refer to a model in which we will set exactly how the interactions between the various components of a system are. Then, we will explore how these interactions may be tuned in order to recover and control anomalous diffusion and how its features depend on the properties of the system. We will explore crucial topics arising in recent experimental observations, such as weak-ergodicity breaking or liquid-liquid phase separation. Second, we will survey the topic of trajectory characterization. Even if our theories are extremely well developed, without an accurate tool for studying the trajectories observed in experiments, we will be unable to correctly make any faithful prediction. In particular, we will introduce one of the first machine learning techniques that can be used for such purpose, even in systems where previous techniques failed largely.

Resumen

La difusión es el fenómeno por el cual partículas de todas formas y tamaños se mueven a través del entorno que les rodea. Su estudio se ha convertido en una potente herramienta a partir de la cual entender el comportamiento de sistemas complejos. Gracias al reciente desarrollo de increíblemente precisas técnicas experimentales, este fenómeno ha generado un enorme interés, tanto desde el punto de vista experimental como teórico. En particular, dicha atención se ha dado en mayor medida en el estudio del movimiento de partículas microscópicas en entornos biológicos. Mediante el análisis de las trayectorias de estas partículas, somos capaces de caracterizar no solo sus propiedades, pero también las de su entorno. El mismo Einstein, autor junto con Smoluchowski de la teoría de la difusión, mostró cómo era posible calcular el radio de los átomos de un líquido simplemente mediante el análisis del movimiento de una partícula suspendida en este. Dicha teoría, que dio pie a lo que hoy conocemos como movimiento Browniano, consideraba que la interacción homogénea de una partícula con su entorno provocaba el movimiento aleatorio de este última.

Aunque el movimiento Browniano haya sido utilizado para describir una enorme cantidad de experimentos, sabemos hoy en día que existen sistemas particulares que se desvían de sus predicciones. Esta divergencia ha dado pie al desarrollo de la teoría de la difusión anómala, en la que, debido a las propiedades de las partículas y sus entornos, la difusión difiere drásticamente de las predicciones de la teoría Browniana. Algunos fenómenos como la ergodicidad, Gaussianidad o el envejecimiento de difusión, particulares de la difusión anómala, son hoy en día cruciales para el entendimiento del movimiento de partículas en sistemas complejos.

En términos teóricos, la difusión anómala tiene unas bases firmes, capaces de explicar gran parte de las observaciones experimentales más recientes. Sin embargo, esta teoría suele centrarse en la descripción de la difusión desde un punto de vista microscópico. Esto quiere decir, analizar un sistema mediante modelos generales, capaces de predecir propiedades colectivas o globales. Aunque las teorías microscópicas consiguen describir correctamente la mayoría de los procesos de difusión, no tienen la capacidad de discernir qué tipo de interacciones dan lugar a la difusión anómala.

El trabajo presentado en esta Tesis tiene dos objetivos principales. El primero es explorar el uso de modelos microscópicos (o fenomenológicos) para entender la difusión anómala. Un modelo microscópico, en contraposición al macroscópico, describe el sistema a partir de sus propiedades específicas. En este caso, a partir del tipo de interacciones que existen entre las partículas y su entorno. El objetivo es entonces entender cuáles de estas interacciones producen difusión anómala. Además, caracterizaremos los parámetros macroscópicos de la difusión, como el exponente anómalo, y mostraremos como depende de las propiedades del sistema. En el camino, exploraremos como fenómenos como la rotura débil de la

ergodicidad (weak-ergodicity breaking) o la separación de fase aparecen en sistemas con interacciones complejas. Nuestro segundo objetivo consiste en el desarrollo de técnicas para la caracterización de trayectorias provenientes de procesos de difusión. Aunque nuestro entendimiento teórico llegue a niveles insospechados en los próximos años, sin un análisis correcto y preciso de las trayectorias experimentales, jamás podremos construir un puente entre teoría y experimentos. Por tanto, el desarrollo de técnicas con las cuales analizar con la mayor precisión posible dichas trayectorias es un problema igual de importante que el desarrollo teórico de la difusión. En este trabajo, estudiaremos como las técnicas de aprendizaje automático (Machine Learning) pueden ser utilizadas para caracterizar dichas trayectorias, llegando a niveles de precisión y análisis muy por encima de las técnicas existentes.

Acknowledgements

First and foremost, I want to thank Maciej for accepting me as his student and letting me work in such a special place he has created. Miguel Angel has guided me through my discovery of Science and research. Carlo has also been there since the beginning, and help us materialize our often crazy ideas. I am extremely grateful to all the colleagues I had the pleasure to collaborate with and from whom I could learn so much: Alessio Celi, Maria García-Parajo, Przemek Grzybowski, José D. Martín-Guerrero, Juan Torreño-Piña and Giovanni Volpe. Specially, I want to thank Alex Pozas-Kerstjens for his patience and teaching me so many things, it has been a pleasure to work with you.

Science is a beautiful path, but only with the right companions. Luckily, I could share mine with the incredible QOT group. Since my first days, with Dani, Albert, Christos, Alexandre, Jess, Nils, Arnau, Manu, Nello and specially Maria, to the ones that joined later and refilled us with their energy: Sergi, Borja, Joana, Binz, Emilio, Valentin, Tymek and a big etcetera. Thanks for making the life in our group so easy!

Science is most and foremost about learning, and being surrounded with so many brilliant people during this past four years has helped me grow both as a scientist but also as a person. The environment ICFOnians have created is the perfect ground from which so many cool ideas and projects flourish. Probably without the hours spent in the 'futbolín', none of this could have been achieved, thanks to all the people that collaborated! Particularly, to our fiercest adversaries, the QIT and SMB groups, with which I not only shared these moments but many more. Some of the parts I enjoyed the most this years have been thanks to Fede, thanks for creating such cool projects!

A great part of this Thesis has been possible thanks to Peter Wittek, who showed us the ML side of Physics. With him I shared not only the passion for Science but also for mountains. One of the chapter of this thesis is dedicated to his memory.

Echando la mirada atrás, esta Tesis ha sido el fruto de un largo camino, en el cual siempre he podido contar con mi familia, Majo, Javi y Germán. Gracias por apoyarme y darme la libertad para crecer. Gracias a Joan Ginard, el primero en mostrarme la Física tal y como la veo hoy en día. Gracias a Veronica Ahufinger, por mostrarme el camino hacia la cuántica y la fotónica y en general al físico que soy ahora.

Siempre he pensado que las pasiones en la vida solo tienen sentido si unas compensan a las otras. Nada de esto hubiera sido posible sin poder contar con gente que me distrajera del día a día y con los que pasar los mejores de los momentos. Gracias a toda la gente de Mallorca en BCN, Jandro, Garfella, Sastre, Victor, Joan, Pep, . . . Gracias a Pol por soportarme estos cuatro años, en los buenos y en los malos momentos. A Joan, Guille, Edu, Joan, Petr y un largo etcétera por todos los momentos arriba de las montañas y bajo ellas.

Contents

List of Publications	iii
Abstract	v
Resumen	vii
Acknowledgements	ix
1 Introduction	1
1.1 Historical remarks	1
1.2 Current state of anomalous diffusion	8
1.3 Plan of the Thesis	10
2 Preliminaries	13
2.1 Brownian motion	13
2.1.1 Discrete Brownian motion: random walks in a lattice	17
2.2 Continuous time random walks	18
2.2.1 General features	20
2.2.2 Moments of displacement	21
2.2.3 Power-law waiting time distributions	21
2.2.4 Ergodicity breaking	22
2.3 Other anomalous diffusion models	25
2.3.1 Coupled space-time random walks	25
2.3.2 Diffusion disordered models	26
2.3.3 Fractional Brownian Motion	27
3 Heterogeneous interactions as source of subdiffusion	29
3.1 Theoretical framework	29
3.1.1 Effective waiting time distribution	31
3.1.2 Mean squared displacement	32
3.1.3 Non-ergodicity	33
3.1.4 Non-Gaussianity	35
3.2 Numerical results	36
3.3 Conclusions	39

4	Subdiffusion in critical environments	43
4.1	Theoretical framework	43
4.1.1	Motion of the particle	43
4.1.2	The Ising environment	44
4.1.3	Interaction particle-environment	46
4.1.4	Steps inside a domain	47
4.2	CTRW in a critical Ising environment	48
4.2.1	Diffusion of the particle	49
4.2.2	Numerical implementation	50
4.2.3	Critical slowing down of the Ising model	52
4.3	Finite size Ising environment and deviations from the critical temperature	54
4.4	Ergodicity breaking	55
4.5	Conclusions	57
5	Anomalous diffusion through porous compartments	59
5.1	Microscopical model for a compartmentalized environment	59
5.2	Mesoscopic description of the system	60
5.3	Mesoscopic motion as a Lévy walk	62
5.3.1	The osmotic approach	63
5.4	Diffusion of a Brownian particle in compartmentalized environments	65
5.4.1	Constant transmittance and stochastic length	65
5.4.2	Stochastic transmittance and constant length	66
5.4.3	Stochastic transmittance and length	68
5.5	Conclusions	69
6	Phase separation in diffusing interacting systems	71
6.1	Microscopical model of interacting particles	72
6.1.1	Average behaviour of the system	74
6.2	Transition to phase separation	75
6.3	Distribution of condensate sizes	78
6.4	Diffusion in condensed systems	80
6.5	Conclusions	82
7	Single trajectory characterization via Machine Learning	85
7.1	Machine learning as a scientific analysis tool	85
7.1.1	Supervised learning	86
7.1.2	Unsupervised learning	87
7.2	Single trajectory characterization as machine learning problem	90
7.2.1	Machine learning method	91
	Random Forest	92
	Training and test datasets	92
	Preprocessing	93

7.2.2	Benchmarking the model with simulated data	94
	Discrimination among diffusion models	95
	Anomalous exponent estimation	96
7.2.3	Experimental scenario: short and noisy trajectories	96
7.3	Transfer learning in simulated and experimental data	97
7.3.1	Results	98
7.4	Conclusions	99
8	Conclusions	103
	Bibliography	111

1 Introduction

1.1 Historical remarks

The world in our surrounding moves. No matter its scale, physical objects move in very particular ways, driven by their properties and their interaction with the environment. From the motion of black holes in the center of our own galaxy to the dynamics of particles in atomic experiments, their speed, direction and acceleration, among others, are widely used to understand their physical nature. Indeed, many theories have been developed to study systems just by looking at their motion. For instance, with the emergence of Newtonian mechanics and the works of Galilei, we have been able to predict the mass of stellar objects by studying their orbit. Understanding the diffusion of light through different materials led to the main discoveries of classical optics, while the scattering of electrons gave us insights on the structure of the atom.

Most physical theories are able to describe completely the outcome of an event, given enough prior information. However, this is not always the case. In complex systems, the degrees of freedom of the system increase so vastly that we can no longer describe its behaviour by a deterministic theory. In this case, physicists rely on a statistical approach: the macroscopic behaviour of the system is described by a small number of microscopical parameters, considered probabilistic and fluctuating around a certain mean. This approach, known as statistical physics, has been thoroughly studied in many scenarios, from mechanics to thermodynamics. It was particularly well suited for the study of the physical systems, in which the stochastic behaviour of micro and nanoscopic particles would give rise to some macroscopic phenomena, as e.g. the temperature of a system being related to the actual velocity of the particles it contains.

Lucretius and the Epicurean philosophy Surprisingly, such ideas were already conceived as early as in the times of the Roman empire. Our main source of knowledge on this topic is the scientific poem 'On the nature of things' (60 B.C.), written by the philosopher and scientist Lucretius (94 B.C. - ?). Considered as one of the most important poems of the Roman age, Lucretius explains to his contemporaries the main concepts of the Epicurean philosophy. During the Ancient age, two main currents of thought existed: from one side, Epicurus and his followers,

usually known as *the atomists*, considered that our surrounding is made of both matter and void. Atoms, indivisible particles of different shape and sizes, would fill some of this void and their combination give rise to everything we see. Opposite to them was Aristotle, who considered that matter was continuous, hence you could divide it endlessly in even smaller pieces. Moreover, he considered that all nature was formed by the four elements: earth, air, water and fire.

Due to its influence, the Aristotelianism persisted from the Greek's time and was considered as the main physical theory also by Romans. Nevertheless, some philosophers still believed in Epicure's vision of the world, being Lucretius one of them. Such belief motivated him to write 'On the nature of things', in which a very interesting idea is introduced, perhaps without him even figuring how important this was. It is summarized in the following verses:

*[...] Another reason you should turn
Your attention to the motes that drift and tumble in the light:
Such turmoil means that there are secret motions, out of sight,
That lie concealed in matter. [...]*

*[...] For atoms are moving on their own,
Then small formations of them, nearest them in scale, are thrown
Into agitation by unseen atomic blows. [...]*

The previous is an excerpt of the poem 'The dance of the atoms', the second volume of Lucretius' work. As a whole, the poem introduces very intriguing concepts: atoms move due to a *secret* motion, which properties are concealed in their matter. Moreover, 'atomic blows' may cause the movement of even greater particles. As we will see later, these concepts are the basis of what we know now as the theory of particle diffusion, which was not established until the beginning twentieth century. Sadly, Lucretius' ideas were soon to be forgotten, mostly by two reasons: in one hand, the rudimentary experimental techniques of that time were far from giving any kind of judgment on the validity of his proposals; on the other hand, the prestige of the Aristotelian current, contrary to the existence of atoms, made it such that Lucretius' ideas were not seriously considered. Moreover, due to its atheist nature, very few copies survived the Middle age and hence probably never arrived to any of the other main characters of our particular story.

Before highlighting the importance of Lucretius ideas and its influence on the work related to this Thesis, let us briefly return to the history of the kinetic theory of gases. Many centuries after the fall of the Roman empire, enormous advances were made. From the seventeenth to the beginning of the twentieth century, works from Bernoulli, Clausius, Boltzmann and Maxwell constructed the basis of statistical thermodynamics. Nevertheless, while we are currently certain of the validity of such theory, this was not so clear for its creators. Even if its macroscopic implications were clearly understood, the lack of experimental evidences on its microscopical predictions made it more a theoretical construct rather than an actual

contrasted theory. Indeed, most of the predictions involved atomic experiments, which were far from doable even at the beginning of the twentieth century.

Brownian motion, a story of many Things were soon to be changed, mostly due to the works of Albert Einstein (1879-1955) [1] and Marian Smoluchowski (1872-1917) [2]. While the kinetic theory of gases focused on atoms and molecules, hence nanoscopic particles, their work considered much bigger bodies, with sizes of few microns. In its basis, the work by Einstein and Smoluchowski extends the common knowledge in statistical thermodynamics about the random motion of molecular gases or liquids. It is considered by some to be the most valuable piece of work in such direction [3], as it finally introduced a feasible prove to the microscopic predictions of all previous authors. Their critical contribution was to consider that the atomic fluctuations, hidden to their contemporary experimental techniques, could indeed affect larger bodies. More precisely, they considered that the collisions of the atoms and molecules with larger bodies would heavily affect the motion of the latter. Due to its fluctuating nature, the collisions were completely stochastic and so was the motion of those larger bodies.

Luckily to both, neither had to convince their fellow experimental physicist to perform any sort of experiments, as the prove had already been there for almost 80 years. It is 1826 and Robert Brown, renowned Scottish botanist, is back from one of his multiple exploratory travels. While examining a recently discovered plant, the *Clarkia pulchella*, he noticed that some particles, ejected from the pollen grains when suspended in water followed an erratic yet continuous motion [4]. Initially, Brown thought that such effect was due to some kind of biological interaction between the particles and the water. In order to test such idea, he proceeded with similar experiments, now with inorganic dust particles, just to find the exact same behaviour. To enhance the historical narrative of such finding, he even observed the motion of dust coming from Egypt's Sphynx, proving that the stagger was similar no matter the origin of the particles. It has to be noted that similar experiments on inorganic particles had been done by Jan Ingenhousz (1730-1799) already in 1784 [5]. However, such observations were somehow dismissed by the community and had little effect on the development of Brownian motion.

While the common knowledge and usual narrative of the Brownian motion history jumps from Brown's experiment to Einstein's diffusion theory, a series of important contributions are found in between. Thought most of them incomplete, each of these showed the importance on the understanding of this phenomenon. Note that, at least from what is understood from their works, none or very few of the following authors knew about the proposals of Lucrecius, or even maybe considered them to be purely philosophical. The first theoretical approach of this new era is associated to Ludwig Christian Wiener (1826-1896), which in 1863 proposed that the behaviour of Brownian particles was indeed produced by the 'internal motion peculiar to the liquid' in which they were suspended [6]. Few years later,

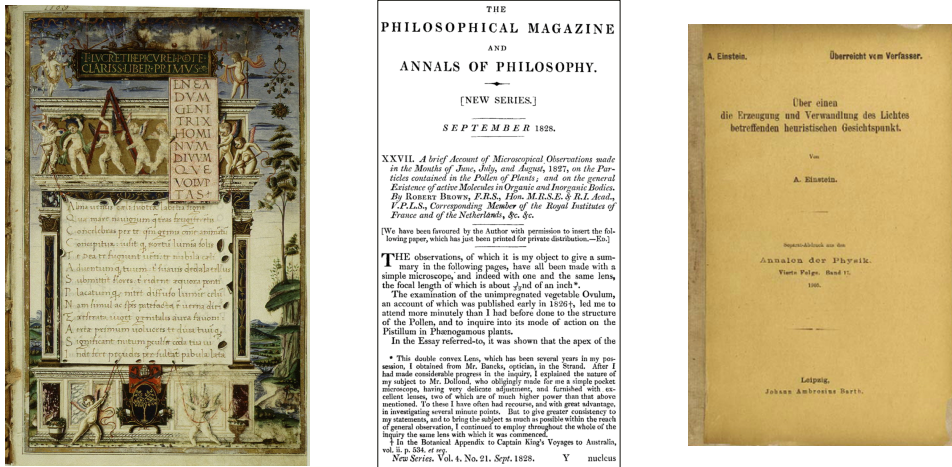


FIGURE 1.1: **Important contributions to the development of the theory of diffusion:** a) Opening of Pope Sixtus IV's 1483 manuscript of *On the nature of things* by Lucretius, scribed by Girolamo di Matteo de Tauris. b) Reproduction of the first page of the original Brown's paper on the observation of Brownian motion [4]. c) Cover of Einstein's paper on the diffusion theory published in Annals of Physics in 1905 [1].

in 1879, William Ramsay (1852-1916) went beyond Wiener's proposal and considered that it was in fact the motion of the liquid's atoms causing such behaviour [7]. This is the first atomistic approach to the problem since Lucretius' ideas.

In 1880, while working in his paper on the method of the least squares, Thorvald N. Thiele (1838-1910) introduced some of the mathematical concepts that later helped to establish the Brownian motion theory [8]. In the same spirit, Louis Bachelier (1870-1946), father of mathematical finances, used in his Thesis similar concepts to explain the evolution of the stock and option markets [9]. Interestingly, such system is now widely studied as a diffusion problem, as the stock market is considered to be one of the most random signals produced by humans. In the experimental side, Louis George Gouy (1854-1926) investigated during 1888 if Brownian motion could be caused by external forces or fluctuations. For instance, he explored if the jittering motion was due to vibrations, convection currents due to the liquid not being at equilibrium or even the presence of artificial illumination in the liquid [10]. Obviously, all those tests failed and assured Gouy the internal nature of the phenomena.

We are back in 1905 and Einstein and Smoluchowski have their works ready for publication. Similarly, the Australian physicist William Sutherland is also finishing his work on diffusion [11]. All seem unaware of each other's work. Moreover,

they also seem unaware of the previous theoretical approaches to Brown's experiments. Nevertheless Einstein was, at least in the later stages of his work, familiar with Brown's observation, as he himself noted in the abstract of his paper: *'It is possible that the motions to be discussed here are identical with so-called Brownian molecular motion; however, the data available to me on the latter are so imprecise that I could not form a judgment on the question.'* In physical terms, Einstein was the first to develop a formal theory for the atomistic version of Brownian motion. As Lucretius and Ramsay, he considered that the atoms in the liquid collided with the suspended microscopical particles. With this concept, he derived the diffusion of such particles and concluded that its motion was solely dependent on the viscosity of the liquid and the size of the suspended particles. This was done by introducing the concept diffusion coefficient, constant characterizing the random motion of any microscopical particle in a given medium. Interestingly, Einstein, and also Smoluchowski, showed that such coefficient was directly related to the microscopical properties of the medium, as well as to various universal constants. In fact, Einstein demonstrated in his article how these new phenomena may be used to calculate the size of atoms of the medium, just by looking at the diffusion of the particle.

Einstein finishes his paper with the following sentence: *'Let us hope that a researcher will soon succeed in solving the problem presented here, which is so important for the theory of heat.'* It took little time for physicists to relate Einstein's theory to Brown's experiment. However, a thoughtful study of the phenomena in terms of the new theory was lacking. Four years later, in 1909, Jean Perrin (1870-1942) carefully reproduced Brown's observations and finally concluded the history of Brownian motion discovery [12]. His observations are reproduced in Fig. 1.2. See that this discovery goes beyond the study of the diffusion of the suspended particles. As it was shown by Einstein in its study of the atom's sizes, the phenomena of Brownian motion opens the door to the microscopical study of the interactions between particles and their environment. For instance, Perrin was able to calculate Avogadro's number by two means: the distribution of the particles over the system and their fluctuations around their initial position. His results hence assessed Einstein's theory both quantitative and qualitatively. Similar experiments, both having as goal the exact calculation of the Avogadro's number, were conducted in 1914 by Ivar Nordlund (1955-1937) [13] and in 1931 by Eugen Kappler (1905-1977) [14].

An important contribution to the development of diffusion models, uncorrelated in its beginning to the diffusion theories, was made by Karl Pearson in 1905. Pearson was deeply interested in the problem of the drunkard's walk, i.e. the walk of a particle whose steps have random directions. The problem was not yet solved, even for a small number of steps. However, thanks to its persistence and help from other fellows such as John G. Bennett and Lord Rayleigh, Pearson finally concluded that *'in open country the most probable place to find a drunken man who is at all capable of keeping on his feet is somewhere near his starting point!'* [15].

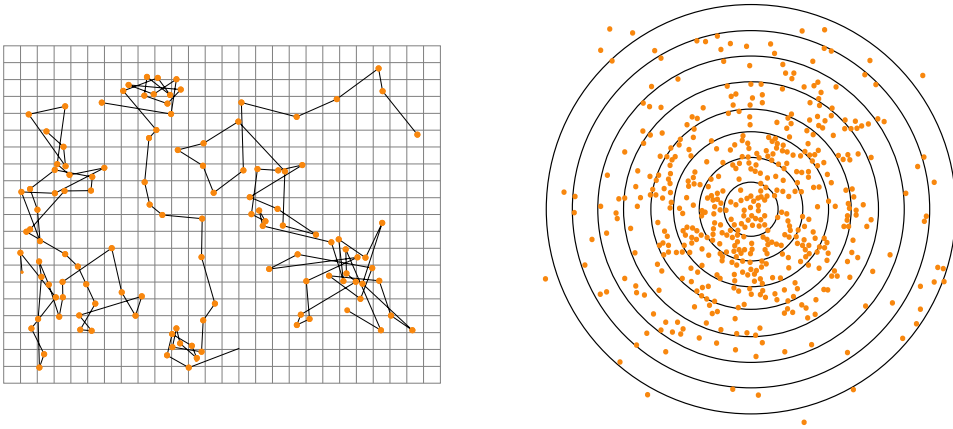


FIGURE 1.2: **Reproduction of Perrin observations:** Left, we show the trajectories observed by Jean Perrin in Ref. [12]. In the right, we show the distribution of positions at a given time, where the center of the circles shows the initial position of the particles. This was used by Perrin to show the Gaussian nature of Brownian motion.

The connection between the drunkard's walk (or just random walk) and Brownian motion was later done by Smoluchowski. We will show such equivalence in Section 2.1.1.

Beyond Brownian particles While in its initial formulations Brownian motion was developed as an extension of the kinetic theory of gases, little by little scientist started to realize the potential of such theory in the description of the diffusion of particles in complex environments. That is how the focus started to be more on the actual motion of the microscopical particle rather than in the actual properties of the media. In that sense, both Einstein and Smoluchowski's theories, as well as Perrin, Nordlun and Kappler's experiments, considered common assumptions. For instance, the time scale at which the successive collisions between atoms and microscopic particles happen had to be small enough, such that the displacements of the particle were completely uncorrelated. Moreover, they considered that single realization of the experiment, if conducted for a significant time, described the average behaviour of many short realizations. Both conditions were key in finding that Brownian motion was well described by a Gaussian distributed process, just as the random walk and as shown in Fig. 1.2. By means of the diffusion equation, one could also see that the variance of such Gaussian distribution, referred usually as the mean squared displacement (MSD) of the particle, was a linear function of time, whose slope is proportional to the diffusion coefficient.

Some years later, the first deviations from such linear behaviour were found. As always, controversy arises when trying to find the actual origin of this physical concept. In this case, we usually associate the discovery of the first 'non' Brownian motion to Lewis Fry Richardson (1881–1953). Widely known for his pioneering work in weather forecasting by means of mathematical analysis, Richardson found out that the relative motion between two particles in a turbulent flow was not well described by the Einstein-Smoluchowski diffusion equation [16]. Instead, Richardson proposed what is currently known as the four-thirds power law [17], which introduced a power law correction to the Brownian motion diffusion equation. This led to the MSD no longer being a linear function of time, but rather having a cubic scaling. This finding paved the way to what we know now as *anomalous diffusion*.

The concept of *anomalous diffusion* is very broad and each year contains more and more phenomena, just as the theory and experimental observations expand. In general, we consider that it arises there where Brownian motion by itself is no longer valid. This may happen in many different forms. For instance, we may see cases in which the Gaussian distribution characteristic of Brownian particles is no longer fulfilled. In other cases, even if Gaussian distributed, the scaling of the MSD is no longer linear. Combinations of such phenomena, as well as the recent appearance of many others, such as ageing or ergodicity, have given rise to a plethora of diffusion models which aim to contain the strange behaviour that particles have when diffusing throughout complex media. While in its initial formulation Brownian motion considered the diffusion of a particle with homogeneous interactions with the media, we know now that such assumption is sometimes not true and that the behaviour of the particle is heavily affected by the heterogeneous interaction with its environment.

The rest of this Thesis will be devoted to the exploration of the confounding world of anomalous diffusion. We will explore it from two points of view: by studying precisely which particle-environment interactions may lead to their anomalous behaviour but also by describing the various methods one may use to characterize the arising of such phenomena. While Lucretius was interested in the nature of the atoms, this work will be directed to much bigger systems, such as the motion of nanoscopic particles in biological environments. Nevertheless, the beauty of such models is their possible generalisation to many other systems, from physical oriented fields such as material science and transport phenomena, to economy and the study of market fluctuations (just as Bachelier introduced) or even the study of information spread in social networks.

Looking back at the history of Brownian motion, it is very interesting to see that way before the invention of the microscope, Lucretius could already envisage the arising of such phenomena. It is quite possible that what he was seeing while looking at highly illuminated dust was far from actual Brownian motion. Nevertheless, it is surprising that even in an era ruled by the Aristotelian current, he could think that the existence of atoms and their motion could affect much larger

bodies. The fact that Brown was unaware of such idea (and even myself until the writing of this Thesis) shows the importance of not dismissing any scientific idea, even if confronted with the established common knowledge.

1.2 Current state of anomalous diffusion

One of the beauties of diffusion models is their suitability to explain complex behaviour in a vast quantity of fields. However, while similar methods are used by very different communities, these are quite separated from each other and have hard time sharing their knowledge. For instance, some of the most recent advances in terms of the theoretical understanding of diffusion has been devoted to the field of biophysics and have hard time to transcend to other communities. Nevertheless, most of the understanding of such processes is mature enough, such that the theoretical basis is already well constructed and contrasted. Of course, this does not mean that everything is known about diffusion, but rather that the foundations from where the new knowledge arises are robust and well understood for quite some time already.

Since the discovery of anomalous processes by Richardson in 1926, mainly three models have been used to describe anomalous diffusion. For subdiffusion, i.e. processes for which the scaling of the MSD is smaller than Brownian Motion, fractional Brownian motion (FBM) and continuous time random walk (CTRW) have been at the basis of most of the recent development. The former was introduced by Kolmogorov in 1940 [18] and later formalized by Mandelbrot and Van Ness in 1968 [19] and the latter, CTRW, was introduced by Scher and Montroll in 1975 [20]. For superdiffusion, for which the scaling is bigger than Brownian motion, a particular extension of CTRW, the Lévy flights, proposed also by Mandelbrot in 1982 [21], is the best known model. The mathematical and physical details of these models will be described later in this Thesis, specially in Section 2.3.

Theoretical framework In terms of theoretical advances in the recent years, many has been done in the understanding of anomalous diffusion. There exist many research lines. From one side, there is a huge interest in the complete understanding of the existing models. Even if introduced more than 50 years ago, we still have much to learn from models such as CTRW and FBM. Moreover, in the last years many different properties of anomalous diffusion have been introduced, never known before. For instance ergodicity, concept we will explore in Section 2.2.4, is now one of the most important features in anomalous diffusion. Studies of the Gaussianity, step length correlations, first passage time,... have enlighten not only the inherent properties of the various diffusion models, but also on how to differentiate among them. There exist nowadays very extensive reviews on the topic. For instance, a very nice introduction to the topic of diffusion can be done by reading Ref. [22]. A complete description of the various diffusion models existing and

their properties can be found in Ref. [23], which has recently been extended with a more in depth look on Brownian motion [24]. In order to understand the differences that emerge between models, Ref. [25] reviews various metrics allowing for that.

Another important line of research is related to the understanding of the microscopical interactions leading to anomalous diffusion. By this we refer to the actual particle-environment interactions that take place in anomalous systems. Note here that the term microscopical is here referring just as a counter part to the macroscopic or effective behavior of the system. For instance, in the case of Brownian motion, the effective model is the one of the stochastic motion of the particle, while its microscopical model describes the collisions between the atoms in the environment and the particle. While anomalous diffusion is understood in terms of effective models as e.g. CTRW or FBM, the actual microscopical interactions leading to such behaviors are elusive in many scenarios. Then, anomalous diffusion arises as a tool to study physical systems, only by observing the motion of particles. This is very much related to the study on the atoms size made by Einstein when he discovered Brownian motion. With much more complex models, we can now give a more detailed description of the actual interactions in stochastic processes. Indeed, and citing explicitly the extensive review of Ref. [26], *'there is clearly a need for theory and simulation of microscopic models that can make qualitative and quantitative predictions of the transport behaviour in crowded environments, at least in vitro.'*

Diffusion in biophysical environments In both cases, i.e. the general study of anomalous diffusion characteristics and of microscopical models, such theoretical developments have been mainly motivated by the recent advances in experimental techniques, allowing for the tracking of micro and nanoscopic particle with unprecedented accuracy. As we already commented, anomalous diffusion is a very general framework, that can be applied in many different fields. Nevertheless, most of its recent advances have been related to the microscopical world, where various kinds of cells, proteins and microscopical particles in general have shown some of the most surprising behaviours associated to anomalous diffusion. Such observations are mostly performed by means of single particle tracking (SPT) techniques, i.e. methods allowing for the tracking, for a sufficient long time, the path of a particle, usually beyond the diffraction limit.

Until some years ago, optical setups were limited in their resolution by the Abbe diffraction limit, a function of the wavelength of the light used to illuminate the sample and the numerical aperture of the microscope. In general, even the most sophisticated instruments were limited to resolutions of ~ 250 nm. Even if many biological bodies such as cells are well beyond that range, viruses, proteins and other molecules are below it. This meant the impossibility of directly characterizing such particles. However, between 1980 and the early 2000s, various

methods were introduced to circumvent such problem. Some of these developments were even awarded the Nobel prize of Chemistry in 2004 [27]. An extensive review on these techniques can be found in Refs. [28, 29, 30]. Moreover, the review in Ref. [26] details on the different biological systems, mostly focusing on crowded environments, where anomalous diffusion arises.

However, as previously said, anomalous diffusion, and the concept of diffusion and random walks is not restricted to the microscopical world. For instance in ecology, random walks are widely use to understand animal search strategies [31, 32]. Thanks to new telemetric data, fuelled by the improvement of animal GPS tracking, biologist are now able to model statistically the movement of animals, how they search they food, how they move in the season changes, ... [33, 34]. As an example, many works have associated the animal (and also human) foraging patterns to the Lévy walk model [35, 36]. Interestingly, such patterns can not only be associated to animals but also to plants [37]. However, there is still debate if this is really the case, or more realistic models need to be introduced [38].

Diffusion in other fields Away from the biological world, and following the trend started by Bachelier in 1909 [9], diffusion models are use in social and economic physics. There main goal is to study the fluctuations generated by human interactions by means of the same stochastic methods used in anomalous diffusion [39, 40]. Even models such as CTRW and Lévy walks find their use for the study of finances [41, 42] and more precisely of the evolution of the stock market [43, 44]. While also animals, us humans move sometimes in vary strange forms and we are prone to our own diffusion models [45, 46], even when moving by car [47].

Returning to the microscopical scale and going even beyond, we find the world ruled by Quantum physics. Also there many of the concepts of anomalous diffusion arise. For instance, the framework of Quantum Brownian motion is often used to the describe the motion of impurities in open quantum systems [48]. Particularly, it has been very successfully used to investigate the motion of particles in Bose-Einstein condensates [49]. Interestingly, there exist regimes in such systems in which anomalous diffusion appears and can even be controlled [50]. Moreover, anomalous diffusion has been detected in transport phenomena such Anderson location [51], the diffusion of matter-waves in disordered systems [52] or quantum walks [53, 54].

1.3 Plan of the Thesis

This thesis is structured as follows. In Chapter 1 we will introduce the basic theoretical framework first of anomalous diffusion. To begin, we will introduce the main concepts of Brownian motion, such as the diffusion equation and the Gaussian propagator. We will start reviewing the different features of diffusion models,

such as the mean squared displacements, and show how to calculate it analytically, but also practically in trajectories arising from experimental observations. We will then relate Brownian motion with a discrete random walk. Then, we will start our exploration of anomalous diffusion. By means of the continuous time random walk (CTRW), the most recurrent diffusion model in the Thesis, we will explore the main characteristics of anomalous diffusion models with special attention to the concept of ergodicity. Then, we will present briefly other kind of anomalous diffusion models and their main characteristics.

In Chapter 3 we will begin our journey in the world of microscopical models for anomalous diffusion. The model presented will consider the diffusion of a particle in a crowded environment, where the interaction with its neighbouring particles induces a tunable anomalous diffusion. The particle follows a normal diffusing CTRW when moving freely. However, its interaction with other particles makes it such that the CTRW is drastically affected and is transformed into a power law CTRW, hence anomalous. We will explore the effect of density and also the presence of annealed and quenched disorder, both analytical and numerically. We will show the difference between these and also analytically calculated the time needed for the particle to reach its anomalous behaviour. The work of this chapter is based on the original work of Ref. [55].

In Chapter 4 we will consider the motion of a particle in a critical environment, such as the one arising from Ising dynamics. The latter forms domains of spins point either up or down. We consider here how the emergence of such compartmentalized environment affects the motion of the particle. More precisely, we consider that the diffusion of the particles is closely related to the size of the domain the particle is moving on. From here, we will explore how criticality affects its motion. We show how in a critical system, the particle shows anomalous diffusion, with an anomalous exponent related to the strength of the interaction between the environment and the particle, but also to the difference between their dynamics' time scales. Then, away from criticality, no matter if it is in presence of finite size effects or because of the departure from the critical temperature, the particle subdiffuses only for a transient time, to then recover normal diffusion. The work of this chapter is based on the original work of Ref. [56].

In Chapter 5 we consider yet another compartmentalized environment. In this case we study the motion of particle following Brownian motion, through an environment made of compartments with varying size and whose boundaries are porous. This means that, when reaching a boundary, the particle has complementary probabilities of either being reflected inside the same compartment or transmitting to the contiguous. Our first contribution is directed at the approach followed to study the diffusion of the particle. Instead of focusing in the microscopical behaviour of the particular, i.e. studying each precise interaction with the boundary, we show how it suffices to track the particle each time it crosses a boundary. Then, the walk is transformed into a space-time coupled CTRW or a Lévy walk with non-alternated rests, depending on the exact configuration of

the system. With such approach, we explore which properties the compartments need to have in order for the particle to show anomalous diffusion. The work of this chapter is based on the original work of Ref. [57].

In Chapter 6 we focus in the phenomena of phase separation. In recent years, this complex behaviour has captured a lot of attention, as many components inside living cells have been shown to compartmentalize without creating any boundary with its surrounding. While there exists many models describing the appearance of such phase, the particular interactions leading to this phenomena are still elusive. Moreover, the actual models often lack a close connection with relevant quantities accessible in single particle tracking experiments. In this chapter we present a minimal microscopical model able to reproduce many of the observations of experimentally tunable phase separation. More precisely, we consider a system in which particles have a certain transient binding probability. We will show how the system overcomes a transition from a phase in which particles move freely, even in the presence of binding, to a phase in which particles form condensates and phase separate. We characterize the phase transition, show how the condensate size distribution behaves in and out of the phase separated scenario and proceed with numerical simulations to test the validity of our model. The work of this chapter is based on the theoretical part of the original work of Ref. [58].

In Chapter 7 we propose novel forms of characterizing anomalous diffusion, based on machine learning techniques. In previous chapters we have focused in study the source of anomalous diffusion from a theoretical point of view. In this chapter we explore different forms of studying experimental trajectories, considering that we have access to a single trajectory from the system of study. We first introduce basic concepts of machine learning, such as supervised and unsupervised learning. Then, we review the existing literature on single trajectory characterization. We show for instance that most of the techniques rely on the ergodicity of the trajectories, which allow for the use of temporal averages. We propose that machine learning architectures, such as the Random Forest, allow for the correct characterization of trajectories even in the presence of ergodicity breaking. Moreover, we show how one may use a machine trained with simulated trajectories to then study experimental trajectories. The work of this chapter is mainly based on the work of Ref. [59]. Moreover, it contains crucial concepts explored and proposed in Refs. [58, 60, 61, 62].

2 Preliminaries

In this chapter we will briefly review the basics of diffusion, starting with an exploration of Brownian motion, to later discuss the properties of anomalous diffusion and the various models used to describe it. As commented in the Chapter 1, there exists nowadays extensive reviews and monographs covering many of the topics discussed in below [22, 23, 24, 63]. Nevertheless, for the completeness of this thesis, we will review now some of them, which will be recursively appearing in following chapters. This chapter is organized as follows: first, we will introduce the concept of diffusion just as introduced by Einstein and Smoluchowski. From here we will present different ways of characterizing the diffusion, all by means of the trajectory of the particle or system of study. We will briefly explain the analogy between continuous and discrete walks. Then, we will introduce the continuous time random walk (CTRW), one of the most important topics of this Thesis. We will use it to introduce some of the key concepts of anomalous diffusion. Finally, we will present other models giving rise to anomalous diffusion.

2.1 Brownian motion

Brownian motion (BM) was developed by Einstein [1, 64] and Smoluchowski [2] as the motion of a particle due to its collisions with its smaller surrounding particles. Both understood that a deterministic theory would be completely overwhelmed by the number of parameters (i.e. the degrees of freedom) to be considered. Hence, they developed the motion of Brownian particles as a stochastic process whose probability density function (PDF) follows the diffusion equation

$$\frac{\partial}{\partial t}P(x, t) = D \frac{\partial^2}{\partial x^2}P(x, t), \quad (2.1)$$

where x is the position of the particle at time t . Considering that the particles start its motion at the origin, i.e. $P(x = 0, t = 0) = 1$, one can solve the previous equation to find that the PDF governing the motion of the particle is Gaussian distributed:

$$P(x, t) = \frac{1}{\sqrt{4\pi Dt}} \exp\left(-\frac{x^2}{4Dt}\right). \quad (2.2)$$

See here that D , the diffusion coefficient, is the only free parameter. This means that it has to enclose all the physical properties of the system. It is interesting here to note that the value of the diffusion coefficient found by Einstein, Smoluchowski and Shuterland, while accounting for similar contributions, was substantially different. The relation between the diffusion coefficient and the physical parameters of the system, known as the Stokes-Einstein-Sutherland relation, is currently expressed as

$$D = \frac{k_b T}{m\eta}, \quad (2.3)$$

where $k_b = 1.38 \cdot 10^{-23} \frac{m^2 kg}{sK}$ is the Boltzmann constant, T is the temperature of the medium, m the mass of the particle and η the friction coefficient.

It has to be noted here that the formulation of BM by means of Eq. (2.1) is not unique. Pierre Langevin developed an analogous model based on Newton's second law in the presence of noise [65]. His approach considers that the position of a particle follows

$$\frac{dx(t)}{dt} = \zeta(t), \quad (2.4)$$

where $\zeta(t)$ is a random variable, Gaussian distributed, with zero mean. Its auto-correlation function is given by $\langle \zeta(t)\zeta(t') \rangle = 2D\delta(t-t')$. As we will see later in this work, Langevin's formulation allows for a simpler interpretation of BM and can easily be extended to different kinds of diffusion models. Anyhow, both formulations yield to the same results, as expected. From the resulting PDF, Eq. (2.2), we can calculate the mean square displacement (MSD) of a Brownian particle as

$$\langle x^2(t) \rangle = \int_{-\infty}^{\infty} x^2 P(x,t) dx = 2Dt. \quad (2.5)$$

This simple relation introduces one of the most important features of diffusion, which will be largely explored during the rest of this Thesis, for a variety of different system. See for instance that in this case, the MSD has a linear dependence with respect to t . We define such behaviour as *normal diffusion*. Conversely, *anomalous diffusion* appears when such relation is no longer linear. The differences between these two classes of diffusion, normal and anomalous, will be deeply explored later.

While Eq. (2.5) is central in the theoretical study of diffusion, it is usually not practical for the systematic study of trajectories arising from diffusion experiments. This is because it is usually very challenging to extract $P(x,t)$ faithfully. To showcase the study of the MSD in a real scenario, let us consider the example of the trajectories presented in Fig. 2.1 (a). We show here three trajectories with different diffusion coefficients, $D = 1, 5$ and 10 . The first analysis one can proceed with is to check whether the particles follow Eq. (2.2). Note here that the probability of the particle being at position x in time t is analogous to the probability of

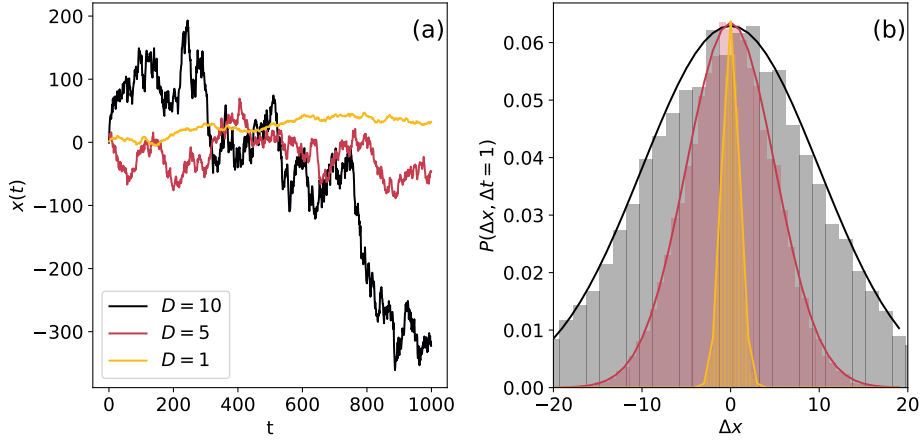


FIGURE 2.1: **Gaussian nature of Brownian motion:** **a)** Example of three Brownian motion trajectories, with different diffusion coefficient D . **b)** Distribution of displacements in an interval of time $\Delta t = 1$ for trajectories presented in a). The shadowed bar plot shows the histogram calculated from the trajectories, while the bold lines show Eq. (2.2) for each diffusion coefficient.

performing a displacement of length Δx in a time Δt .

In Fig. 2.1 (b) we plot the probability $P(\Delta x, \Delta t = 1)$ for each of the three trajectories as a bar plot. The bold line show the value of $P(x, t = 1)$ calculated from Eq. (2.2) for each D . See here for instance how switching from positions and times to their displacements allows to reformulate Eq. (2.5) in much practical form. Nevertheless, as commented before, constructing a plot such as the one in Fig. 2.1 (b) needs sufficiently long trajectories, such that we have enough points to construct the distribution.

In the case in which $P(x, t)$ can not be exactly calculated, and the MSD cannot be retrieved from Eq. (2.5), other approaches exists. For instance, on may calculate the displacement made by the particle in an interval Δ , averaged over the whole length of the trajectory. This is known as the time mean squared displacement (tMSD), which expression is

$$\overline{\delta^2}(\Delta) = \frac{1}{t - \Delta} \int_0^{t-\Delta} [x(t' + \Delta) - x(t')]^2 dt', \quad (2.6)$$

where t is the length of the trajectory considered. The interval time Δ is usually referred as the time lag (t_{lag}).

Similarly, one may consider now the displacements made in such interval t

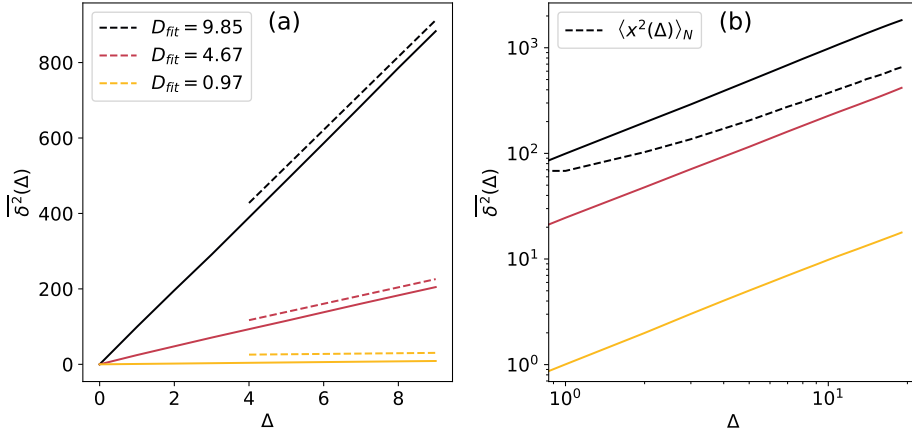


FIGURE 2.2: **Brownian motion mean squared displacement:** **a)** Time mean squared displacement for the previous trajectories. Dashed is the fit done to each tMSD, whose slope is presented in the legend. **b)** Same plot as b) but in log-log scale. See here that all the bold lines have slope equal to 1, showing the behavior $\overline{\delta^2}(\Delta) \sim \Delta$. The dashed line shows the ensemble mean squared displacement averaged over 10^4 trajectories with $D \in [0, 10]$. Note that at the long time limit the ensemble and time averages show the same behavior.

averaged in this case over various realizations of the same walk. If one considers N distinct and uncorrelated walks, the previous quantity, known as the ensemble mean squared displacement (eMSD), can be calculated as

$$\langle x^2(\Delta) \rangle_N = \frac{1}{N} \sum_{i=1}^N [x_i(t' + \Delta) - x_i(t')]^2, \quad (2.7)$$

where in practical terms, we usually choose $t' = 0$.

Considering now the positions, and most importantly the displacements arising from Eq. (2.2), one can show that $\overline{\delta^2}(\Delta) = \langle x^2(\Delta) \rangle_N = 2Dt$, just as predicted by Eq. (2.5). From these two calculations, we can start to characterize the diffusion of the particles. For instance, we can now use it to extract their diffusion coefficient. This is shown in Fig. 2.2 (a), where the tMSD was calculated for the three trajectories of Fig. 2.1. Note that in order to perform a good average, $\Delta \ll t$. Once calculated the tMSD, we proceed to fit linearly the resulting line and extract from it the diffusion coefficient. We see that even if in some cases, the linear fitting gives rise to particularly good results (e.g. $D_{fit} = 0.97$ compared to 1 and $D_{fit} = 9.85$ compared to 10), this method may lead to poor results (e.g. $D_{fit} = 4.67$). To

solve this problem, and in general the problem of single trajectory characterization, more sophisticated methods are being proposed, as we will see in Chapter 7.

If we now perform the logarithm to either the tMSD or the eMSD, it easy to see that

$$\log(\overline{\delta^2}(\Delta)) \propto \log(\Delta), \quad (2.8)$$

where the diffusion coefficient is now just an offset and the MSD has slope one. We show this in Fig. 2.2 (b) for both the tMSD and eMSD, which coincide in their slope in the long time limit. While in the case of Brownian motion we do not gain excessive information from such evaluation, the slope of Eq. (2.8) is exactly the anomalous exponent, hence a strong signature of the departure from normal diffusion.

2.1.1 Discrete Brownian motion: random walks in a lattice

In general, the motion of particles in physical environments is continuous. This means that while the sampling time (i.e. the time at which the position is recorded) is usually regular, the position of the particle has continuous values. Similarly, Brownian motion is also defined as a continuous process, where the step arising from $P(x, t)$ can take any value. However, when considering phenomenological models for the diffusion of particles, it is often useful to consider a simplified, discrete version of the problem. While the suitability of such approach will be clear in the following chapters, we will prove that a discrete random walk converges to Brownian motion, and more generally to a Wiener process.

In a discrete random walk, one considers the motion of a particle which at each step has complementary probabilities of going in any of the allowed directions. For instance, in a one dimensional case, the particle has p probability of going left and $1 - p$ probability of going right. The length of each step is considered to be regular during all the walk. Let us take here a walk in which the particle performs steps of size Δx . A usual realization of this kind of walks is the motion of a particle in a regular lattice, in which the particle can only move from vertex to vertex, and their distance is Δx . If the walk consist in n steps, the position at time $t = \Delta t n$, being Δt the time taken to perform a step, is

$$y(t) = \Delta x(x_1 + x_2 + \cdots + x_n), \quad (2.9)$$

where $x_i = +1$ when the particle moves to right and $x_i = -1$ when it moves to the left. From here we have that the expected value $E[x_i] = 2p - 1$ and its variance $\text{Var}[x_i] = 1 - (2p - 1)^2$. Using these, we can calculate

$$E[y(t)] = n\Delta x(2p - 1) \quad (2.10)$$

$$\text{Var}[y(t)] = n(\Delta x)^2 [1 - (2p - 1)^2]. \quad (2.11)$$

Considering for instance $\Delta x = \sigma\sqrt{\Delta t}$ and $p = [1 + (\mu/\sigma)^2\Delta t]/2$, we have $E[x_i] \rightarrow \mu t$ and $\text{Var}[x_i] \rightarrow \sigma^2 t$ for $\Delta t \rightarrow 0$, which is equivalent to Brownian motion with mean μ and variance σ . If one takes $\Delta x = \sqrt{2D\Delta t}$ and $p = 1/2$ we recover the case presented in Eq. (2.2). See that the equivalence is a direct consequence of the Central Limit Theorem, as the sum of independent variables in Eq. (2.9) gives rise to a normal distribution with same mean and variance. Even though many properties, such as fractality, are conserved in this analogy, others, such as invariance against rotations, are not.

In general, in order to faithfully approximate a Wiener or Brownian process of length L , one must consider a discrete random walk of length $L/\Delta x^2$. This makes the need to be in the regime $\Delta x \gg L$, which is ensured by either considering $\Delta x \rightarrow 0$ or $L \gg 1$. In the case of the models presented in following chapters, the latter will always be ensured, as we will always consider their long time limit, where $t \rightarrow \infty$ and $L \rightarrow \infty$.

2.2 Continuous time random walks

In the previous section we have studied the motion of a particle which diffuses freely in an unbounded space, both in its continuous and discrete limits. While Brownian motion considers that the motion of the particle is due to the microscopic interactions with the surrounding particles, it also considers them as homogeneous. However, in physical systems, one usually faces the presence of heterogeneities. This means that the particle may interact differently with different parts of the systems. As a consequence, its motion is perturbed from the previous Brownian (or normal) diffusion.

Such effects arise in very different forms in the statistics of the particle. One of the most common is the departure from the linear scaling of the MSD, such that we now have

$$\langle x^2(t) \rangle \propto t^\alpha, \quad \text{with } 0 \leq \alpha \leq 2, \quad (2.12)$$

where α is the anomalous exponent and signals arising of *anomalous diffusion*. Note that this is just one of the traces of anomalous diffusion, as for example we now know about anomalous system which show a linear scaling of the MSD but their PDF is not Gaussian [66]. In terms of the anomalous exponent, there exist two very distinct regimes: subdiffusion, where the anomalous exponent α is $0 \leq \alpha < 1$ and superdiffusion, where $1 < \alpha \leq 2$. To understand the effect of such exponent, one may think of the MSD as the radius of the circle, centered at the initial position of the particle, whose perimeter marks the furthest point one expects to find the particle at time t . In subdiffusion, the particles explore less space (the radius is smaller) while the opposite occurs in superdiffusion.

In this Thesis we will mainly focus in the subdiffusive case. Its appearance may be linked to very different phenomena. We will review in this chapter many

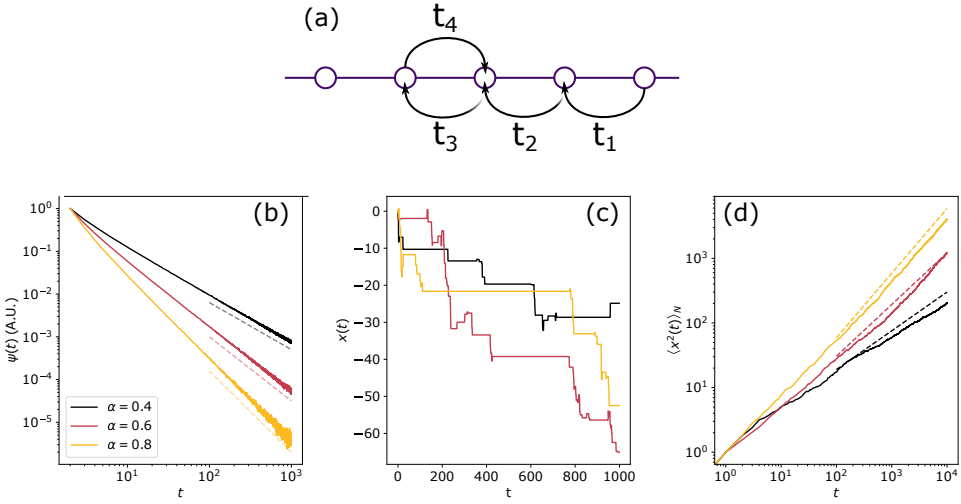


FIGURE 2.3: **Continuous time random walk and its characteristics:** **a)** Schematic of the walk: a particle moves in a regular lattice with waiting times t_i . **b)** Waiting time distribution, given by Eq. (2.22), for different α . Dashed lines show the expected behavior $t^{-1-\alpha}$. **c)** CTRW trajectories arising from these distributions. **d)** Ensemble MSD performed over 1000 trajectories for trajectories with the given α . Dashed lines show the expected behavior t^α .

of such. However, due to its importance in the rest of the Thesis, we will use as vehicle for the exploration of anomalous diffusion the continuous time random walk (CTRW).

Mathematically, the CTRW has a very simple formulation. Let us consider here its discrete version. CTRW considers a random walker that moves through a regular lattice, just as the one of Eq. (2.9). However, in this case the walker waits a given time t_i before performing each of the steps. We defined such times as the *waiting times*, i.e. the time the walker has to wait before performing a step. In general, we will consider that the waiting times have a certain distribution $\psi(t)$. CTRWs were first proposed in Ref. [20] and are now one of the main anomalous diffusion used for instance to describe the diffusion of particles in very different scenarios [67]. Specially, they are used to describe systems which present certain traps, which immobilize temporarily the traced particles. Then, such trapping times can be directly mapped to the waiting times of the CTRW framework.

2.2.1 General features

One of the main advantages of the CTRW is that all its behaviour can be directly related to $\psi(t)$, which allows for a very simple derivation of its main features. Note here that we are considering the case of a CTRW in a regular lattice, i.e. all steps have equal size but random direction. One usually starts by defining the survival probability, i.e. the probability of a particle to stay on a site for a time longer than t ,

$$\Psi(t) = \int_t^\infty \psi(t') dt' = 1 - \int_0^t \psi(t') dt'. \quad (2.13)$$

Recall here that $\psi(t)$ is the waiting time distribution. From here we can calculate the probability of the particle performing exactly n steps up to time t as

$$\chi_n(t) = \int_0^t \psi_n(t) \Psi(t - \tau) d\tau, \quad (2.14)$$

which in the Laplace space takes the very simple form of

$$\chi_n(s) = \psi^n(s) \frac{1 - \psi(s)}{s}. \quad (2.15)$$

The previous can be used to calculate the PDF of the position of the particle at time t , analogous to Eq. (2.2), which in this case is given by

$$P(x, t) = \sum_n^\infty P_n(x) \chi_n(t), \quad (2.16)$$

where $P_n(x)$ is the probability of reaching x at the n -th step of the random walk. We consider here that such probability can be written as a function of its characteristic function λ in Fourier space, as $P_n(k) = \lambda^n(k)$. The latter is defined as the Fourier transform of the probability density $p(x)$, i.e. the probability of travelling a distance x in a single step, which in the case of a regular CTRW is just the delta function. Performing the Laplace-Fourier transform of Eq. (2.16) we find that [63]

$$P(k, s) = \frac{1 - \psi(s)}{s} \frac{1}{1 - \lambda(k)\psi(s)}. \quad (2.17)$$

Note here that the previous equation is general for any CTRW and that not all CTRW are subdiffusive. Such property will arise from particular definitions of the waiting time $\psi(t)$. The previous CTRW framework is general enough to accommodate most of the uncoupled walks, i.e. the walks in which the step length and the waiting time are not related. For instance, if one considers an exponential waiting time PDF, $\psi(t) = \tau e^{-t/\tau}$, and an exponential characteristic function, $\lambda(k) = \exp(-\sigma^2 k^2/2)$, we recover the exact Brownian motion PDF of Eq. (2.2).

2.2.2 Moments of displacement

Of our particular interest is the calculation of the moments of displacement of $P(x, t)$, as the MSD is defined as its second moment. In general, they are defined, in the Laplace space, as

$$M_n(s) = (-i)^n \left. \frac{d^n P(k, s)}{dk^n} \right|_{k=0}. \quad (2.18)$$

As said, we are interested in the second moment, which we can calculate as

$$M_2(s) = \langle x^2(s) \rangle = -\frac{d^2 P(k, s)}{dk^2} = \frac{\psi(s)}{s(1-\psi(s))} \langle l^2 \rangle + \frac{2\psi^2(s)}{s(1-\psi(s))} \langle l \rangle^2, \quad (2.19)$$

where $\langle l^2 \rangle$ is the variance of $p(x)$ and $\langle l \rangle$ its mean. Note that in the case of an unbiased walk, we have that $\langle l \rangle = 0$, which means that the second term of the previous equation vanishes. If we consider now the same exponential waiting time PDF as before, we find that

$$\langle x^2(s) \rangle = \frac{1}{1+s\tau} \frac{1}{s(1-1/(1+s\tau))} \langle l^2 \rangle = \frac{1}{s^2\tau} \langle l^2 \rangle. \quad (2.20)$$

Performing the inverse Laplace transform, we find the time dependence of the MSD,

$$\langle x^2(t) \rangle = \frac{\langle l^2 \rangle}{\tau} t, \quad (2.21)$$

i.e. a CTRW with exponential waiting time distribution shows normal diffusion. Moreover, in one dimension the prefactor $\langle l^2 \rangle / \tau$ is directly connected to the diffusion coefficient D , with which we would recover Eq. (2.5).

2.2.3 Power-law waiting time distributions

While CTRW can give rise to normal diffusion, as shown in Eq. (2.21), it is mostly known for its particular connection to anomalous diffusion. In the previous example, we have considered a waiting time distributions with defined means, more precisely $\langle t \rangle = \tau$. We will treat now the case in which the first moment of the distribution $\psi(t)$ diverges. Particularly, we are interested in the case in which the distribution has power law tails, also called long or fat tails. In its most simple form, we consider here

$$\psi(t) \propto t^{-\alpha-1}, \quad (2.22)$$

with $0 \leq \alpha \leq 1$. We will now calculate the MSD using Eq. (2.20). A key difference from the previous case is the need of the use of the Tauberian theorem [68] for the correct calculation of the Laplace transform of $\psi(t)$, mainly due to its divergence.

The theorem states that at $t \rightarrow \infty$, a given function $f(t)$ fulfils

$$f(t) \cong t^{\rho-1}L(t) \iff f(s) \cong \Gamma(\rho)s^{-\rho}L(1/s), \quad (2.23)$$

where $\Gamma(\cdot)$ is the Gamma function, $L(t)$ is a slowly varying function of its argument and $0 < \rho < 1$. Moreover, the previous theorem considers normalized functions, i.e. $\int_0^\infty f(t)dt = 1$ and $f(s \rightarrow 0) = 1$. From its definition in Eq. (2.22), it is easily seen that $\psi(t)$ does not fulfil the previous condition, hence the Tauberian theorem leads to incorrect results. To solve such problem, one considers instead the survival probability $\Psi(t)$ from Eq. (2.13) in the Laplace space,

$$\Psi(s) = \frac{1 - \psi(s)}{s}. \quad (2.24)$$

From the Eqs. (2.13) and (2.22), we see that $\Psi(t) \propto t^{-\alpha}$. Then, applying (2.24), we have that the Laplace transform of the waiting time distribution is

$$\psi(s) \approx 1 - \tilde{\tau}^\alpha s^\alpha, \quad (2.25)$$

Inserting the previous in Eq. (2.19) and performing again an inverse Laplace transform, we get that the MSD of a power-law CTRW is

$$\langle x^2(t) \rangle \propto t^\alpha. \quad (2.26)$$

See that in the defined regime of α , i.e. $0 \leq \alpha \leq 1$, the MSD is subdiffusive. Moreover, its degree of *subdiffusivity*, i.e. the value of the anomalous exponent, is directly related to slope of the waiting time distribution $\psi(t)$.

From a phenomenological point of view, the explanation for the subdiffusion in CTRW is related to the divergence of $\psi(t)$. Due to the later, there is a non zero probability for the walker to be trapped in a given site for an infinite time. See that this will never occur in an exponential distribution, in which infinite times are exponentially unlikely. Interestingly, this feature has another very important effect. As a walker may be trapped for an infinite time, it is not able to explore the whole space during its walk, even in the limit $t \propto \infty$. We refer to this as the breaking of ergodicity, a central feature in anomalous diffusion.

2.2.4 Ergodicity breaking

The ergodic theorem, coined by L. Boltzmann in 1898 [69], states that a 'system in some region of the phase space of microstates with the same energy is proportional to the volume of this region, i.e. that all accessible microstates are equiprobable over a long period of time'. The breaking of ergodicity is then related to the system not fulfilling the previous theorem and hence not being able to visit the whole phase space.

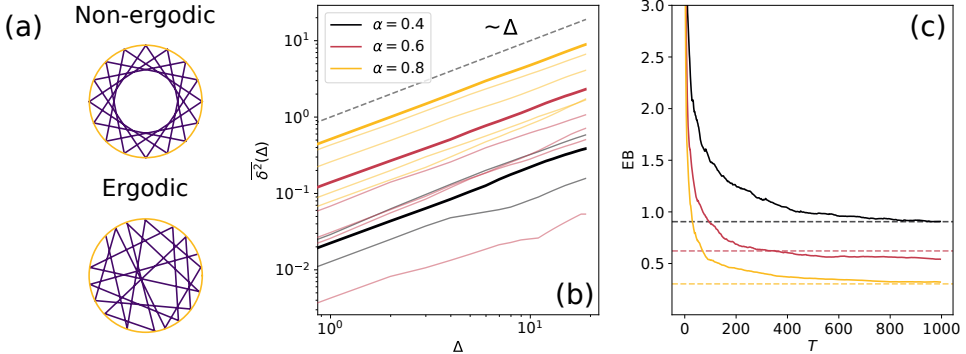


FIGURE 2.4: **Weak ergodicity breaking in the CTRW:** **a)** Schematic representation of ergodic and non-ergodic processes. **b)** Time MSD for various CTRW with different α . Wider lines show the tMSD of the trajectories presented in Fig. 2.3. We show the linear scaling, as well as the random nature of the tMSD. **c)** Ergodicity breaking parameter for a set of 1000 CTRW trajectories with various α . Dashed lines show the theoretical prediction of Eq. (2.30).

Commonly, it was associated to infinite barriers which separated the different microstates of the system. Later on, Bouchaud showed how some systems may only break ergodicity *weakly*, which means that the phase space is ‘*not broken into mutually inaccessible regions*’ [70]. In Fig. 2.4 (a) we exemplify this behavior: the upper trajectory will never visit the central part of the bounded space, while the lower one is able to explore the whole space. Hence, in non-ergodic systems, a single trajectory is unable to faithfully describe the features of the system, as it may only visit some part of the phase space.

In terms of diffusion trajectories, ergodicity breaking is well represented by the difference between the eMSD and the tMSD:

$$\overline{\delta^2}(\Delta) \neq \langle x^2(\Delta) \rangle_N. \quad (2.27)$$

See that this is directly opposed to what we saw in Section 2.1, where we proved that these two averages were equal for Brownian motion. Indeed, the previously defines two big families in diffusion processes: the ergodic and the non-ergodic. Note that the breaking of ergodicity has a direct impact in the characterization of experimental trajectories, as the tMSD differs from the eMSD and hence from the MSD, and is no longer a correct measure for most of their features. We will comment on this concept throughout this Thesis and specially in Chapter 7.

In the case of an unbiased CTRW, it has been shown that the tMSD of trajectories with same α are indeed ‘*non-identical and the tMSDs remains a random variable*’ [71]. Thus, the tMSD is another stochastic feature of the system, for which we

can study the mean and distribution. For the former, one can use Eq. (2.6) to find that

$$\langle \overline{\delta^2(\Delta)} \rangle \sim \frac{2D_\alpha}{\Gamma(1+\alpha)} \frac{\Delta}{t^{1-\alpha}}. \quad (2.28)$$

Opposite to what we showed for the MSD in Eq. (2.26), the tMSD is linear with Δ . We show this behaviour in Fig. 2.4 (b). We present there the tMSD calculated for various trajectories, with different anomalous exponents. See there that not matter α , each $\overline{\delta^2(\Delta)} \sim \Delta$. Moreover, their value varies from trajectory to trajectory, showing its random value. Note also that in Eq. (2.28), we also have a non-linear dependence with time. This effect is usually referred as *ageing*. This exemplifies the fact that the longer the process, the more probable it is to get trapped for a long time, hence lowering the displacement of the particle (even stopping it at all). Usually, one consider that the tMSD in the simple form $\overline{\delta^2(\Delta)} \sim D(t)\Delta$, where $D(t)$ accounts for the time dependence in Eq. (2.28).

Another interesting feature is the actual distribution of $\overline{\delta^2(\Delta)}$. More precisely, one can calculate the distribution of the dimensionless variable $\xi = \overline{\delta^2} / \langle \overline{\delta^2} \rangle$ as [71]

$$\lim_{t \rightarrow \infty} P(\xi) = \frac{\Gamma^{1/\alpha}(1+\alpha)}{\alpha \xi^{1+1/\alpha}} l_\alpha \left[\frac{\Gamma^{1/\alpha}(1+\alpha)}{\xi^{1/\alpha}} \right], \quad (2.29)$$

where $l_\alpha(\cdot)$ is the one-sided Lévy stable PDF. While the distribution encloses the complete behaviour of the process, in an experimental scenario it is usually difficult to access sufficient trajectories as to correctly fit any function. To solve such problem, a much simpler measure of the ergodicity breaking can be done by studying the fluctuations of tMSD and their variance. A particular form of doing so is given by the ergodicity breaking parameter (EB) [71]

$$\text{EB} = \lim_{t \rightarrow \infty} \frac{\langle (\overline{\delta^2})^2 \rangle - \langle \overline{\delta^2} \rangle^2}{\langle \overline{\delta^2} \rangle^2} = \frac{2\Gamma^2(1+\alpha)}{\Gamma(1+2\alpha)} - 1. \quad (2.30)$$

Importantly, the EB is independent of any scaling of Δ or t and only depends on the anomalous exponent α . The behaviour of the EB is as follows: for normal diffusion (i.e. $\alpha = 1$), the EB decays asymptotically zero, while decreasing α , hence enhancing subdiffusion, increases such asymptotic value. In Fig. 2.4 (c) we present the values for the EB for various α . The bold lines show the EB calculated over 1000 trajectories with same anomalous exponent. At long times, the value approaches asymptotically the dashed lines, representing the theoretical value calculate by means of Eq. (2.30). Note that in Fig. 2.4 (c) that the EB was calculated as a function of the sampling time T , meaning that the trajectories where cut at length T before calculating EB. Such measures shows the actual behaviour of EB,

and proves that Eq. (2.30) is only valid at $T \rightarrow \infty$, analogous in this case to $t \rightarrow \infty$, but with closer connection to the numerical implementation.

2.3 Other anomalous diffusion models

While the main scope of this thesis is the study of phenomenological models leading to CTRW-like models, we will at some points explore their connection with other diffusion models. Moreover, in the last chapter of the thesis we will present a method to differentiate between these. In this section, we will review the main characteristics of three families of models: coupled space-time random walks, disordered diffusion models and fractional Brownian motion. As we will show, the first two are closely related to CTRW and tend in some regimes to the results presented in the previous sections. The latter has been for decades one of the main examples of anomalous diffusion, due its rather simple definition by means of a fractional Langevin equation (in contrast to Eq. (2.4)).

2.3.1 Coupled space-time random walks

Until now, we have considered walks in which the distribution of waiting times and step lengths were completely uncorrelated. This was clear from the Eq. (2.16), which could be simplified so that the generator of the walk is $\psi(x, t) = p(x)\psi(t)$. In previous sections, we have considered various forms of $\psi(t)$, to finally study the case of a power law distribution in more detail. For the step length distribution, we have mostly considered either a Gaussian distribution and their discrete analogue (see for instance the end of Section 2.2.1). However, many other distributions are possible. Of special importance are the Lévy distributions, which give rise to the so-called Lévy flights. In its most general form, one considers a random walk in which the step-lengths with a heavy-tailed PDF,

$$p(x) \propto \langle x \rangle^{-1-\alpha}, \quad (2.31)$$

with $0 < \alpha < 2$. Let us consider a generator of the form of $\psi(x, t)$ and the usual power-law waiting time distribution of Eq. (2.22). Then, we can use Eq. (2.16) to find the PDF of the particle:

$$P(x, t) = \frac{s^{\beta-1}}{s^{\beta} + k^{\alpha}}. \quad (2.32)$$

See that the previous PDF has a diverging second moment, hence its connection with *real*, in the sense of physically possible diffusion processes is very small. Nevertheless, Lévy distribution have been widely observed in many experimental scenarios. To solve such problem, one of the proposals has been to couple the step

and waiting time distributions, i.e. $\psi(x, t) = p(x)\psi(t|x)$ or $\psi(x, t) = \psi(t)p(x|t)$. These processes are commonly known as Lévy Walks. An extensive review on the topic can be found in Ref. [72]. Further details on the characteristic of this walks will be presented in Chapter 5.

2.3.2 Diffusion disordered models

For some time, CTRW has been one of the few diffusion models able to show weak ergodicity breaking, phenomena that was widely seen in different experimental scenarios. However, the presence of infinite trapping events, needed for anomalous diffusion, is somewhat a very strong condition which does not usually arises in biological scenarios. To solve such issue, there has been some recent developments in diffusion models which could accommodate many of the *anomalous* features but could be easily connected to the experimental observations in biological scenarios.

A prominent direction has been the study of the motion of a Brownian particle for which the diffusion coefficient is non-constant. In 2014, two very conceptually similar models were introduced: the diffusing diffusivity model [73] and the patch model [74]. The former explains the motion of a particle which shows anomalous yet Brownian diffusion, as seen experimentally in Refs. [75, 76]. This means that while the MSD is still linear with time, the PDF of the walk is no longer Gaussian, as it was for Brownian particles (see for instance Eq. (2.2)). This arises from the diffusivity of the diffusion coefficient D . The particles are considered to perform Brownian motion (or an unbiased random walk, in discrete formulation) but their diffusion coefficient D changes over time. Originally, it was considered that D was indeed performing its own random walk. Later, an analogous derivation was introduced, for which it was demonstrated the *'equivalence of the diffusing diffusivity process with a super-statistical approach with a distribution of diffusivities, at times shorter than the diffusivity correlation time'* [66].

While the diffusing diffusivity model answered some of the questions related to the non-Gaussianity of the displacement distribution, it focuses mostly in cases where the diffusion is normal. On the other hand, the patch model has as main goal the study of anomalous diffusion with weak ergodicity breaking. There are various versions of the model, we will focus here in the annealed transit time case, which considers a particle moving with Gaussian displacements, just as in Eq. (2.22). The particle starts by sampling a diffusion coefficient D_1 with which it will diffuse for a time t_1 . After this time, a new pair (D_2, τ_2) is sampled. In general, the model considers that the pairs are drawn with distribution $P_{D,\tau} = P_D(D)P_\tau(\tau|D)$, with $P_D(D) \sim D^{\sigma-1}$, $\sigma > 0$ and the expected value $E[\tau|D] = D^{-\gamma}$. The particle then shows anomalous diffusion with exponent σ/γ for $\sigma < \gamma < \sigma + 1$ and $1 - 1/\gamma$ for $\sigma + 2 < \gamma$. Such behaviour has then been observed in the motion of receptors in living cells [77].

2.3.3 Fractional Brownian Motion

Fractional Brownian motion (FBM) is one of the most studied and used diffusion model, mainly due to its simple formulation but also to its arising in many different biological scenarios. Mandelbrot and van Ness introduced the model back in 1969 [19]. Nevertheless, Kolmogorov proposed an analogous formulation already twenty years before [18]. FBM is usually formulated by means of the fractional Langevin equation

$$\frac{dx(t)}{dt} = \xi_{fGn}(t). \quad (2.33)$$

See that its definition is analogous to the definition of the Brownian motion we presented in Eq. (2.4). In that case, ξ was defined as an uncorrelated Gaussian noise. In the case of FBM, ξ_{fGn} is defined as a fractional Gaussian noise, which is normally distributed but shows power-law correlations in time

$$\langle \xi_{fGn}(t_1) \xi_{fGn}(t_2) \rangle = \alpha(\alpha - 1) D_\alpha |t_1 - t_2|^{\alpha-2}, \quad (2.34)$$

where D_α is here the diffusion coefficient. Following the notation proposed in Ref. [23], we will define FBM based on α , the anomalous exponent. However, note that in its usual definition, FBM is studied in terms of the Hurst exponent $H = \alpha/2$. In the proposed way, the connection between diffusion and the Langevin equation is made from the its initial formulation.

Coming back to Eq. (2.34), we see that for $0 < \alpha < 1$ the noise is negatively correlated, while for $1 < \alpha < 2$ is positively correlated. To understand the implication of this, let us first define the PDF of the *free* FBM, in close analogy to Eq. (2.2), as

$$P(x, t) = \frac{1}{\sqrt{4\pi D_\alpha t^\alpha}} \exp\left(-\frac{x^2}{4D_\alpha t^\alpha}\right). \quad (2.35)$$

From here, we can calculate autocorrelation of FBM displacements as

$$\langle \Delta x(t_1) \Delta x(t_2) \rangle = D_\alpha (t_1^\alpha + t_2^\alpha - |t_1 - t_2|^\alpha). \quad (2.36)$$

With this, the link between the noise correlation and diffusion can be easily exposed. See that for negative correlation ($0 < \alpha < 1$), the displacements Δx_1 and Δx_2 will have opposite sign, implying that the particle is effectively bouncing. This effect has often been associated to the motion of a particle in a viscoelastic medium, where the particle bounces while interacting with its environment [78]. In the case of positive correlations, the signs of the displacements will be equal, i.e. displacements in one direction induce the next to be in the same direction. This induces the appearance of superdiffusion, as the motion is now directed [79, 80].

The previous statements about the departure from normal diffusion are clear if

one calculates the MSD of the walk, using Eq. (2.5) and Eq. (2.35) to find $\langle x^2(t) \rangle = 2D_\alpha t^\alpha$. Now, from Eq. (2.36) we can also calculate the tMSD as

$$\overline{\delta^2}(\Delta) = 2D_\alpha t^\alpha, \quad (2.37)$$

which implies that $\overline{\delta^2}(\Delta) = \langle x^2(\Delta) \rangle$, i.e. FBM is an ergodic stochastic process. This shows a crucial difference between the models we have previously described and FBM. In this direction, ergodicity has usually been used to differentiate between these, while recently a plethora of new methods have been introduced [59, 81, 82, 83]. In Chapter 7 we will further comment on this, as we will explore there a novel machine learning technique which may be used for this end.

3 Heterogeneous interactions as source of subdiffusion

In this chapter we will begin the exploration of phenomenological anomalous diffusion models. As we have widely commented, the arising of anomalous diffusion has been understood for quite some time already. Nevertheless, its connection with the actual microscopical interactions between the tracked particles and their environments is still unclear. Moreover, such phenomena can vary significantly from system to system. We want to focus here in a specific family of models, in which the presence of spatio-temporal disorder leads to anomalous diffusion. We present here a model in which such disorder appears due to the interactions from a particle, defined as *prey*, with its neighbouring particles, defined as *hunters*. We consider that the interactions are heterogeneous, meaning that the prey interacts differently with each hunter. More precisely, we consider that the hunter-prey interactions induce changes in the motion of the particle, which is by itself following a continuous time random walk. We will show how these interactions lead to the anomalous diffusion of the prey and how the distribution of heterogeneities affect the anomalous exponent. We will also study the appearance of non-ergodicity and non-Gaussianity in the diffusion of the prey. Moreover, we will show how the density of hunters affects the diffusion of the prey. The latter gives a powerful tool to test the validity of the model in real biological scenarios.

3.1 Theoretical framework

We consider a system in which a random walker, the *prey*, moves in a system surrounded of N independent random walkers, defined as *hunters*. We consider that both kind of walkers move in a d -dimensional regular lattice with $m = L^d$ sites, where $d = 1, 2$. Moreover, we consider that the system has periodic boundary conditions to ensure: 1) that the density of hunters is constant over time; 2) that the distribution of walkers in space is not affected by the finite size of the system. An schematic of the system is presented in Fig. 3.1.

While the step length of all walkers is regular, given in this case by the lattice site distance, the time between steps is considered irregular. This defines a continuous time random walk (CTRW) [20], in which the times between steps are

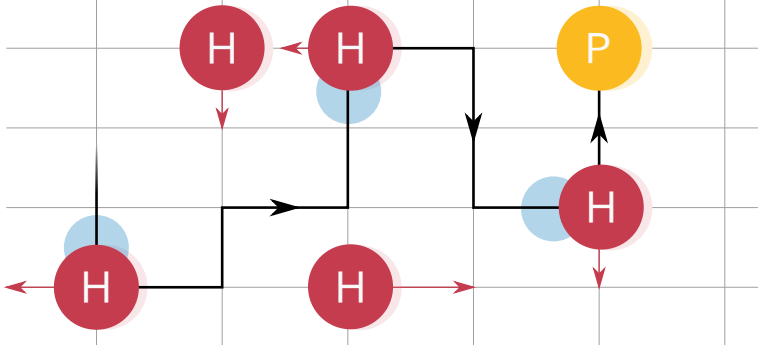


FIGURE 3.1: Scheme of the model: the prey (P) and hunters (H) perform a random walk in a regular lattice. Each time the coincide, the diffusion of the prey is affected as described in Eq. (3.4).

usually defined as the *waiting times* of the walker. We consider here that the waiting times of both prey and hunters are retrieved from an exponential distribution

$$\psi_0(t) = (1/\tau) \exp[-t/\tau]. \quad (3.1)$$

Following the usual CTRW theory presented in Chapter 2, one can show that such distribution, together with a step size distribution $p(x) = \delta(x - 1)$, leads to normal diffusion, i.e. $\langle x^2(t) \rangle = \frac{1}{\tau} t$. Additionally, we consider now that each time the prey and one or more hunters coincide in a given site, the waiting time distribution of the former is transformed to

$$\psi_\kappa(t) = (1/\kappa\tau) \exp(-t/\kappa\tau). \quad (3.2)$$

where κ is a stochastic variable drawn from a probability distribution

$$P_\kappa(\kappa) \approx \kappa^{-\sigma} \quad \text{with } \sigma > 1. \quad (3.3)$$

Note that κ is indeed the source of disorder in the model and will be shown to be the cause of the departure from normal diffusion. Finally, we assume that the change of the waiting time distribution only occurs for the prey, while the hunters remain with the distribution of Eq. (3.1) at all times. This means that the hunters will always diffuse normally.

We consider now two kind of disorders. First, one in which a new κ is drawn for every prey/hunter coincidence. We refer to this as the *annealed* disorder. A different disorder realization considers that each hunter is assigned a given κ since the initialization of the system. Then, each time the particle interacts with that hunter, it draws the same κ . We refer to this as the *quenched* disorder. In the case

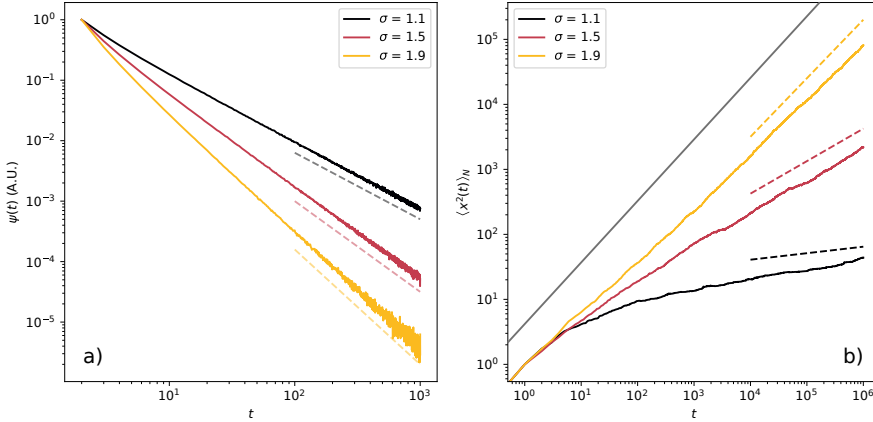


FIGURE 3.2: **(a)** Analytical (dashed line) vs numerically-calculated (solid line) waiting time distribution for $\sigma = 1.6$. **(b)** Ensemble mean squared displacement calculated for different values of σ , showing the subdiffusive behaviour in the asymptotic regime and the agreement of the exponent α with the theoretical predicted values. The black solid thin line indicates the exponent $\alpha = 1$. These results correspond to $N = 8$ hunters and $L = 20$ sites.

of large density, common in most biological scenarios, the prey has a very low probability of hitting the same hunter before having hitting many others. Hence, it can be considered that at each encounter the prey is indeed sampling a new value of κ . Therefore, in this scenario the annealed and quenched disorder converge to the same behaviour. We explore the validity of this statement in Section 3.2.

3.1.1 Effective waiting time distribution

From the model defined above we have that the waiting time distribution of the prey, $\psi(t)$, has two contributions: one accounting for the free motion of the prey, i.e. $\psi(t) = \psi_0(t)$, and one accounting for the prey-hunter coincidences, i.e. $\psi(t) = \psi_k(t)$. The latter has a probability p_H (the probability of hitting a hunter), while the former has probability $p_{NH} = 1 - p_H$ (the probability of not hitting hunters). Considering that the system has m sites, that the number of hunters N is constant over time and that they occupy all the space with equal probability, the not hitting probability is also constant during the evolution of the system and equals to $p_{NH} = \left(\frac{m-1}{m}\right)^N$. From here, we can define the effective waiting time distribution of the prey as

$$\psi(t) = p_{NH} \psi_0(t) + p_H \int_0^\infty P_\kappa(\kappa) \psi_\kappa(t) d\kappa. \quad (3.4)$$

See that in the case of hitting events, the waiting time $\psi_k(t)$ is weighted by the distribution probability of κ . The final waiting distribution of the prey is then closely related to the disorder distribution. We consider for instance a power law distribution of the disorder

$$P_\kappa(\kappa) = (\sigma - 1) \cdot \theta[\kappa - 1] \kappa^{-\sigma}, \quad (3.5)$$

where $\theta[\cdot]$ represents the Heaviside step function. The previous considers that the interaction between prey and hunters can only slow down the motion the former, as it sets a minimum value of $\kappa_{min} = 1$. Indeed the value of κ can be, by means of the MSD, directly related to the diffusion of the prey as $D = 1/\kappa$. See then that the higher the value of κ , the lower the diffusion coefficient of the prey. Setting the range of $\kappa \in [1, \infty)$ ensures that $D \in (0, 1]$. Using this change of variable, we can now perform the integral of the second term of Eq. (3.4) to find

$$\frac{1}{\tau} \int_0^1 D^{\sigma-1} e^{-\frac{Dt}{\tau}} dD = \frac{1}{\tau} \left(\frac{t}{\tau}\right)^{-\sigma} (\Gamma[\sigma] - \Gamma[\sigma, t/\tau]), \quad (3.6)$$

where $\Gamma[\sigma, t/\tau] = \int_{t/\tau}^{\infty} r^{\sigma-1} \exp[-r] dr$ is the upper incomplete Gamma function, which converges to zero as $t \rightarrow \infty$. Hence, we can neglect its contribution in the long-time limit regime. Moreover, the first term of Eq. (3.4) exponentially decays to zero in this regime, which means that it can also be neglected. In Section 3.2 we will comment on the behaviour at short times. Combining all previous statements, we have that the waiting time distribution of the prey is effectively described at $t \rightarrow \infty$ by

$$\psi(t) \approx p_H \frac{\Gamma[\sigma]}{\tau} \left(\frac{t}{\tau}\right)^{-\sigma} = \frac{1}{\tau} \left(\frac{t}{\tau}\right)^{-\sigma}, \quad (3.7)$$

where $\left(\frac{t}{\tau}\right)^{\sigma-1} = p_H \Gamma[\sigma]$.

3.1.2 Mean squared displacement

Once we have defined the model and studied the waiting time distribution for the CTRW performed by the prey, the next step to characterize diffusion is to calculate the mean squared displacement (MSD), i.e. Eq. (2.5) from Chapter 2. Indeed, the MSD gives us a powerful tool to compare the model with experimental observations, as it is usually easier to extract it, rather than, for example, the waiting time distribution. For CTRW, we have shown in Chapter 2 that the MSD in the Laplace space is a function of the waiting time distribution, with the form [22]

$$M_2(s) = \frac{\psi(s)}{s[1 - \psi(s)]} \langle \ell^2 \rangle. \quad (3.8)$$

Using the theory developed in Section 2.2.3, applied in this case to the waiting time distribution of Eq. (3.7), we find that its Laplace transform is

$$\psi(s) \approx 1 - \tilde{\tau}^\alpha s^\alpha, \quad (3.9)$$

where we have defined $\alpha = \sigma - 1$ (recall that $1 < \sigma < 2$, hence $0 < \alpha < 1$). Now using Eq. (3.8) and performing the inverse Laplace transform, we finally find the expression for the MSD,

$$M_2(t) = \mathcal{L}^{-1}[M_2(s)](t) \approx \frac{1}{\Gamma(\sigma)} \left(\frac{t}{\tilde{\tau}} \right)^\alpha. \quad (3.10)$$

We see here two very interesting dependences. First, the scaling of the MSD is directly related to the power law behaviour of the waiting time distribution by means of the relation between their exponents, $\alpha = \sigma - 1$. More importantly, we see that when $\sigma < 2$ the anomalous exponent is smaller than one, $\alpha < 1$. From this, it is clear that the disorder introduced by the interactions between the prey and the hunters can indeed produce anomalous diffusion in a system which initially (i.e. the prey without interactions) was normally diffusing. Moreover, depending on the distribution of the disorder introduced by the interactions, we may see completely different behaviours of the MSD.

Another important factor is given by the appearance of $\tilde{\tau}$ in the MSD. This variable is indeed related to the density of hunters,

$$\tilde{\tau} \propto \left[1 - \left(\frac{m-1}{m} \right)^N \right]^{\frac{1}{\alpha}}. \quad (3.11)$$

We see then not only a dependence on the scaling behaviour of the disorder, but also to its *amount*, in the sense of how many times the waiting time of the prey is changed w.r.t its free form. Indeed, this establishes a relevant relationship between the MSD (easily calculated from trajectories acquired in any SPT experiment) and the presence and quantity of disorder. See for instance that in dilute system, in which $m \gg N$, the prefactor $\tilde{\tau} \sim \rho$, where $\rho = N/m$ is the density of hunters. The MSD is then a correct measure for the density of interacting hunters and their disorder distribution.

3.1.3 Non-ergodicity

As stated in previous chapters, non-ergodicity implies that the time-averaged mean squared displacement (tMSD) over a given trajectory is not equal to the

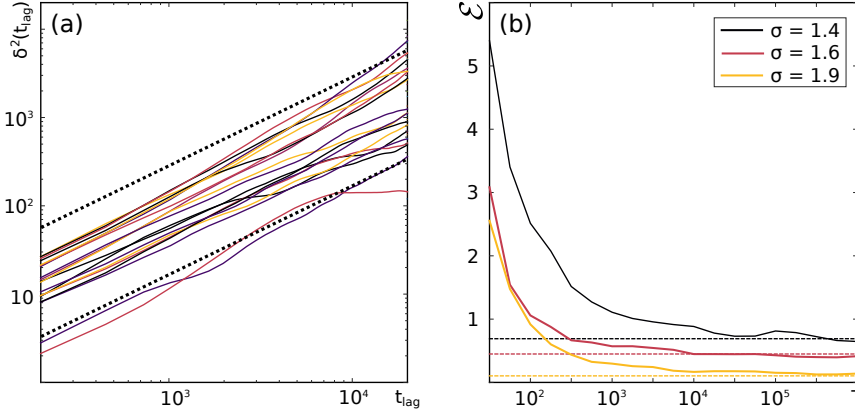


FIGURE 3.3: **(a)** Time averaged mean squared displacement obtained for 20 representative prey trajectories with $\sigma = 1.8$, $N = 6$ and $L = 20$. The curves show a linear behaviour but large scattering of their amplitude at all time lags, as expected for weak non-ergodic behaviour. Dashed lines correspond to linear behaviour and are meant as a guide to the eye. **(b)** Ergodicity breaking (EB) parameter calculated as a function of total time of measurement t for several values of σ and $N = 10$. At large t all the curves asymptotically tend to the value predicted by Eq. (3.13), shown as horizontal dashed lines. As σ is reduced, the system departs more from ergodicity and the EB shows larger asymptotic value.

average performed over a set of trajectories. We defined the latter as the ensemble mean squared displacement (eMSD). To faithfully characterize the presence of non-ergodicity, we use the Ergodicity Breaking parameter (EB), defined as [71]:

$$\text{EB} = \lim_{t \rightarrow \infty} \frac{\langle (\overline{\delta^2})^2 \rangle - \langle \overline{\delta^2} \rangle^2}{\langle \overline{\delta^2} \rangle^2}, \quad (3.12)$$

where

$$\overline{\delta^2}(t, t_{\text{lag}}) = \frac{\int_0^{t-t_{\text{lag}}} [x(t' + t_{\text{lag}}) - x(t')]^2 dt'}{t - t_{\text{lag}}},$$

is the tMSD of the given trajectory $x(t)$. The EB is zero for ergodic processes while $\text{EB} > 0$ for non-ergodic. For CTRW, we showed in Section 2.2.4 that power law waiting time distributions implied a linear tMSD w.r.t t_{lag} while its amplitude was random. From this, and considering that the distribution follows $\psi(t) \approx t^{-(1+\alpha)} / |\Gamma(-\alpha)|$, it was shown that the EB is [71]

$$\text{EB} = \frac{2\Gamma^2[\sigma]}{\Gamma[2\sigma - 1]} - 1. \quad (3.13)$$

This result holds also exactly for the diffusion of the prey, as in the long time limit its behaviour can be directly mapped into a CTRW with waiting time distribution $\psi(t)$.

3.1.4 Non-Gaussianity

To finish the theoretical study of the prey and hunters model we will study the Gaussianity of the propagator $P(x, t)$ of the prey. The latter, describing the probability of the prey being at time t in position x , gives the complete description of its behaviour. While it is Gaussian for Brownian particles, most of the anomalous models are now known to behave away from Gaussian distributions. Different ways exist to study the non-Gaussianity of a function. In this case, we will use so-called non-Gaussianity parameter, which compares the second and fourth moments of $P(x, t)$ as [84]

$$\vartheta(P(x, t)) = \frac{\langle x^4 \rangle}{a(d)\langle x^2 \rangle^2} - 1, \quad (3.14)$$

where d is the dimension of the walk and $a(d)$ is defined as the ratio of the second and fourth moment for a Gaussian propagator. To calculate $a(d)$, we consider the Gaussian propagator

$$P(x, t) = (4\pi\rho(t))^{-d/2} \exp[-x^2/4\rho(t)], \quad (3.15)$$

where x is the displacement in a d -dimensional space \mathcal{R}^d , x its modulus, and $\rho(t)$ is the variance and has dimensions of length to the square. Then, one can calculate all even momenta as

$$\begin{aligned} \langle x^{2n} \rangle &= \int_{\mathcal{R}^d} d^d x x^{2n} P(x, t) \\ &= \frac{(4\rho)^n}{(4\pi\rho)^{d/2}} \frac{\partial^n}{\partial k^n} \int_{\mathcal{R}^d} \exp[-k x^2/4\rho] \Big|_{k=1} \\ &= \frac{(4\rho)^n}{(4\pi\rho)^{d/2}} \frac{\partial^n}{\partial k^n} \left[\frac{4\pi\rho}{k} \right]^{d/2} \Big|_{k=1} \\ &= (-4\rho)^n \frac{d}{2} \frac{d+2}{2} \dots \frac{d+2(n-1)}{2}. \end{aligned} \quad (3.16)$$

From here, it suffices to consider $n = 2, 4$ and use it to calculate

$$a(d) \equiv \frac{\langle x^4 \rangle}{\langle x^2 \rangle^2} = \frac{d(d+2)}{d^2} = 1 + \frac{2}{d}. \quad (3.17)$$

Being $a(d)$ the ratio for a Gaussian propagator, $\vartheta(P(x, t) = 0$ is a necessary but not sufficient condition for $P(x, t)$ to be Gaussian. Nevertheless, ϑ is zero for any Gaussian process and $\vartheta \neq 0$ implies the so-called non-Gaussianity.

To study non-Gaussianity in our model, we consider the effective picture of the motion of the prey being a CTRW in $d = 1$ with waiting time distribution given by Eq. (3.7). As our walk is considered discrete and with equal step size throughout the whole walk, the step distribution is given by a delta distribution, $p(x) = \delta(x, 1)$. Using $\psi(t)$ and $p(x)$ one can calculate $P(x, t)$ in Laplace-Fourier space as (see also Section 2.2.1)

$$P(k, s) = \frac{1 - \psi(s)}{s} \frac{1}{1 - \lambda(k)\psi(s)}, \quad (3.18)$$

where $\lambda(k) = \int \exp[-ikx]p(x)ds$ is the Fourier transform of the step size distribution. From the previous, all moments can be obtained using

$$M_n(s) = (-i)^n \left. \frac{d^n P(k, s)}{dk^n} \right|_{k=0}, \quad (3.19)$$

and in particular the fourth moment $M_4(s)$ is

$$M_4(s) = \frac{\psi(s)}{s} \left(\frac{\langle \ell^4 \rangle}{1 - \psi(s)} + \frac{6\langle \ell^2 \rangle \psi(s)}{(1 - \psi(s))^2} \right). \quad (3.20)$$

We already know from the previous section that $\psi(s) \approx (1 - \tilde{\tau}^\alpha s^\alpha)$. Moreover, as we are interested in the long time behaviour, we are only concerned about the leading terms when $s \rightarrow 0$. In such case, we have that

$$M_4(s) \approx 6\langle \ell^2 \rangle^2 s^{-1-2\alpha} \tilde{\tau}^{-2\alpha}. \quad (3.21)$$

Performing the inverse Laplace transform, we see that

$$M_4(t) \approx 6M_2(t)^2, \quad t \gg \tilde{\tau}. \quad (3.22)$$

As for $d = 1$ we had $a(d) = 3$, this equation leads to $\lim_{t \rightarrow \infty} \vartheta(t) = 1$, which proves the non-Gaussianity of the presented model.

3.2 Numerical results

Once we have set the theoretical framework of the prey and hunters' model, we will simulate its dynamics by means of Monte Carlo dynamics in 1D. We will consider the case of a prey moving in an unbounded space surrounded by N hunters. As we are interested in the long time behaviour, in which numerics and theory

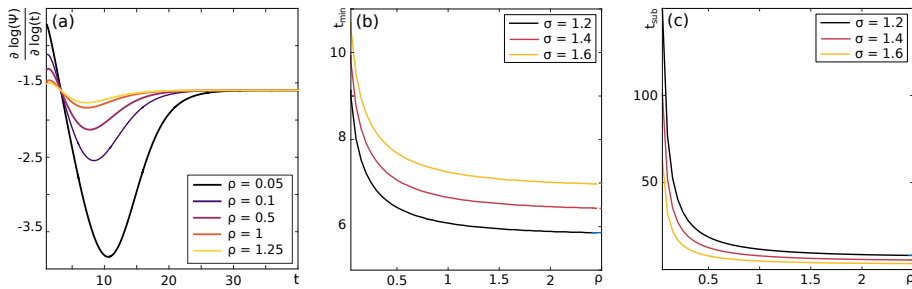


FIGURE 3.4: **(a)** Logarithmic derivative of the distribution of waiting times as in Eq. (3.4) for $\sigma = 1.6$ and different values of the density of hunters ρ ($L = 20$). For large t , the derivative tends to the expected value of $-\sigma$, corresponding to the exponent of Fig. 3.2(a) at long times. **(b)** Time t_{\min} at which the minima of the curve in panel (a) are reached, as a function of the density. The larger the density, the quicker the logarithmic derivative of the waiting time distribution tends to its asymptotic value σ (shorter t_{\min}). **(c)** Analytically calculation of the time t_{sub} at which the subdiffusive behaviour occurs as a function of ρ .

can be compared, we will consider that $\tau = 1$, which means that the waiting times arising from Eq. (3.7) will be three and four orders of magnitude higher. Moreover, unless otherwise stated, we will consider the annealed version of the model, i.e. the case in which a new κ is drawn at each prey/hunter coincidence.

We begin our comparison by studying the waiting time distribution of the prey. The results are shown in Fig. 3.2(a) for various values of σ . We also plot as dashed lines the theoretical prediction of Eq. (3.7), showing a great correspondence between each other. In panel (b) we show the eMSD calculated with a set of $n = 1000$ trajectories for each value of σ . This panels showcases the emergence of subdiffusion, coinciding with the prediction $\sim t^\alpha$, plotted as dashed lines in the figure.

With the same set of trajectories we calculate now the tMSD, shown in Fig. 3.3(a). We see there the typical behaviour of CTRW trajectories, where the tMSD has a linear dependence with t_{lag} while its amplitude is random. The latter is seeing as the spread of each plotted tMSD. While this implies non-ergodicity, as the tMSD is not equal to the eMSD presented in Fig. 3.2(b), a quantitative study of ergodicity breaking is presented in Fig. 3.3(b) by means of the EB parameter. We see that the numerical calculation of the EB parameter for the simulated trajectories converges to the value predicted by Eq. (3.13). We see also that as σ is reduced, we get a larger value of the EB, implying that the systems increases its ergodicity. It has to be noted that for $\sigma = 2$ we recover a normal diffusive CTRW, for which the EB is then equal to zero, as expected in this kind of processes.

One of the main features of the model is that the long time behaviour of the anomalous exponent and the ergodicity breaking do not depend on the density of clusters ρ . However, it has contributions to the general behaviour of the system at

shorter times. This is due to the dependence of Eq. (3.7) on p_H . Indeed, one can see that as we increase ρ , the second term in Eq. (3.4) becomes dominant at short times. To study this behaviour, we calculate the logarithmic derivative of $\psi(t)$ for different densities and show the result in Fig. 3.4(a). Interestingly, all curves are equal at $t = \sigma\tau$ with value $\frac{\log(\psi(t))}{\log(t)} = \sigma$. The general behaviour is independent of ρ , as all curves decrease until reaching a certain minima, to then increase to reach asymptotically the value σ and remain on it for bigger t .

While all densities behave similarly, the time to reach the asymptotic value σ is a function of ρ . While the converge to this point is not easily accessible, one can indeed calculate the time t_{\min} at which the logarithmic derivative reaches its minimum. In Fig. 3.4(b) we plot such value. We see there that for any σ , the smaller the density, the bigger t_{\min} . This means that the time at which the model reaches its asymptotic behaviour, set in this case by long time limit eMSD $\langle x^2(t) \rangle \sim t^\alpha$, increases as the density of hunters decreases.

In Fig. 3.5 (a) we present the eMSD for various densities at $\sigma = 1.2$, in one dimension. As predicted, the smaller the density, the longer it takes to reach the predicted anomalous exponent for the eMSD. We plot there both the annealed model (continuous lines) and the quenched model (dashed lines). While the slope reached by the two models is the same, we see that the smaller the density, the bigger the difference in the eMSDs. In this low density scenario, a prey in the annealed case has a larger time exploring the whole disorder distribution, as it has a high probability of repeatedly coinciding with the same hunter and thus drawing the same value κ many times. For high densities, such probabilities lowers considerably, as many hunters, with different κ , surround the prey. A similar effect happens when considering a 2D system, as shown in Fig. 3.4(e). There we see that the difference between annealed and quenched fades away even a lower densities.

Returning to the asymptotic approach to the expected anomalous exponent, we can now use the eMSD to estimate the time of such event. One can lower bound the appearance of the subdiffusive behaviour by exploring at which time the power-law behaviour of Eq. (3.10), dominant at longer times, intersects and overcomes the linear behaviour, dominant at short times. Such event takes place at $t_{\text{sub}} = \frac{10^{1-\alpha}}{p_H \Gamma(\sigma)^2}$. As expected and showed in Fig. 3.4(d) for the annealed case, there is dependence between t_{sub} and ρ , mediated in this case by the presence of p_H in the former. Note that, as described before, the behaviour of t_{\min} and t_{sub} are closely connected.

Once we have characterized the appearance of the subdiffusive behaviour as a function of time, we can relate the offsets in M_2 due to such effect. Indeed, we can calculate the distance between the two curves of the eMSD for different values of ρ , once they have reached the subdiffusion. Considering that the number of sites m is the same, two different densities imply two different numbers of particles N_i and N_j . Then, the distance between the two M_2 curves is given by

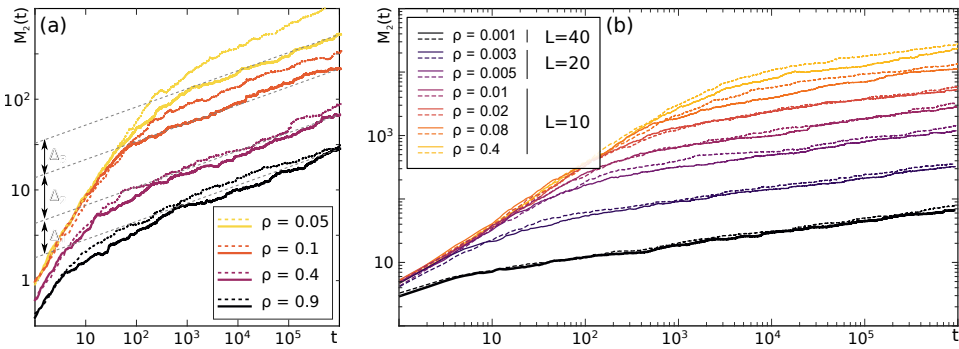


FIGURE 3.5: **(a)** eMSD for $\sigma = 1.2$ in 1D as obtained at different densities for annealed (continuous lines) and quenched disorder (dashed lines). The long-time scaling exponent of the eMSD is independent of the density and the type of disorder. In the asymptotic regime, curves obtained for different densities and type of disorder are separated by a distance Δ . **(b)** eMSD for $\sigma = 1.2$ in 2D for various densities and system sizes, for the annealed (continuous lines) or quenched disorder (dashed lines). See that the convergence of the two cases is even greater in higher dimensions.

$\Delta = \log(p_H(N_j, m)/p_H(N_i, m))$, which can be simplified to $\Delta = \log(N_j/N_i)$ in the dilute limit.

3.3 Conclusions

In this chapter, we have studied the effect of disorder in the continuous time random walk of a particle, defined as the *prey*. Such disorder appears due to the heterogeneous interactions between the prey and the surrounding particles, defined as the *hunters*. Phenomenologically, the model shows the effect of the presence of dynamic traps on the diffusion of the prey. We considered for instance that when the prey coincides with a hunter, the waiting time of the former is affected, in such a way that it is not longer drawn from an exponential distribution but from one with heavy tail. In the mathematical approach, we have studied how the effective waiting time distribution of the prey, described as the sum of distribution weighted with complementary probabilities (see Eq. (3.4)), leads to anomalous diffusion in the long time limit. Moreover, we have seen how the anomalous exponent is directly related to the disorder distribution in the system.

We have considered two realizations of the system, i.e. in the presence of either annealed or quenched disorder. While both show similar long time scalings, we have seen how the correlations arising in the quenched scenario induces some important changes in the diffusion of the particle, specially in the low density regime. We investigated such differences both in one and two dimensions, with

similar results: the more dilute the system, the bigger the differences in the behaviour. Due to the correlations, and mostly to the *speed* at which the disorder distribution is explored, we see that in the quenched system the particles takes longer to reach the anomalous, asymptotic behaviour.

Similarly, we have also studied how the density of hunters may affect the diffusion of the prey. While again, the asymptotic behaviour is equal for all cases, we see that the time taken to reach such value is clearly related to such density. We see that the smaller the density, the longer the time to reach subdiffusion t_{sub} . We show this both analytically (Fig. 3.4) and numerically (Fig. 3.5). We also showed that the density is the only important parameter, and not the size of the system.

The proposed framework relies on the assumption of a broad distribution of the diffusion rates (or diffusion coefficients) of the interacting partners. We consider this assumption rather reasonable since the hunters in our model might represent different chemical species and on the basis of broad diffusivity distributions reported for chemically identical cellular components [85]. Moreover, our general requirements for the distribution of rates include the particular case in which the diffusivity is the sum of several squared Gaussian random variables, e.g. due to the presence of a large number of degrees of freedom [86].

An important feature of the model is the possibility of being experimentally tested, thus allowing one to distinguish its occurrence from other theoretical frameworks. This is nowadays technologically possible by means of multicolour single particle tracking techniques. As an example, in a dual colour single particle tracking experiment it is possible to simultaneously follow the motion of two closely spaced particles with time resolution of few milliseconds and resolve their relative distance with a precision of the order of 10 nm [28, 87]. Analogously to single particle tracking, these experiments provide trajectories from which the time- and ensemble-averaged MSD can be calculated, thus allowing one to test the appearance of non-ergodicity. In addition, the technical advantages afforded by dual colour tracking make it possible to experimentally verify the occurrence of interactions between diffusing species, measure the duration of such events, and check whether they affect the diffusivity of the particles involved [88, 89, 87]. These experiments can be carried out by labelling chemically identical components as well as different species, thus testing the formation of both homo- and hetero-oligomers. This technique has already been successfully used to study interactions of several membrane components. In addition, other promising approaches to investigate interaction-dependent diffusion include hyper-spectral microscopy [90], as well as the combination of single particle tracking with recent methods based on advanced statistical tools [91] and on the spatio-temporal analysis of fluorescence fluctuations [92], which have been shown to provide a wealth of information into dynamic molecular processes of biological relevance.

Moreover, while these experimental strategies allow one to discriminate on the occurrence of the previous theory in a specific system, the model allows one

to directly calculate microscopic parameters of the system under investigation. Indeed, the timescale for the onset of subdiffusion in the eMSD curve provides an estimation of the average density of hunters, thus quantifying the level of crowding experienced by the prey. In addition, the scaling exponent of the eMSD is a proxy for the degree of heterogeneity of the environment. However, for a robust determination of these parameters one needs to collect a sufficient number of eMSD data points over the appropriate timescale. For example, in order to precisely extract the time at which subdiffusion arises, one needs to collect a sufficient number of eMSD data points spanning over at least two orders of magnitude centred around such a timescale. In typical SPT experiments, this range is bounded by the time-resolution and the trajectory duration [28]. The time resolution (i.e. the inverse of the recording frame rate), besides setting the shortest eMSD time point, also determines the lag between successive points and thus the number of data points within the measured range. The maximum trajectory length is instead ultimately limited by the photon budget of the fluorescent emitter. Therefore, although it is desirable to collect a large number of photons in each frame in order to achieve the precise localization of the particle [28], this would limit either the number of points or the maximum duration of the trajectory. Therefore, the experimental conditions must be finely tuned in order to obtain the best trade-off between tracking precision, time resolution and trajectory length. Although it is currently possible to obtain eMSD with hundreds of data points between a few milliseconds to tens of seconds, new strategies have the potential to push these bounds even further [93]. In this scenario, the model presented above might be a useful tool to investigate anomalous transport and its implications, while providing an alternative interpretation to the causes of non-ergodic subdiffusion. Moreover, in combination with recently proposed techniques, many of them discussed in Chapter 7, the model may help understand not only the arising of non-ergodic, but also the properties of the environment where the particle is diffusing.

4 Subdiffusion in critical environments

In this chapter we will introduce a microscopic model in which a particle diffuses through an environment which has different, heterogeneous regions or patches which affect its diffusion. In general, and as we have seen in previous Chapters, the diffusion of a particle is closely related to its own properties, but also to the particularities of the environment. In this cases, we consider a very abstract and general consideration: we will propose that the diffusion of the particle is related to the size of each patch it visits. While it may arise as a purely theoretical proposal, we will show in Chapter 5 that such behaviour may easily be reproduced by compartmentalized environments. In this case, we are interested in how the distribution of patch sizes may affect the diffusion of the particle. More precisely, we will consider that the environment is generated via the Ising model, a spin model with critical behaviour. The patches are then the connected domains of spins pointing in the same direction. Depending on the its temperature, the Ising model is known to show very distinct domain size distributions. We will explore how the diffusion of the particle, which is by itself performing a continuous time random walk (CTRW), is affected by the particularities of the environment. For instance, we will show how the particle diffuses anomaly when the Ising system is at critical temperature. Then, the environment can depart from criticality in two ways: first, due to finite size effect; second, by the change of temperature. In both cases, the particle will only diffuse anomaly for a transient time, which depends on how far away the environment is from criticality. We will show that the particle's motion shows weak ergodicity breaking at criticality, while at non-critical environments the particle recovers ergodicity after a characteristic time.

4.1 Theoretical framework

4.1.1 Motion of the particle

We consider the motion of a particle in a discrete space, which is a lattice of dimension d and side length L in two dimensions. The results presented here can be extended to more dimensions, but in such case, one has to do this generalization

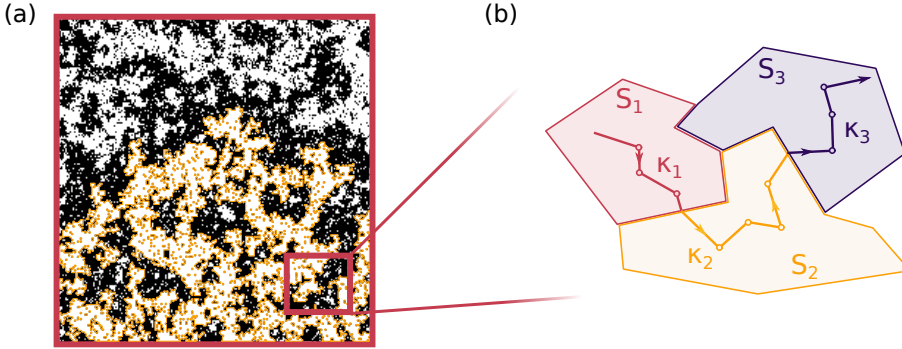


FIGURE 4.1: **Schematic of the CTRW performed by the particle in an Ising environment.** (a) Squared Ising lattice close to the critical temperature, $k_B T_c \approx 2.2691J$, with k_B the Boltzmann constant, and side length of $L = 500$. White (black) pixels represent spins point up (down). In yellow we highlight the biggest domain of the system, coinciding here with the percolating domain. (b) An scheme of a particle's motion through three different domains. Here, κ is determined from the size of the domain in which it sits, according to Eq. (4.4).

carefully, and take care of some details, as we comment later. The particle performs a CTRW along the lattice. Being the latter evenly spaced, the walk consist in regular steps of length ℓ , i.e. the distance between to vertex of the lattice. This is analogous to considering a delta step size probability distribution function (PDF), $p(x) = \delta(\ell - \langle x \rangle)$. The waiting time distribution, i.e. the time the walker waits in a given site before performing the next step, is given by an exponential PDF

$$\phi_\kappa(t) = \frac{1}{\kappa\tau} \exp[-t/\kappa\tau], \quad (4.1)$$

where τ accounts for the time scale of the walk. Similarly to Chapter 3, κ is considered here the source of disorder in the walk of the particle and will enclose the effect of the environment to the diffusion of the particle. As we showed previously, κ is indeed the inverse of the diffusion coefficient D of the particle. With this, depending of the values of κ , and more precisely its distribution $P(\kappa)$, we will see very distinct behaviour in terms of the diffusion of the particle. As shown in previous chapters, distributions with infinite mean but finite variance, such as $P(\kappa) \sim \kappa^{-\sigma}$ with $1 < \sigma < 2$, induce anomalous diffusion, i.e. $\langle x^2(t) \rangle \sim t^{\sigma-1}$.

4.1.2 The Ising environment

extend? We consider now an environment described by Ising dynamics. This means that at each site of the two dimensional lattice we consider a spin, which

can point in two directions: up ($s_i = 1$) or down ($s_i = -1$). We consider that the interactions of the spins with their neighbours is described with a two dimensional Ising Hamiltonian

$$H_{\text{Ising}} = -J \sum_{\langle ij \rangle} s_i s_j. \quad (4.2)$$

Here $\langle ij \rangle$ refers to the spins interacting only with their nearest-neighbors pairs in the lattice. These systems have been widely studied, mostly to describe ferromagnetic materials [94]. Moreover, their general properties make them great candidates to describe many kind of critical systems, as for example the heterogeneities present in plasma membranes [95, 96]. In two dimensions, the Ising model is known to have a phase transition at a critical temperature T_c , where the system changes from a phase in which all spins point in the same direction (ferromagnetic phase, $T < T_c$) to a phase in which the spins tend to align in the opposite direction of their neighbours (antiferromagnetic phase, $T > T_c$).

It is usual in Ising systems to see the appearance of domains: connected areas in which all spins point in the same direction. The size of such domains S , and more importantly the distribution of domain sizes $P(S)$, are connected with the temperature. Close to the phase transition, the domain size distribution behaves as

$$P(S) \propto S^{-\tau} \exp[-S/S^*], \quad (4.3)$$

where $\tau = 187/91 \approx 2.05$ is a critical exponent [97, 98] and S^* is the characteristic size of a domain. As the system approaches the critical temperature, we see the emergence of very large and even infinite domains, similar to what occurs in a percolation scheme. This is so due to the characteristic size being directly connected to the correlation length of the system, which is known to diverge at criticality [97, 98]. In such case, $S^* \rightarrow \infty$ and the distribution $P(S)$ becomes a power law. Note that this behaviour is also seen in a three dimensional lattice, with $\tau = 2.53$ [98], such that the results presented below are then extendable to the three dimensional walk of the particle.

In Fig. 4.1(a) we show a system of spins evolving under Ising dynamics at a temperature close to the critical one, $k_B T_c \approx 2.2691J$, for $L = 1000$. Dark (light) pixels represent spins pointing down (up). In yellow we highlight the biggest domain, which under periodic boundary conditions can be considered to be infinite. As it can be seen, such domain corresponds also to the percolating domain, i.e. a region of connected sites which goes from one limit of the systems to the opposite without breaking. In these, one can then consider that $S^* \rightarrow \infty$ and then recover the power law behaviour in Eq. (4.3).

Nevertheless, in order to assess the validity of Eq. (4.3), we use Monte Carlo simulations to evolve spins systems of various sizes ($L = 200, 500$ and 1000 spins) near the critical temperature. In Monte Carlo simulation of spin systems, one considers the flip of single or many spins, depending on the method, and only accepts them if the total energy of the system has lowered. To avoid getting stuck

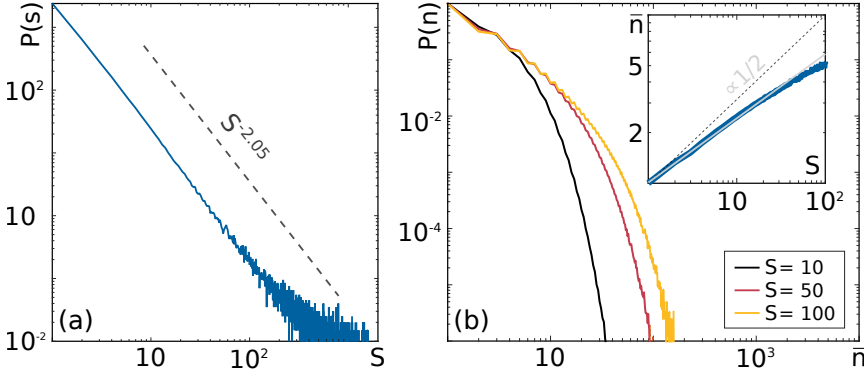


FIGURE 4.2: **Domain size distribution and average number of steps \bar{n} in a domain of size S** (a) Distribution of domain sizes for 200 patterns calculated at the critical temperature, $k_B T_c \approx 2.2691J$, for $L = 500$. (b) Numerically calculated probability distribution of the numbers of steps taken before exiting a domain of size S when the initial position is in the border. To do the calculations we select all the patterns of a given size S , perform X simulations of a particle starting at random positions in the border of the domain, and retain the time at which the particle leaves the domain. Inset: average time \bar{n} for leaving a domain of size S in log-log scale, showing that \bar{n} grows approximately as S^μ , with $\mu \sim 0.3$.

in local minima, it is usual to accept also flips that increase the energy with a certain, small, probability. The systems are evolved for long times, in order to attain an equilibrium state. Once reached, we numerically checked that $P(S)$ is indeed a good description of the domain size distribution, even for small S , as it is shown in Fig. 4.2 (a).

4.1.3 Interaction particle-environment

Once we have defined the two players of the system, the CTRW walker and the Ising environment, we consider a model in which the walk is affected by the environment in such a way that the disorder parameter κ of Eq. (4.1) is proportional to the size of the domain the particle is at a given time step. Namely, we consider that

$$\kappa = S^\eta. \quad (4.4)$$

An schematic representation of the walk is presented in Fig. 4.1(b). As shown, the particle moves for a number of steps in a domain of size S_1 . At each of these steps, its disorder parameter is equal to κ_1 , just until it traverses to a new domain of size S_2 in which it will change to κ_2 . We consider here that the direction at which the spins are pointing does not affect in any sort the diffusion of the particle. Moreover, we consider here that the Ising environment is at equilibrium,

which means that its dynamics are much slower than the ones of the particle. For simplicity, we will consider that the environment does not change at all during the walk of the particle. Nevertheless, we will assess the effect of the dynamics of the particles below.

The defined interaction makes it such that the motion of the particle is now closely related to its probability of finding a domain of size S in its step j , $P(s, j)$. This probability will again be closely related to the dynamics and time scales of both the particle and the environment. It is obviously also related to the distribution of domain sizes $P(S)$. Moreover, it will also depend on the previous history of the particle, i.e. $P(S, j | S', j - 1; S'', j - 2; \dots)$. The non-Markovian nature of this probability increases its complexity in such a way that no analytical solutions may be found for the motion of the particle. Nevertheless, there exists two limiting cases in which one may assume that the behaviour of the particle is Markovian: when its motion is either much faster or slower than the dynamics of the environment. We will deepen both cases in following sections.

4.1.4 Steps inside a domain

As commented previously, there exists two limiting regimes in which the description of the model is substantially simplified. We will focus now in the case in which the particle moves much faster than the evolution of Ising environment. Practically, this means that while moving, the particle does not perceive any change in the environment, hence we consider it to be static. In terms of the mathematical description given in the previous section, we consider here that the time τ in Eq. (4.1) is sufficiently smaller than the dynamical critical time ζ of the environment (see Sec. 4.3).

Even with the previous consideration, $P(S, j | S', j - 1; S'', j - 2; \dots)$ is still Markovian, as the probability of visiting a domain of given size at step j depends of the sizes of the domains already visited. Finding an analytical expression for such probability is not a trivial task, and may be indeed impossible. To solve such difficulty, we will tackle the problem in a different way: we will consider that when visiting a domain of size S , the particle performs n steps on it. Obviously, n will be a function of the size S but also of its shape and the entrance and exit point of the particle. Note here that we consider that the domain is not moving while the particle explores it, due to the difference in evolution scales. To avoid excessive complexity, we start by considering here the that average number of steps \bar{n} if a domain of size S is proportional to the one done in a domain of circular shape, i.e. $\bar{n} \propto S^{1/2}$.

To confirm the previous assessment, we perform a series of numerical simulations for a system of $L = 500$ at the critical temperature. First, we evolve 200 different realizations of an Ising environment, until reaching their equilibrium state. At this point, we extract all the domains formed and calculate what is the average number of steps a random walker may take to exit the domain, for various

random initial positions in the boundary. We see that the distribution of the number steps for any given S follows an exponential distribution, as shown in Fig. 4.2 (b). We then proceed to calculate the mean number of steps as a function of the domain size S and show this results in the inset of Fig. 4.2 (b). As it can be seen, expected behaviour departs from the simplified case in which we considered that the domains had circular shapes. Numerically, we perform a fitting to find that $\bar{n} \propto S^{0.3}$.

All the previous is correct for a static environment. In the cases in which the dynamics are not negligible, the relation between \bar{n} and S has to be reassessed. See that in the opposite limiting case, i.e. the evolution of the environment is much faster than the motion of the particle, in average only one step will be performed at each domain. This is so because the environment evolves so fast that at each new step of the particle it has effectively reset itself. See now that in any other scenario, the rates between the two dynamics (particle and environment) must be enclosed between these two limiting cases (the static and the resetting environments). We consider then that in its most general form, the mean number of steps can be rewritten as $\bar{n} \propto S^\mu$, with $0 \leq \mu \leq 0.3$, where now μ is a free parameter that accounts for the difference in the time scales between the particle and the environment.

4.2 CTRW in a critical Ising environment

We will begin our study of the model by assessing the case in which the Ising environment is close to criticality. As we will comment throughout this chapter, criticality only exists in Ising systems when they have infinite size. Away from this condition, finite size effects appear in the system, making such that its critical properties may even disappear. To address such problem, we consider in this section that the temperature of the system is close to T_c , but also that the Ising environment is infinite.

With the considerations presented in previous sections, we can now derive the probability $P_{new}(S)$ of entering a new domain of size S at every new step. This probability has to consider first the probability of that domain to exist, namely $P(S)$. Then, taking into account that our environment has a finite size, we need to account for the probability of being in such domain among all the available space. In our case, we consider a two-dimensional lattice of side length L , which means that the previous is just $\frac{S}{L^2}$. Finally, we need to account the mean number of steps performed in that domain $\bar{n} \propto S^\mu$. Putting everything together, we have

$$P_{new}(S) \propto P(S) \cdot \frac{S}{L^2} \cdot S^\mu \propto S^{-\zeta+\mu}, \quad (4.5)$$

where we have defined $\zeta = \tau - 1$. As the disorder parameter κ is directly related with S by means of Eq. (4.4), we can now use such relation to calculate the probability of the particle to draw a new value κ at a certain step as

$$P_{\text{new}}(\kappa) = P_{\text{new}}(S) \frac{dS}{d\kappa} \propto \kappa^{-\sigma(\mu)}, \quad (4.6)$$

where

$$\sigma(\mu) = \frac{\zeta - 1 - \mu}{\eta} + 1. \quad (4.7)$$

We see now two different regimes. In the case where $\mu < \zeta - 1$, the dynamics of the environment is very fast, as μ is close to zero. In such case, the particles sees a completely new environment at each step, meaning that it is able to explore conveniently the distribution $P(S) = S^{-\tau}$. In the opposite case in which $\mu \leq \zeta - 1$, the evolution of the environment becomes much slower and it is difficult for the particle to completely explore $P(S)$. Indeed one sees that in terms of the distribution P_{new} , the probability of sampling big κ 's increases exponentially in this case. In the same spirit, the probability of entering an infinite domain and remaining on it up to $t \rightarrow \infty$ increases substantially, again preventing the correct sampling from P_{new} . Moreover, see that P_{new} is no longer a normalizable probability. To solve this, one needs to introduce a cut-off to the domain size, which solves both problems: the diffusion in infinite domains and the normalization. Nevertheless, we will see that in terms of diffusion, the cut-off has a very similar effect as to the diffusion in an infinite domain. We will further discuss about this point in Section 4.3.

4.2.1 Diffusion of the particle

We will focus now in the case of a well defined P_{new} (i.e. $\mu < \zeta - 1$) and leave the discussion of the opposite case for Section 4.3. In such case, we can use Eq. (4.1) to calculate the effective waiting time distribution of the CTRW in the Ising environment by performing the convolution

$$\begin{aligned} \psi(t) &= \int_1^\infty P_{\text{new}}(\kappa) \phi_\kappa(t) d\kappa \\ &= \frac{1}{\tau} \left(\frac{t}{\tau} \right)^{-\sigma(\mu)} (\Gamma[\sigma(\mu)] - \Gamma[\sigma(\mu), t/\tau]), \end{aligned} \quad (4.8)$$

where τ represents a characteristic time scale and $\Gamma[\cdot]$ ($\Gamma[\cdot, \cdot]$) is the complete (upper incomplete) Gamma function. From here, one can use the usual CTRW theory we developed in Chapter 2 to calculate the mean squared displacement of the

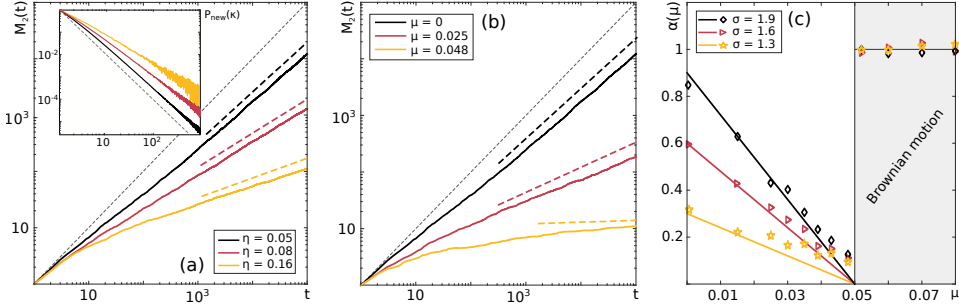


FIGURE 4.3: **Ensemble-averaged mean squared displacement at criticality.** (a) eMSD for different theoretical values of η and $\mu = 0$ for infinite size Ising environments at critical temperature. The movement is subdiffusive, that is $M_2(t) \propto t^\alpha$, with $0 \leq \alpha \leq 1$. Dashed black line represents the Brownian motion limit. Coloured dashed lines show the theoretical prediction of Eqs. (4.7) and (4.9) (same for (b)). Inset: The corresponding probability distribution function $P_{\text{new}}(\kappa)$ used for the simulations. (b) eMSD obtained for different values of μ and $\eta = 0.05$. The expected subdiffusive behaviour is observed. (c) Relation between the eMSD exponent $\alpha(\mu)$ and the time scale parameter μ . In this panel, symbols represent the numerical calculations while lines are theoretical predictions. We see that for $\mu > \zeta - 1 = 0.05$ normally diffusing Brownian motion occurs, i.e. $\alpha(\mu) = 1$.

particles (MSD) as

$$M_2(t) \approx \frac{1}{\Gamma(\sigma(\mu))} \left(\frac{t}{\tau} \right)^{\alpha(\mu)}, \quad (4.9)$$

with $\alpha(\mu) = \sigma(\mu) - 1$. This shows that the motion of the particle is closely related to the behaviour of the particle-environment interaction. More precisely it is linked to: the interplay between the time scales of the environment and the particle, by means of μ ; the distribution of domains, governed by ζ ; the relation between the domain size and the disorder parameter, given by η . The various parameters combine by means of Eq. 4.7. To our interest, there exists a regime in which $1 < \sigma(\mu) < 2$, which implies the anomalous diffusion of the particle.

4.2.2 Numerical implementation

In order to test the accuracy of the predicted anomalous exponent of Eq. (4.9), we perform a series of numerical simulations for the random walk of the particle. Strictly, we should simulate a random walk in lattice of spins with Ising dynamics and evolve the whole system by means of Monte Carlo methods. However, the computational cost of such simulation is extremely high, mostly due to the Ising lattice dynamics. Moreover, by simulating the Ising system we introduce the so-called finite size effects. As the simulation of an infinite system is impossible,

considering a computationally feasible introduces such effects on the system. To avoid such problem and to faithfully simulate the walk of the particle in an infinite Ising system, we propose an analogous implementation.

First, we will draw a value of S by means of the distribution $P_e(S) = (\zeta - 1)S^{-\zeta}$, which takes into account the probability of a domain of such size to exist and the probability of the particle to land on it. In order to sample from this distribution, we will use the inverse transform sampling distribution method. In such method, one considers the sampling of a random whose cumulative distribution function (CDF) is well described. In our case, we can calculate it directly from P_e as

$$\mathcal{C}_S(\bar{S}) = (\zeta - 1) \int_1^{\bar{S}} S^{-\zeta} dS = 1 - \bar{S}^{1-\zeta}. \quad (4.10)$$

Once defined the CDF, one needs to find its inverse, i.e. \mathcal{C}_S^{-1} . Defining U as a random number drawn from a uniform distribution $\in [0, 1]$, the method ensures that the numbers arising from $S = \mathcal{C}_S^{-1}(U)$ are distributed just as P_e . In our case, we have

$$S = (1 - U)^{1/(1-\zeta)} \quad (4.11)$$

After sampling the size of the domain currently visited by the particle, we calculate the corresponding value of κ by means of Eq. (4.4). The waiting times for the CTRW of the particle are then calculated with Eq. (4.1). As the walk takes place in a two dimensional lattice, four possible directions are possible for the particle at each step. For each, we calculate its expected waiting time

$$t_j = \frac{\ln(U)}{w_{ij}} \kappa, \quad (4.12)$$

where i is the actual site and j accounts for its four neighbours. The rate w_{ij} accounts for the probability of jumping to each of them. As we defined the random walk as unbiased, we will consider that $w_{ij} = w_i \forall j$. Then, the particle will jump to the neighbouring site with shortest waiting time.

Finally, following the rationale of Section 4.1.4, we consider that the particle performs $n = S^\mu$ steps inside each domain. Note that for each step, a new waiting time has to be retrieved from Eq. (4.1). After these n steps, the process starts again by calculating a new S by means of Eq. (4.11). From a collection of trajectories simulated with the previous recipe, we can now calculate the ensemble mean squared displacement (eMSD) and compare it to the value given by Eq. (4.9).

We show the results of such simulations in Fig. 4.3 for various scenarios. In Fig. 4.3(a) we show how the change of the exponent η , i.e. the one mediating the relation between the waiting times and the size of the domains, affects the diffusion. We consider here a fixed $\mu = 0$. First, in the inset, we see the distribution of κ extracted for each simulation. According to the theory a distribution $P(\kappa) \propto \kappa^{-\sigma}$ causes the appearance of subdiffusion with anomalous exponent $\alpha = \sigma - 1$.

Moreover, the bigger the effect of the size on the waiting times (i.e. the bigger η), the more subdiffusive the motion of the particle is. We see such effect in the main figure, where the exponent for each eMSD can be calculated analytically (dashed lines) for each η .

In similar fashion, we explore in Fig. 4.3(b) the effect of the environment evolution to the diffusion of the particle with a fixed $\eta = 0.05$. Recall that the smaller μ , the faster the evolution of the Ising system, causing the diffusion of the particle to be normal. This is due to the resetting of the environment: in a static environment, the particle has a high probability of entering a big domain and staying there for many of steps. Because of the size, the waiting times of such steps are longer than the ones expected for small domains. Hence, the particles moves much slower, effect seen in the decrease of the anomalous exponent as we increase μ and get closer to the static environment.

Finally, in Fig. 4.3(c) we summarize the previous results. We show there the same effect of the previous figure: the slower the evolution of the environment, the more subdiffusive the motion of the particle. This holds until we reach the point $\mu = \zeta - 1$ at which the particle recovers Brownian motion. As commented, this happens because the distribution $P_{\text{new}}(\kappa)$ is no longer normalizable. A cut-off must be introduced in order to work with correctly behaving PDFs. As we will see with more details in following sections, such cut-off causes the departure from anomalous diffusion. The different markers show the fitted anomalous exponent of the simulations, while the bold lines represent the predicted behaviour by Eq. (4.9).

4.2.3 Critical slowing down of the Ising model

An important feature arising in critical systems, as the one considered in this section, is the exponential slowing down of its evolution. In the case of the Ising model, it is known that the time correlation of a spin s_i is given by

$$\langle s_i(t) s_i(0) \rangle \propto \exp[-t/\zeta], \quad (4.13)$$

where ζ is the dynamical critical time, which diverges at the critical temperature. It is then through the comparison between ζ and τ from Eq. (4.1) that one can relate the dynamics of the environment and the particle. As commented previously, two regimes arise. When $\zeta \ll \tau$, the evolution of the environment is much faster than the one of the particle. This limit corresponds to $\mu = 0$ and showcases the case in which the environment is effectively reset at each of the particle's step. Thus, the subsequent visited domains are uncorrelated. The opposite case, in which $\zeta \gg \tau$ (corresponding now to $\mu = 0.3$), the environment is effectively static with respect to the motion of the particle.

To understand the critical slowing down, it is useful to use the dynamical critical scaling hypothesis [99, 100], which states that the dynamical critical exponent

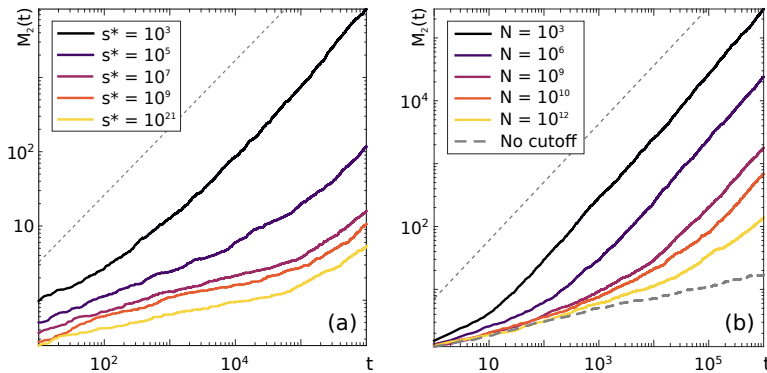


FIGURE 4.4: **Ensemble-averaged mean squared displacement out of criticality.** (a) eMSD for $\alpha = 0.05$ and different deviations from the critical temperature, described by the typical size S^* . A transient subdiffusive behaviour occurs for intermediate times. As S^* is increased, the onset of diffusive dynamics occurs at a longer time. (b) eMSD for $\alpha = 0.2$ and different values of the size N of the Ising environment at critical temperature. As shown the movement is diffusive in the long term behaviour. In intermediate times, the finite size cases show the same subdiffusive behaviour than the infinite size case (bottom curve). The position at which it departs from subdiffusion is larger as the size is increased. Dashed lines show the Brownian motion limit.

ζ is given by

$$\zeta \propto \xi^z, \quad (4.14)$$

with z being the dynamical critical exponent. The calculation of the dynamical exponent is in itself a huge challenge. Indeed, various numerical approaches have found that $z = 2.167$ [101, 102]. Nevertheless, the problem is widely connected to the correct simulation of the Ising model for very long times. Usually, such simulations are performed by Monte Carlo and need the use a large number of random numbers. Hence, the quality of such random numbers, namely them being uncorrelated, is key for the correct estimation of ζ . To this aim, quantum random number generators (QRNG) have been proposed [103]. Due to the true randomness of such generator, certified by the use of quantum systems, the numbers will be completely uncorrelated, leading to much better Ising simulations and thus to a better numerical estimation of ζ .

In Eq. (4.14) we see the appearance of the correlation length ζ , defined as $\zeta = |T - T_{\text{crit}}|^{-1}$. See that at $T = T_{\text{crit}}$, the correlation length diverges, and so does ζ . This implies that in the scenario of a real infinite, critical Ising model, one can never find a time scale $\tau > \zeta$, hence we must always have $\mu \neq 0$. Nevertheless, in practical terms we will always work for system which, even if close to criticality, depart from it either by the finite size effect or by fluctuations in the temperature

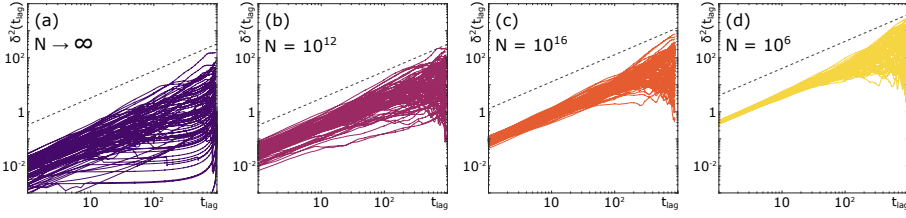


FIGURE 4.5: **(a)** Time-averaged mean squared displacement for $\alpha = 0.4$ in the infinite size Ising environment. As shown, the tMSD remains a random variable in time, as seen by the large scattering observed at all time lags. **(b)-(d)** Same calculation but in the presence of a maximum size $N = L^2 = 10^{16}, 10^{12}$ and 10^6 , respectively.

of the system.

4.3 Finite size Ising environment and deviations from the critical temperature

We will study now the effect of the depart from criticality on the diffusion of the particle. As commented previously, there are two ways a system becomes non-critical: first, if its temperature is $T \neq T_c$ and second, if the system is not infinite. Of interest to us, in both scenarios the dynamical critical time no longer diverges. In the case of non-critical temperatures, the correlation length no longer diverges. We have then $\zeta \propto L^z$. In the case of finite system, the correlation length is finite too hence preventing too ζ to diverge. See for instance that for certain values of the time scale τ is now possible to recover $\mu = 0$. For a finite system this happens when $\tau \gg L^z$ while for non-critical temperature we must have $\tau \gg \zeta^z$.

In terms of the distribution of domain sizes, see that in Eq. 4.3 we have now the appearance of an exponential cut-off. Away from criticality, the probability of finding an infinite domain reduces exponentially. Thus, there exists a characteristic size S^* above which it is exponentially rare to find domains. In the case of a finite system, it is clear that the biggest domain must have size $S \leq N$. For non-critical temperatures, we will consider S^* to be the biggest possible domain. We consider then that below such values, the distribution of domain sizes still follow $\propto S^{-\tau}$ while the probability of $S > S^*$ is set to zero.

This effect translate to the disorder parameter too, for which the PDF of Eq. (4.6) is now transformed to

$$P(\kappa) = \begin{cases} \propto \kappa^{-\sigma(\mu)} & \text{if } \kappa < \bar{\kappa} \\ 0 & \text{if } \kappa > \bar{\kappa}, \end{cases} \quad (4.15)$$

Note that this solution also holds for the case $\mu \geq \zeta - 1$, where the probability distribution $P_{\text{new}}(\kappa)$ could be normalizable without the introduction of an exponential cut-off (see Section 4.2.1). Following Eq. (4.15), the integral in Eq. (4.8) can be written as

$$\begin{aligned} \psi(t) &= \int_1^{\bar{\kappa}} P_{\kappa}(\kappa) \psi_{\kappa}(t) d\kappa \\ &= \frac{1}{\tau} \left(\frac{t}{\tau}\right)^{-\sigma} \left[\Gamma\left(\sigma, \frac{t}{\bar{\kappa}\tau}\right) - \Gamma\left(\sigma, \frac{t}{\tau}\right) \right]. \end{aligned} \quad (4.16)$$

We can notice that since $\Gamma[\sigma, 0] = \Gamma[\sigma]$, Eq. (4.16) converges to Eq. (4.8) for $\bar{\kappa} \rightarrow \infty$. On the basis of the timescales involved, we can identify two temporal regimes: (I) $\tau \ll t \ll \bar{\kappa}\tau$, and (II) $t > \bar{\kappa}\tau$. In the first regime, the times are very large but still smaller than the cut-off in κ . In this limit, $\Gamma\left(\sigma, \frac{t}{\bar{\kappa}\tau}\right)$ tends exponentially to zero and we can neglect its contribution. Contrarily, we can consider that $\Gamma\left[\sigma, \frac{t}{\bar{\kappa}\tau}\right] = \Gamma[\sigma, 0] = \Gamma[\sigma]$. Therefore, the eMSD will behave as in Eq. (4.9). In regime (II), that is, when time is larger than all the timescales τ and $\bar{\kappa}$, we expect that both Gamma functions tend exponentially to zero, thus giving normal diffusion at long times.

In Fig. 4.4(a) we show the numerically calculated eMSD for different values of S^* , when $\alpha = 0.05$. For finite values of S^* , a subdiffusive plateau occurs at intermediate times. As S^* is increased, thus getting closer to the critical temperature, one gets a larger subdiffusive plateau. In Fig. 4.4(b) we show the eMSD for the infinite and different finite size Ising environments. The time, at which the eMSD departs from the slope corresponding to the infinite size environment and tends to slope equal to one, is shorter as the lattice size decreases.

4.4 Ergodicity breaking

We will investigate now the presence of weak ergodicity breaking (WEB) in the model. For that, we will use the theory developed in Section 2.2.4. Recall for instance that WEB could be quantified by means of the Ergodicity breaking parameter EB, defined as

$$\text{EB} = \lim_{t \rightarrow \infty} \frac{\langle (\overline{\delta^2})^2 \rangle - \overline{\delta^2}^2}{\langle \delta^2 \rangle^2}. \quad (4.17)$$

We showed how normal diffusion processes showed $\text{EB} \rightarrow \infty$, while the value increase with the presence of non-ergodicity. Moreover, for a CTRW with heavy-tailed waiting-time PDF (as in Eq. (4.8)), we showed that the EB parameter fulfils

$$\text{EB} = \frac{2\Gamma^2[\sigma]}{\Gamma[2\sigma - 1]} - 1. \quad (4.18)$$

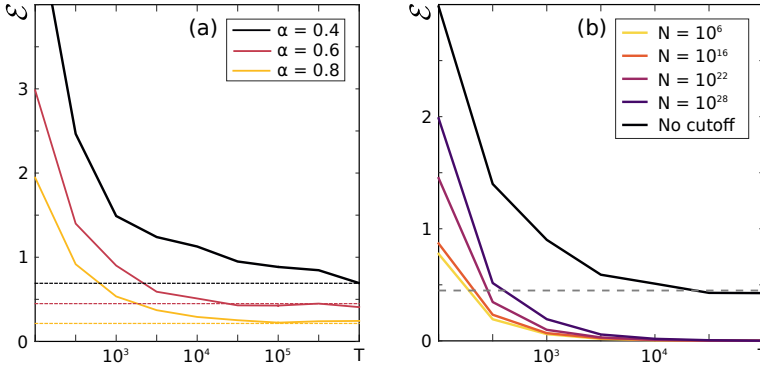


FIGURE 4.6: **(a)** Ergodicity breaking parameter for different values of α in the infinite size environment case. This parameter tends asymptotically to the value predicted by Eq. (4.18) [we indicate the asymptotic value of the ergodicity breaking parameter, $\bar{\mathcal{E}}$, for each α with horizontal lines]. **(b)** Ergodicity breaking parameter for $\alpha = 0.4$ both for the infinite and finite size environment cases. For all finite cases the curves tend to zero asymptotically for the maximum measurement time taken here, $t = 10^6$. This means that the behaviour is ergodic at long times for finite size if the measurement time is large enough. The time at which it reaches the zero value is larger as the size of the environment is increased.

Therefore, we used our simulations to determine the tMSD for several particles and thus verify the occurrence of ergodicity breaking in our model. In the fast environment limit at criticality and infinite size system, as shown in Fig. 4.5 (a), we found that the tMSD exhibits linear behaviour at short time lags. Moreover, tMSD curves corresponding to different trajectories are largely scattered, as expected for non-ergodic dynamics. This observation is quantitatively reflected in the value of the EB parameter measured at long times [see Fig. 4.6(a)], which moreover tends to the corresponding non-zero values given by Eq. (4.18) (dashed lines), thus in full agreement with the theoretical prediction. The EB parameter gives also a good tool to study deviations from criticality studied in the previous sections. We see in fact that as the particle departs away from the subdiffusive behaviour due to finite size and off-criticality effects, the ergodicity of the system increases. We plot in Fig. 4.5(b)-(d) the tMSD for $\alpha = 0.4$ and different maximum size, and we compare it with the infinite size Ising environment Fig. 4.5(a). The plots show the dispersion is decreased as the size of the lattice is reduced. Also, the $\bar{\mathcal{E}}$ reached asymptotically for all finite size cases is zero, while the time at which this value is reached is longer as the environment is made larger [see Fig. 4.6(b)]. Thus, for all finite size environments, no ergodicity breaking is predicted asymptotically.

4.5 Conclusions

In this chapter, we have introduced a model in which a particle performs a continuous time random walk in a regular lattice, at which vertices are spins. These are governed by Ising dynamics, i.e. a Hamiltonian evolution given by Eq. (4.2). Close to the critical temperature, domains of spins are created, their sizes distributed as a power law. In his walk, the particle is affected by such domains, in such a way that its diffusion coefficient is proportional to the domain size, up to a certain exponent. These heterogeneities make it such that the diffusion of the particle is anomalous in some regimes.

More precisely, we have shown that in the case of a critical environment, i.e. when the system is at critical temperature and its size is infinite, the exponent of power law behaviour of the domain size distribution can be directly linked to the scaling of the diffusion of the particle. We have studied the system in two extreme scenarios: when the dynamics of the particles is much faster than the evolution of the spin system, and the opposite case. This contributes heavily on the diffusion of the particle, as the slower the evolution of the system, the more anomalous the diffusion. This is true until a certain threshold, at which the waiting time distribution of the particle is no longer normalizable without the introduction of an exponential cut-off and its diffusion becomes normal.

We have also studied how the departure from criticality affects the diffusion. Non critical systems arise in two scenarios: either when the system is no longer at critical temperature or when its size is finite. Both cases, while intrinsically different, have a similar effect on the system. Effectively, we saw that both could be described by the introduction of an exponential cut-off in the domain size distribution. This makes such that the particle shows transient subdiffusion only for a short period, while in the long time limit it diffuses normally.

Finally, we have studied the emergence of weak ergodicity breaking in the particle's diffusion. We have seen that, analogous to the existing CTRW theory, the particle has a non-zero ergodicity breaking parameter for any case in which subdiffusion was emerging in the eMSD. In general, we have seen that even if the initial walk of the particle was defined as a normal diffusion CTRW with exponential waiting times, the presence of disorder in the system can cause the appearance of anomalous diffusion and ergodicity breaking.

5 Anomalous diffusion through porous compartments

In Chapter 4, we presented a model where a particle was diffusing through an environment made of domains and whose diffusion coefficient was related to the size of each domain. However, the exact rationale for the latter was never addressed, as it was presented as a phenomenological phenomena appearing in a variety of systems. In this chapter, we will present a model, very similar to the previous, in which now the size of the domains directly affects the diffusion of a particle, without the need of an ad hoc definition. We consider here a particle performing an unbiased random walk through a network of compartments separated by porous barriers. As the particle reaches one of these boundaries, it transmits or reflects with complementary probabilities. While the diffusion of the particle is normal inside the compartments, the presence of barriers with heterogeneous transmittances makes it such that the long time diffusion of the particle is indeed anomalous. We will show how the distribution of sizes of the compartments and the distribution of their boundaries transmittances affect the diffusion of the particle.

Due to the complexity of the interaction between the particles and the boundaries, the study is usually impossible by means of analytical methods. We will introduce in this chapter a novel coarse-grain approach which maps the behaviour of the particle to a space-time coupled random walk, in which successive step lengths are connected to the time taken to perform them.

5.1 Microscopical model for a compartmentalized environment

We consider here an environment made of N compartments with various sizes $\{L_i\}_{i=1}^N$, with $N \gg 1$ and $L_i \in [1, \infty)$. In general, we will consider that these sizes are drawn from a probability distribution function $g(L)$. The compartments form a meshwork with high connectivity, which means that each of them is connected with a big number of the others. In such case, a particle moving through the meshwork has a very small probability of revisiting a given compartment. Their

boundary is considered as partially reflective: a particle reaching the boundary has non-zero probability of traversing the boundary and exiting the compartment. Similarly, there is a complementary probability that the particle gets reflected back to the same compartment. The transmittance probability of each of the N compartment is an stochastic variable drawn from the set $\{T_i\}_{i=1}^N$, $T_i \in (0, 1]$. The reflectance is then defined as $R = T - 1$. Similar to the compartment size, we consider the transmittances to be drawn from a probability distribution function $q(T)$.

In the proposed scheme, the compartments can take any form in any dimension as our coarse-grain method can be adapted to deal with such situations. Nevertheless, to showcase the validity of the method and for the sake of simplicity, we will consider that the compartments are one-dimensional. This does not mean that the meshwork needs to be too a one dimensional body. One can imagine for example the case of a tubular system where different *quasi* one dimensional tubes are connected with arbitrary angles between each other.

Given this environment, we introduce now a particle which performs an unbiased random walk inside the compartments. Due to the partially reflective nature of the system, the particle is confined in a compartment until it is able to transmit to one of the colliding ones. The time the particle takes to exit a compartment is then a function of its size L and boundary transmittance T . An schematic representation of the system is presented in Fig. 5.1.

5.2 Mesoscopic description of the system

The diffusion through a compartmentalized environment has been widely studied, as it is usual to find such biological environments such as the motion through cell membranes[104, 105]. However, from a theoretical point of view, it has always been difficult to analytically characterize these systems due to their complexity. Examples of such approaches consider the motion of the particle to be the solution of a Langevin equation with various boundary conditions (e.g. Dirichlet, Neumann, ...). In general, one considers the presence of the boundaries as an obstacle in the path of the particle and studies their microscopical interaction. However, the stochastic behaviour in the compartment sizes and boundaries transmittances increases the complexity of the system in such a way that valid analytical solutions are very hardly attainable.

To face such difficulty, we propose a coarse-grain description of the system. In our approach, the system of compartments is transformed to an irregular lattice in which the vertex correspond to the boundaries of the compartments. While in previous descriptions, defined in the *microscopic* scale, the position of the particle was tracked at regular times $\ll L^2/D$ with D being the diffusivity of the particle, in the new *mesoscopic* approach the particle is tracked only when crossing the boundary of the compartments. Note that by construction, the asymptotic behaviour of

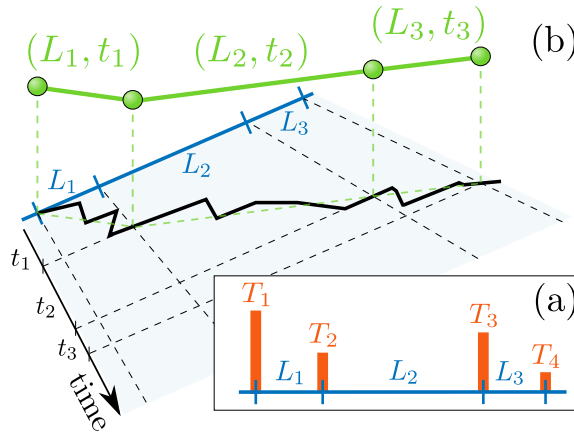


FIGURE 5.1: **Schematic of the system.** (a) Example of a one dimensional compartmentalized environment, with compartment size L and boundary transmittance T . Higher boundaries represent lower transmittance. For simplicity we plot the meshwork as formed by the segments of a line. (b) Motion of the particle in such environment. The dark line represents the microscale description of the motion and the green one indicates its mesoscale description, in this case a Lévy walk with steps given by their length and flight time (L, t) .

the particle is equal in both approaches. Hence, the mesoscopic approach consists in a simplified solution of the system valid in the long time limit.

In terms of the motion of the particle, the initial random walk defined in Section 5.1, taking place in a regular lattice, has now been transformed in a random walk in an irregular lattice. Moreover, while the flight times, i.e. the time taken to make a step, were considered regular in the initial formulation of the problem, in the coarse-grain approach such times are related to the exit time of the a given compartment. The walk is then completely defined by the set of step lengths L_i (i.e. the set of compartment size), and the set of exit times t_i , a function of both the size of compartments L_i and boundary transmittance T_i .

The initial problem has then been transformed into a coupled space-time continuous random walk: a walk in which the flight times and step lengths are coupled, just as the ones described in Section 2.3.1. In our case, the time of a step is given by the conditional probability of the particle to stay a time t in a compartment of size L and transmittance T , $\phi(t|T, L)$. From here, we can write the joint probability for the particle to be in a compartment of length L and boundary transmittance T for a time t as

$$\psi(t, L, T) = \phi(t|T, L)g(L)q(T). \quad (5.1)$$

While the previous probability describes entirely the behaviour of the particle inside the compartments, an important consideration has to be taken into account while defining the mesoscopic approach. When a particle enters a compartment, it can exit it from one of the two boundaries: the one through which it entered and the opposite one. Considering that the position of the particle is only tracked at the crossing of the boundary, these two lead to a very different result in the mesoscale. In the former, the particle is seen while entering and exiting the compartment in the exact same boundary and thus not having moved at all. In terms of the couple space-time CTRW, we will consider this feature as the rest of the particle. When exiting from the opposite boundary, the particle is seen as having moved a step of length equal to the size of the compartment. To summarize, when entering a compartment, the particle has a probability of resting $\varphi_r(L, T)$ and a complementary probability of performing a step $\varphi_w(L, T)$.

With the previous, we have transformed the initially complex motion of the particle through the meshwork of compartments into a much simpler system. Merging all previous considerations, the walk now takes the form of a Lévy Walk with rests [106, 107] in which the joint probability of Eq. (5.1) can be considered the propagator of the walk, as L is now transformed into the step length x at certain time t , given a boundary transmittance T .

5.3 Mesoscopic motion as a Lévy walk

As explained in Chapter 2, Lévy walks are one of the most studied diffusion models, due to their success at describing many physical scenarios. Moreover, their framework accommodates very different behaviour, from subdiffusion to superdiffusion. As commented, the model presented in Section 5.1, transformed with the method of Section 5.2 gives rise to a Lévy Walk with rests. Usually, such walks were defined either with equal walking and resting probabilities or by considering that the walker alternates between rests and steps. In our case such probabilities are indeed a function of the parameters of the system. In the general Lévy Walk framework introduced in Ref. [108], one starts by considering two populations: the population of particles at rest and the population of particles *flying* (or walking). The system is then governed by the probability density functions (PDF) of finding a resting or flying particle at position x at time t . To define them, we need first to consider the walk ($\psi_w(t)$) and rest ($\psi_r(t)$) times distribution, i.e. the time it takes for a particle to make a step and the time it rests in a given position. Their form is analogous

$$\psi_{w(r)}(t) = \int_1^\infty dL \int_0^1 \varphi_{w(r)}(L, t) \psi(t, L, T) dT. \quad (5.2)$$

Note that, from its definition, $\psi_r + \psi_w = 1$.

Another important feature in this framework is the flux of particles finishing their rest and starting to move from point x at time t . In our case, we will add to such flux the fact that the particle is in a compartment of transmittance T . The flux can be then defined via the self consistent equation

$$v(x, t)_T = \int_{-\infty}^{\infty} \int_0^t \psi_r(\tau) \int_0^{t-\tau} \psi(\tau', y, T) v(x - y, t - \tau - \tau')_T d\tau' d\tau dy \quad (5.3)$$

$$+ \psi_r(t) P_0(x). \quad (5.4)$$

From the previous, we can define the PDFs of the resting and walking particles as

$$P_r(x, t)_T = \int_0^t \Psi_r(\tau) \int_0^{t-\tau} \psi(\tau', y, T) v(x - y, t - \tau - \tau') d\tau' d\tau dy + \Psi_r(t) P_0(x) \quad (5.5)$$

and

$$P_w(x, t)_T = \int_0^t \Psi(\tau, y, T) v(x - y, t - \tau) d\tau, \quad (5.6)$$

where $\Psi_r(t) = \int_t^{\infty} \psi_r(t') dt'$ is defined as the survival probability, i.e. the probability of a particle not walking until time t and $\Psi(x, t, T) = \int_t^{\infty} \psi(x, t', T) dt'$ is the PDF of the displacement of the walker during the last uncompleted step. Note that the total PDF of the walk fulfils $P_{\Sigma} = P_r + P_{\text{fly}}$. In our case, we have that

$$P_{\Sigma}(x, t) = \int_0^1 P_{\Sigma, T}(t, x, T) dT. \quad (5.7)$$

By means of a Fourier-Laplace transform, we can calculate the total PDF of the particle as

$$P_{\Sigma, T}(k, s, T) = \frac{\Psi_r(s) P_0(k) + \{\varphi_w(x, T) \Psi(x, s, T)\}_k \psi_r(s) P_0(k)}{1 - \{\varphi_r(x, T) \psi(x, s, T)\}_k \psi_r(s)}, \quad (5.8)$$

where we defined $\{f(x)\}_k$ as the Fourier transform of $f(x)$. If one considers the case of equal resting and walking probabilities, i.e. $\varphi_w = \varphi_r = 1/2$, the general Lévy walk with rests of Ref. [108] is recovered.

5.3.1 The osmotic approach

In general, the calculation of $P_{\Sigma, T}(k, s, T)$ is subordinated to finding an expression for $\varphi_w(L, T)$. The later is a challenging task and will depend heavily on the shape of the compartment [109]. Even in the simplified one dimensional example, finding such expression is not easily attainable. Nevertheless, there exists concrete

examples in which an analytical solution can be found. For instance, in the limiting case in which the boundaries are completely transmitting, i.e. $T = 1$, one finds that

$$\varphi_w(L, T = 1) = \varphi_w(L) = 1 - \frac{L}{L+1} \sim L^{-1}, \quad (5.9)$$

which implies that, the longer the compartment, the lower the probability of exiting it from the opposite side the particle has entered (and analogously, the lower the probability of making a step in the mesoscopic model).

Aside from such extreme cases, the difficulty of finding $\varphi_w(L, T)$ remains. A usual approach to such problems is to consider an annealed system [110], i.e. to assume that the particle enters each new compartment at its center. Effectively, this erases completely the rests from the walk, as the particle will always travel a distance $L_i/2$ before exiting a compartment of size L_i . Hence, we now have that $\varphi_w(L, T) = 1 \forall L, T$ and the walk is transformed into a Lévy walk with flying times depending on the jump length [111].

Physically, the previous assumption is motivated by the presence of osmotic boundaries. These have the property of only allowing the particles to cross the boundary in one direction. We will refer to this specific example as the *osmotic* approach while the general case will be referred as the *non-osmotic* approach. See that in the former, the particles will always travel a distance L_i before escaping the i -th compartment. With this consideration and eliminating the effect of the rests, Eq. (5.8) can be largely simplified to find

$$P_{\Sigma}^{(\text{OA})} = \frac{\Psi(k, s)}{1 - \psi(k, s)}, \quad (5.10)$$

The motion of the particle can then be characterized by means of the mean squared displacement (MSD), which takes the form of $\langle x^2(t) \rangle = -P''(k, s)|_{k=0}$. Using the framework introduced in Ref. [74], the MSD can be rewritten as

$$\langle x^2(s) \rangle = \int_0^1 dT \left[\frac{-\psi''(k, s, T)|_{k=0}}{s[1 - \psi_w(s)]} + \frac{-\Psi''(k, s, T)|_{k=0}}{1 - \psi_w(s)} \right]. \quad (5.11)$$

Throughout the following sections we will use the previous equation to solve the motion of the particle. While the osmotic approach may seem at first glance an important change in the statistics of the particles with respect to the general case, we will show that, in the long time limit, both present a similar behaviour in terms of the MSD. Thus, if the opposite is not stated, the osmotic case will be the one considered for the rest of the Chapter.

5.4 Diffusion of a Brownian particle in compartmentalized environments

In this section we will use the method proposed in previous sections to characterize the motion of the particle in various scenarios. We will differentiate three cases: first, the boundary transmittances will be stochastically drawn from a certain PDF while the compartment lengths are equal; second, we will comment on the paradigmatic case of constant and equal boundary transmittances with stochastic compartment length; third, we will consider the most general case in which both the transmittances and lengths are drawn from their respective PDFs. By means of numerical simulations of the microscopic walk of the particle, we will show that the mesoscopic approach presented is indeed the suitable approach to solve the walk of the particle in such systems.

Common to all cases is the conditional probability, which relates the exit times of a compartment of size L and the transmittance T . Note that in the osmotic approach, the particle has to travel a distance L to exit a compartment. Considering that the particle is performing an unbiased random walk, it will take in average L^2 steps to exit such compartment. In terms of the transmittance, it is clear that the smaller it is, the longer the particle will take to exit the cluster. Numerically, we find that the average time taken to exit a compartment is $\langle t \rangle \propto (L/T)^2$. Moreover, in the limit of large L and small T , we see that the distribution of exit times follows an exponential, i.e. $\phi(t|T, L) \propto \exp -tL^2/T^2$. However, in other regimes we see a departure from such behaviour. Nevertheless, the quadratic relation of the average time and L/T is always maintained. Therefore, we consider here the simplest form for ϕ whose average is in accordance with such statement. Namely, we consider

$$\phi(t|T, L) \sim \delta(t - (L/T)^2). \quad (5.12)$$

While there has been numerous attempts to find an exact form of the previous distribution (see for instance Refs. [112, 113]), such solutions are always very involved and not suitable for the analytical study we are proceeding with in this chapter. Nevertheless, we will show by means of various numerical simulations that even the simple function Eq. (5.12) is able to capture the behaviour of the system and leads to satisfactory results in the long time limit regime.

5.4.1 Constant transmittance and stochastic length

We will start by considering the case of a constant distribution of transmittances, i.e. $q(T) = \delta(T - \bar{T})$, with $\bar{T} \in (0, 1]$, while the compartment length are drawn from the power law distribution

$$g(L) = \beta L^{-1-\beta}. \quad (5.13)$$

From here one can calculate the flight times by performing the convolution of Eq. (5.1) over the previous PDF to find

$$\psi_L(t) = \int_1^\infty \phi(t|L, \bar{T})g(L)dL \propto t^{-1-\beta/2}. \quad (5.14)$$

The joint distribution from Eq. (5.1) is in this case given by

$$\psi(t, T, L) \sim \delta(t - (L/T)^2)\delta(T - \bar{T})\beta L^{-1-\beta}. \quad (5.15)$$

Inserting the previous two results in Eq. (5.11) we find that $\langle x^2(t) \rangle \sim t \forall T$, i.e. the particle performs normal diffusion. This shows how the absence of disorder in the boundary transmittance, while being at distributed randomly over the system, makes it such that the original Brownian diffusion of the particle is not perturbed. It has to be noted that such results hold for all cases but $T = 0$, for which it was demonstrated in Ref. [114] that anomalous diffusion occurs. While one may expect that fully reflecting boundaries may lead to confinement and thus an anomalous exponent equal to zero, it was indeed demonstrated that the exponent is closely connected to the distribution of compartment sizes. For $T > 0$, it may be argued that there exist some pathological cases in which the particle may be confined for an infinite time in a certain compartment, hence erasing the anomalous diffusion behaviour. The previous statement can be compared to the one made in CTRW, where the absence of infinite trapping times leads to normal diffusion.

5.4.2 Stochastic transmittance and constant length

We consider now the opposite case, in which the compartments have constant length, i.e. $g(L) = \delta(L - \bar{L})$, while the boundary transmittance have a power distribution, given in this case by

$$q(T) = \alpha \left(\frac{1}{T} \right)^{1-\alpha}. \quad (5.16)$$

We will refer to this as the spatially ordered case. See that being the compartments all of equal size, the steps in the mesoscale are too of equal length. This makes it such that the walk is transformed into a CTRW, where the waiting times correspond to the exit times. The distribution of waiting times is then just given by

$$\psi(t) = \psi_w(t) = \int_0^1 \phi(t|\bar{L}, T)q(T)dT \propto t^{-1-\alpha/2}. \quad (5.17)$$

As described extensively in previous chapters, once we have the waiting time distribution of a CTRW, it is straightforward to calculate the MSD. For the case of

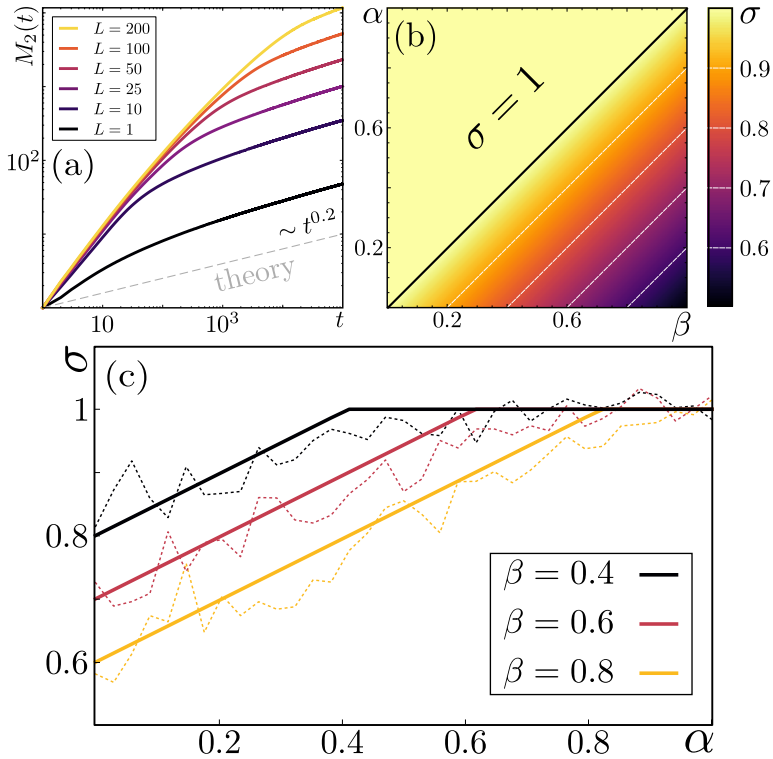


FIGURE 5.2: (a) MSD of a particle moving in a system of compartments of equal length and boundary transmittances distributed following (5.16), with $\alpha = 0.2$. All curves are calculated for the microscale and tend to the predicted subdiffusive motion given by (5.18). A larger L leads to a larger time for the onset of subdiffusion to occur. The dashed bottom line corresponds to the mesoscale and coincides with the theoretical prediction. (b) Value of the exponent of the MSD in a system with stochastic compartment sizes and boundary transmittance, given by (5.20). (c) Comparison between the predicted results of the previous case and numerical simulations of the microscopic walk (dashed lines).

study, we find that

$$\langle x^2(t) \rangle^{(\text{SO})} \xrightarrow{t \rightarrow \infty} t^{\alpha/2}. \quad (5.18)$$

The particle will then show subdiffusion for $0 < \alpha < 2$. This means that the presence of disorder in the system, in this case brought up by the distribution of T , Eq. (5.16), induces a change from the original Brownian behaviour of the particle towards subdiffusion. This is consonant to what we have seen in previous chapters: any interaction between the particle and the environment inducing a power

law behaviour to the waiting times distribution of a CTRW will lead to anomalous diffusion. In order to prove such statement, which has obviously being done by means of the mesoscopic method and in the osmotic approach, we simulate the microscopic behaviour of the particle for various sizes \bar{L} and $\alpha = 0.4$. We show the results in Figure 5.2(a). As seen, the long time behaviour is independent of the length of the compartments. However, the bigger they are, the longer it takes for the particle to attain the expected value. This effect happens because in bigger compartments, the particle takes longer to reach the boundary and thus to effectively sample the distribution $q(T)$.

5.4.3 Stochastic transmittance and length

Lastly, we consider the case in which both the boundary transmittances and the compartments length are stochastic, given by $g(L)$ and $q(T)$ and defined in Eqs. (5.13) and (5.16), respectively. The walk is in this case truly a Lévy Walk, as now the step lengths in the mesoscale, analogous to the compartments length, vary following $g(L)$. Opposed to the previous case, we refer to this as the spatially ordered case. In a similar fashion, we can then calculate the flight times by performing the convolution of the walk's propagator $\psi(t, L, T)$ with Eqs. (5.13) and (5.16) as

$$\psi_w(t) = \int_0^1 dT \int_1^\infty dL \phi(t|L, T) g(L) q(T) = \alpha t^{-1-\gamma}, \quad \text{with } \gamma = \begin{cases} \alpha & \text{if } \beta > \alpha, \\ \beta & \text{if } \beta < \alpha. \end{cases} \quad (5.19)$$

Using these results and the Laplace transform of Eq. (5.1), we can calculate the MSD by means of Eq. (5.11). Performing the inverse Laplace transform we find that

$$\langle x^2(t) \rangle^{(\text{SD})} \xrightarrow{t \rightarrow \infty} t^{\frac{1}{2}(2-\beta+\gamma)}. \quad (5.20)$$

As in previous cases, we see that there exists a regime in which the disorder, now present both spatially and in the boundary transmittances, makes the particle to switch from normal to anomalous diffusion. We show for instance in Fig. 5.2(b) the value of the anomalous exponent for the range of α and β allowed (i.e. the for which Eqs. (5.13) and (5.16) are normalizable). We see there two very distinct regimes. When $\alpha > \beta$, the motion of the particle is still normal. This means that the presence of spatial disorder is able to compensate the disorder introduced by the boundaries, in such a way that for values where the spatially ordered case was subdiffusive, it is now normal diffusing. For values of $\alpha < \beta$, the anomalous exponent behaves linearly with respect to each variable, until reaching the limiting value $\sigma = 1$. To check whether the successive approximations done in the mesoscopic scale are valid for the description of the microscopic walk, we fit the

exponent of multiple simulations of such walk. We plot the results as dashed line in Fig. 5.2(c), while the bold lines represent the values predicted by Eq.(5.20).

5.5 Conclusions

In this chapter, we have introduced a coarse-graining method that we use to study diffusion through complex environments. This method is useful to study systems in which the microscopic behaviour of the particles is too involved to be described analytically. To obtain a description of the motion in such cases, we propose a procedure that allows one to transform the microscopic walk into well-known theoretical models, such as Lévy Walks or continuous time random walks. The coarse-grained transformation maps the original walk performed at the microscale into a simplified movement at a larger scale (which we term mesoscale) that captures the relevant properties of the environment. This allows for a complete analytical characterization of the diffusion in terms of its observables, such as the mean square displacement.

To illustrate the use of the proposed method, we consider the diffusion in an environment consisting of compartments with random sizes and/or transmittances. To resolve the diffusion of the system at the microscale, one needs to consider the complex interaction of the particle with the boundary of each compartment. For some simple systems, e.g. when all the compartments have the same size, it is possible to get an analytical solution of the microscale motion. In these cases, we show that a heavy-tailed distribution of boundary transmittances is a necessary requirement to induce subdiffusion. However, for more intricate spatially-disordered environments, it is often difficult to obtain an analytical solution at the microscale. This is the scenario where our method allows to get insights on the motion while neglecting microscopic details. As an example, we demonstrate that when the compartments length is a stochastic variable, geometric disorder alone cannot generate subdiffusion. However, it can affect the one generated by the heterogeneity in the boundary transmittance. Namely, increasing the geometric disorder reduces the degree of subdiffusion, as it increases the value of the anomalous exponent towards one. We thus fully characterize the mean-square displacement exponent as a function of the parameters controlling the heavy-tailed distributions of both the lengths and barrier heights.

The model presented in this article might be a useful framework to interpret diffusion in a variety of systems composed of compartments of varying size and barriers. A striking example of such kind of system is provided by eukaryotic cells, highly compartmentalized at different spatial scales to provide optimal conditions to perform specific functions [115]. The presence of compartments has been shown to affect the diffusion of transmembrane proteins in the plasma membrane, e.g. as a consequence of a self-similar actin network acting as semipermeable barrier [104].

An interesting outlook of our model consists in the possibility of its further generalization, as to include previously proposed models for diffusion in complex environment. For example, our approach shares important features with the previously proposed comb model [116]. In fact, the comb model can be considered as a continuous-time random walk with stochastic waiting time, the latter derived from first-passage time. This system can be analysed through our coarse-grained approach upon conversion of the waiting time distribution into a stochastic transmittance. The realization of the comb model including convective terms [117], could be further implemented in our approach, e.g. through the use of asymmetric transmittance.

6 Phase separation in diffusing interacting systems

The phenomena of phase separation has recently emerged as a key factor in biological transport. Physically, such phenomena consist on the separation in two clearly distinguished phases from a previously homogeneous mixture. One common example is the one formed by two immiscible liquids as water and oil. Many recent observations have shown how phase separation occurs at different levels in biological environments such as the cell membrane, creating membrane-less compartments which favour distinct biological functions [118, 119]. In terms of its theoretical understanding, phase separation is in a very similar state as anomalous diffusion: even if the macroscopic behaviour is well understood, it still lacks of precise microscopical models, which will explain the actual interactions leading to such phenomena.

In its most general form, phase separation has been widely studied in terms of the heterogeneous mixing of two components. Two principal principles have been shown to lead to it: spinodal decomposition [120] and nucleation [121]. These two methods usually rely on macroscopic features of the system such as the entropy. In this direction, one of the most used models in describing phase separation in biological environments has been the Flory-Huggins model, originally proposed to the study of the thermodynamics of polymer systems [122]. Nevertheless, as with anomalous diffusion, it is usually hard to connect macroscopic features such as entropy to the actual microscopical interactions of the systems. While there exists works in such direction, they usually rely on very specific descriptions of the models, heavy numerical simulations or experimentally inaccessible properties.

In this chapter, we will present a minimal microscopical model in which phase separation emerges above a certain critical point. We consider here particles which stochastically bind to each other, forming condensates. Moreover, the diffusion of the particles is heavily affected by them being in condensates. We will show how this simple model shows a transition from a phase in which, even in the presence of binding, the particles move freely throughout the space to a phase in which particles form condensates and hence phase separate. While in previous chapters the focus has been mainly put in the motion of the particles, here we will first study the dynamics of the condensates, i.e. how they are formed and how

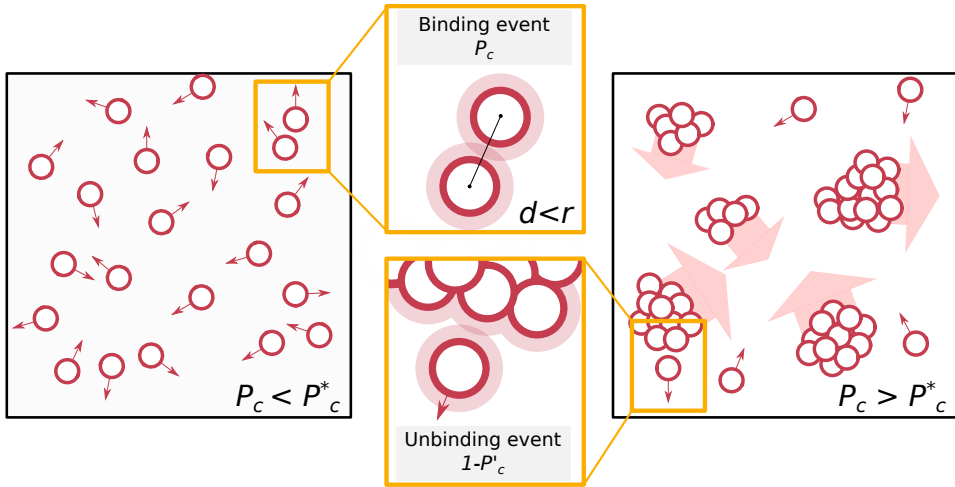


FIGURE 6.1: **Scheme of the model** In the left, we show the system below the critical point, where even in the presence of binding events (happening with probability P_c) most of the particles move freely. On the right, we show the system above the critical point, for which the system phase separate. Even in the presence of unbinding events, condensates are form. While particles show small diffusion inside the condensates, these also move as individual bodies (big, light arrows).

their size evolves. We will characterize with it the phase transition, showing how the critical point can analytically be calculated. Later, we will investigate on the diffusion of the particles and showing how the diffusion coefficient can be used as a tool to study phase separated systems.

6.1 Microscopical model of interacting particles

We consider a system of N particles moving in a bounded space of size L . The model is indeed general for any dimension. Nevertheless, in one dimensional systems, one needs to consider that particles can ‘jump’ (i.e. a quasi-1D system) or traverse each other, such that they can be found at any point in space. In the opposite case, the solution of the model can be defined as the persistent exclusion process (PEP)[123], commonly used in run-and-tumble dynamics and also showing phase separation in some schemes [124]. For simplicity, the following dissertation will be conceptually focused in a two dimensional system.

We consider that each particle has a radius of action r . If the distance between two particles is smaller than $2r$, they bind with probability P_c . Due to this binding, they will start forming condensates whose size M is defined as the number of

particles in the condensate. Then, given a condensate of size M , the probability of n particles to escape from it, i.e. the probability of them to unbound is given by

$$P_{\text{esc}}(n, M) = (1 - P'_c)^n P_c^{M-1-n} \binom{M-1}{n}, \quad (6.1)$$

i.e. the probability that the n -th particle escapes times the probability of all the other particles to stay. Note here that the minimal size of any condensate is 1, thus the maximal number of particles allowed to escape is $M - 1$. We have defined here P'_c as the probability of a particle to stay in a formed condensate, while $(1 - P'_c)$ is the probability of escaping from it. The fact that $P_c \neq P'_c$ considers that in a biological context, breaking a binding may be harder than creating it, which means that particles already forming a condensate have a higher probability of staying in them. In general, we will consider that $P'_c = \eta P_c$, with $1 < \eta < 1/P_c$.

Similarly, we can calculate the probability $P_{\text{abs}}(n, M)$ of a condensate of size M absorbing n new particles. First, the particle has to be in the radius of action of the condensate $S_c \approx rM$. To account for this, we need to consider the probability P_s of a particle being in such radius. Considering that the particle follows a diffusion model which explores space equiprobably in the long time limit (e.g. Brownian motion, FBM, ATTm) and also that $L \gg r$ so that the boundaries do not affect the later, we have that $P_s \approx S_c/L$. At last, $P_{\text{abs}}(n, M)$ can be written as

$$P_{\text{abs}}(n, M)_{L,r} = P_s^n (1 - P_s)^{N-M-n} \binom{N-M}{n} P_c^n + P_s^{n+1} (1 - P_s)^{N-M-(n+1)} \binom{N-M}{n+1} P_c^n (1 - P_c) \binom{n+1}{n} + \dots = \quad (6.2)$$

$$= \sum_{k=0}^{N-M-n} P_s^{n+k} (1 - P_s)^{N-M-(n+k)} \binom{N-M}{n+k} P_c^n (1 - P_c)^k \binom{n+k}{n}. \quad (6.3)$$

In words, the previous equation considers the cases when n particles are in the vicinity of the condensate and n are absorbed, $n + 1$ are in the vicinity but only n are absorbed, ...etc. Note here that if we consider an infinite space, i.e. $L = \infty$, the probability of condensates of any size to absorb new particles is zero, while the probability of particles escaping is non-zero. This implies that, in infinite systems, there will not be condensates in the long time limit. This means that only bounded systems will show the appearance of condensates. The latter has a closer connection with the biological systems of study, as the particles are usually diffusing through compartmentalized environments.

6.1.1 Average behaviour of the system

Once defined P_{esc} and P_{abs} , we can now calculate the average number of escaped and absorbed particles for a given condensate size M . For the former, we have that

$$\langle n_{\text{esc}}(M) \rangle = \sum_{n=1}^M n P_{\text{esc}}(n) = (M-1)(1-P_c). \quad (6.4)$$

For the latter, due to the complexity of Eq. (6.3), we are not able to write a compact analytical expression. Nevertheless, its calculation can still be done in an exact form by means of

$$\langle n_{\text{abs}}(M)_{L,r} \rangle = \sum_{n=1}^M n P_{\text{abs}}(n, M)_{L,r}. \quad (6.5)$$

The behaviour of $\langle n_{\text{esc}} \rangle$ and $\langle n_{\text{abs}} \rangle$ for a system of $N = 50$ particles moving in a box of size $L = 5$ is shown in Fig. 6.2, for different values of the binding probability P_c and considering $\eta = 1$. See that $n_{\text{esc}}(M)$ is a linear function of M whose slope is given by $(1 - P_c)$, as shown in Fig. 6.2 (c). For $n_{\text{abs}}(M)$, we get a more complex behaviour. In Fig. 6.2 (a), we show such function for a radius of action $r = 0.1$. We see that the mean number of particles absorbed increases non-linearly with the size of the condensate. However, when the condensate size reaches $M = N/2$, this number starts to decrease. This is because, as more particles are added to the condensate, less are free to be absorbed, until we reach the maximum size of the condensate $M = N$, in which $n_{\text{abs}}(M) = 0$.

An interesting case arises when we increase the size of the radius of action, until reaching the point $M > L/r$ for which $S_c > L$. In such case, the probability of any free particle to be in the radius of action of the cluster is set to $P_S = 1$. This transforms $P_{\text{abs}}(n, M)$ into

$$P_{\text{abs}}(n, M)_{P_S=1} = P_c^n (1 - P_c)^{N-M-n} \binom{N-M}{n}. \quad (6.6)$$

Then, we can recalculate the mean number of absorbed particles, which in this case can be solved analytically to find:

$$\langle n_{\text{abs}}(M)_{P_S=1} \rangle = (N - M)P_c. \quad (6.7)$$

In Fig. 6.2 (b) we show an example with $r = 0.3$. In such case, for a cluster of size $M = 16$ we will have that $S_c = 5.1 > L$. It can be seen from that point that $\langle n_{\text{abs}}(M) \rangle$ matches exactly the linear dependence given by Eq. (6.7).

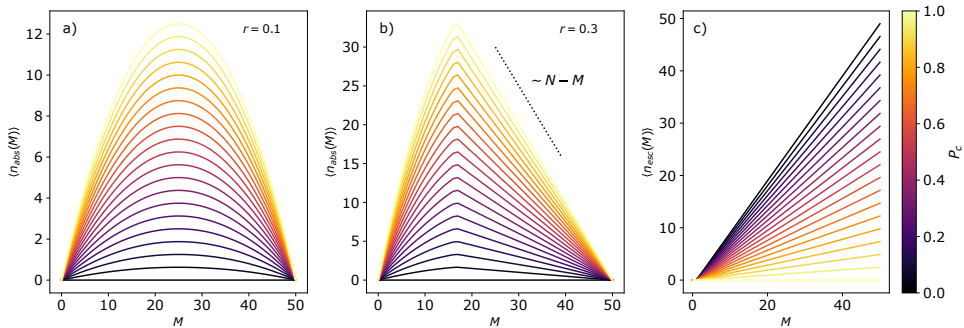


FIGURE 6.2: **Averaged behaviour of the model:** **a), b)** Mean number of particles absorbed by a condensate of size M , for system size of $L = 1$, with $N = 10$ particles, and a radius of action $r = 0.1, 0.3$ respectively. **c)** Mean number of particles escaping of a condensate of size M .

6.2 Transition to phase separation

With the previous definition of the condensate dynamics, we can now study what is the mean number of particles in a condensate for the different free parameters of the system. Indeed, each condensate has a flux of particles, which we define as

$$\Delta n(M) = \langle n_{\text{abs}}(M) \rangle - \langle n_{\text{esc}}(M) \rangle_{L,r}. \quad (6.8)$$

If the flux is positive, the condensate grows its size, as there are in average more particles getting absorbed than escaping. In the case of a negative flux, the opposite occurs. In Fig. 6.3 (a) and (b) we show $\Delta n(M)$ for two values of the radius of action, $r = 0.1, 0.3$, in a system of size $N = 50$ and $L = 5$. Note again that due to the complexity of Eq. (6.3), we cannot find a compact analytical solution for Δn . Nevertheless, in the case in which $P_S = 1$, $n_{\text{abs}}(M)$ was a linear function that could be analytically solved. This linear behaviour expectedly also appears in $\Delta n(M)$. Indeed, we can use Eqs.(6.4) and (6.7) to obtain

$$\Delta n(M)_{P_S=1} = n_{\text{esc}}(M=1) - n_{\text{abs}}(M=1) = P_c(N-1) - M + 1. \quad (6.9)$$

See then that in Fig. 6.3 (b) $\Delta n(M)$ behaves linearly for $M \geq 17$. We plot there a dotted line whose slope is $-M$, showing the accordance between Eq. (6.8) and Eq. (6.9).

There exists a particular value \bar{M} , for which the flux is zero, $\Delta n(\bar{M}) = 0$. This means that at \bar{M} the number of particles escaping and getting absorbed are equal, i.e. the size of the condensate *stabilizes*. Effectively, this implies that the condensates will grow or diminish until reaching such value. Then, \bar{M} gives also the

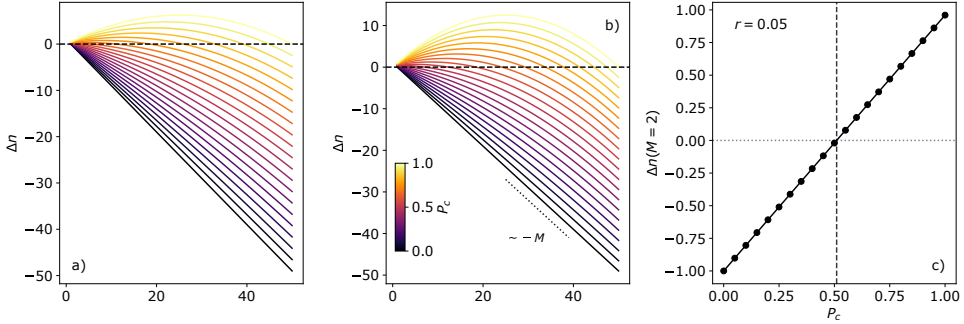


FIGURE 6.3: **Flux of particles in condensates and the phase transition:** a,b) Difference between absorbed and escaped particles as a function of the cluster size M for system size of $L = 1$, with $N = 10$ particles, and a radius of action $r = 0.1, 0.3$ respectively. Dotted line in b) show the expected behaviour in the linear regime. c) Stabilized cluster size \bar{M} as a function of the clustering probability P_c for the same system and various values of the radius of action r . The dotted line shows again the expected behaviour in the linear regime, which fits exactly with the solution for the system with $r = 0.3$ for $M > L/r$.

average size of the condensates present in the system. See in Fig. 6.3 (a) and (b) that Δn crosses only one time the line equal to zero. By studying such crossing, we can calculate what is the average (or stabilized) size of the condensates. We show this result in Fig. 6.4 (a), for a system of $N = 50$ particles, $L = 5$ and various radius sizes.

We see there two different phases: for low P_c , the average size of the condensates is one, which means that most of the particles are moving freely. At a given *critical* P_c , the condensates start growing until we reach $P_c = 1$, for which the system completely collapses in a single condensate.

The fact that the average size is given by the crossing of Δn at zero makes it very simple to calculate where the phase transition will occur. We are considering here that the transition occurs where the condensates have in average at least two particles. Then, the critical P_c can be calculated by studying at which P_c the flux at $M = 2$, i.e. $\Delta n(M = 2)$ crosses zero. We show this in Fig. 6.2 (c). We see that for low P_c , such flux is negative, so the condensate of size 2 tends to loose particles. Then, for bigger P_c , it becomes positive, meaning the possibility of creating bigger condensates. The point at which it crosses zero marks the transition point.

While Δn has not a compact form for all M , it still has quite a simple expression for low M . It is the case for $M = 2$, for which we have

$$\Delta n(M = 2) = P_c \frac{2r(N - 2) + \eta L}{L} - 1. \quad (6.10)$$

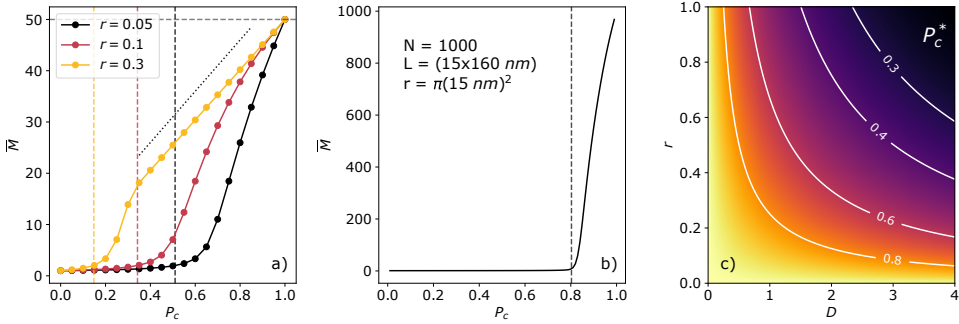


FIGURE 6.4: **Phase transition characterization: a,b)** Difference between absorbed and escaped particles as a function of the cluster size M for system size of $L = 1$, with $N = 10$ particles, and a radius of action $r = 0.1, 0.3$ respectively. Dotted line in b) show the expected clustering behaviour in the linear regime. **c)** Stabilized cluster size \bar{M} as a function of the radius of action r . The dotted line shows again the expected behaviour in the linear regime, which fits exactly with the solution for the system with $r = 0.3$ for $M > L/r$.

From here, solving the previous equation for $\Delta n(M = 2) = 0$, we find that the critical P_c^* is

$$P_c^* = \frac{L}{2r(N-2) + L\eta}. \quad (6.11)$$

We plot such value as vertical lines in Fig. 6.4 (a). We see that while it correctly describes the phase transition, this change is heavily affected by finite size effects, i.e. the system is too small to capture sharply the transition. However, for much bigger systems, as shown in Fig. 6.4 (b), the behaviour is much better reproduced. Moreover, for such big systems, one can approximate Eq. (6.11) by

$$P_c^* \approx \frac{1}{2rD + \eta}, \quad (6.12)$$

where we have defined $D = N/L$ as the density of the system. Note now that the critical point depends solely on the density and radius of action. We show in Fig. 6.4 (c) the behaviour of P_c^* for a range of r and D . See that, for systems with small r , the transition occurs at bigger values of P_c , as the particles have a harder time for finding each other. A similar argument can be given for small D , where the system is so dilute that the particles can not find each other and condensate. As we increase any of the two variables, the critical point lowers, until we reach regimes in which the system condensates at any P_c .

6.3 Distribution of condensate sizes

In previous sections we have studied analytically the *average* behaviour of the system. We are now interested in studying the probabilistic behaviour of it. This helps us to get a better understanding of the condensate behaviour, but also allows us to get features which may be easier to access in an experimental scenario. We will focus our study in the probability distribution function (PDF) of condensate size $P(M)$.

In order to calculate it, we need to consider a recurrent system of equations. To understand its construction, let us consider a small system of three particles. Then, let us define $E_{n,M} = P_{\text{esc}}(n, M)$ and $A_{n,M} = P_{\text{abs}}(n, M)$. The probability of finding a condensate of size $M = 1$ is then given by

$$P(1) = P(1)A_{0,1} + P(2)E_{1,2}A_{0,2} + P(3)E_{2,3}A_{0,1}. \quad (6.13)$$

Similar equations are then constructed for $P(2)$ and $P(3)$. The latter equation considers then all possible ways of creating condensates of size M from all the rest of sizes. Note here that $E_{m,m} = 0$ and that we always consider, both in simulations and in the theory, that escaping events take place before the absorbing ones.

In general, $P(M)$ is found to be

$$P(M) = \sum_{k=1}^N P(k) \sum_{i=0}^{k-1} P_{\text{esc}}(i) P_{\text{abs}}(M - k - i). \quad (6.14)$$

The previous defines a set of N equations with N variables $P(M)$, for $M = 1, \dots, N$. In order to solve such system, we consider the usual approach in stochastic matrix theory. A stochastic matrix (also called probability matrix) is a square matrix with non-negative real elements, each of them representing a probability. They are often used to describe the evolution of a Markov chain. See for instance that the set of equations generated by Eq. (6.14) can be written in matrix form as

$$\begin{pmatrix} x_{11} & x_{12} & \dots & x_{1N} \\ x_{21} & x_{22} & \dots & x_{2N} \\ \vdots & \ddots & \ddots & \vdots \\ x_{N1} & x_{N2} & \dots & x_{NN} \end{pmatrix} \begin{pmatrix} P(1) \\ P(2) \\ \vdots \\ P(N) \end{pmatrix} = \begin{pmatrix} P(1) \\ P(2) \\ \vdots \\ P(N) \end{pmatrix}, \quad (6.15)$$

where x_{ij} are given by Eq. (6.14). Now the matrix X , leftmost matrix in the previous equation, is a stochastic matrix. More precisely, it is a left stochastic matrix, as each column is equal to one, i.e.

$$\sum_{i=1}^N x_{ij} = 1 \quad \forall j. \quad (6.16)$$

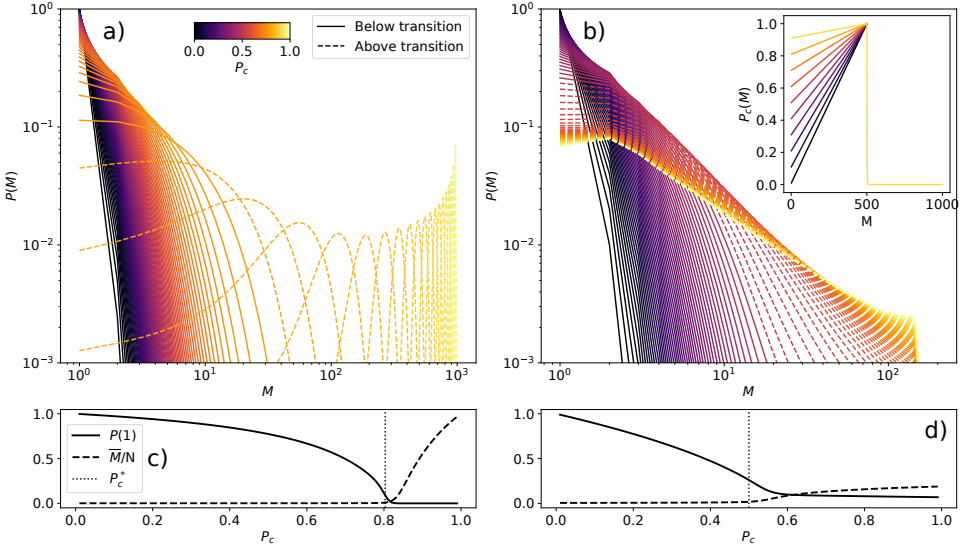


FIGURE 6.5: **Condensate size distribution:** **a)** Distribution of cluster sizes $P(M)$ for system of size $L = 1$, $N = 10$, $r = 0.1$ and various values of P_c . **b)** Normalized number of free/clustered particles for the previous system. Dashed vertical line corresponds to the phase transition between the clustered/non-clustered phases. This results are retrieved from 10^5 simulations of 100 time steps, sufficient long time for the system to reach its equilibrium.

We can then use the stochastic matrix theory to solve the system of equations. For that, we give an initial ansatz for the vector of probabilities \vec{P} . Then, we multiply this vector by the matrix X . The fact that X is a left stochastic matrix makes it such that the sum of the terms of \vec{P} will always be equal to one. We perform this procedure until convergence.

In Fig. 6.5 (a) we show this PDF for various P_c , for a system with $N = 1000$, $L = 15 \times 160$ nm and $r = \pi 15$ nm² (the same as in Fig. 6.4 (b)). We see two very distinct regimes: for $P_c < P_c^*$, $P(M)$ is a Gaussian distribution with mean zero and variance increasing as we increase P_c . Then, for $P_c > P_c^*$ we find a similar Gaussian shape, with a longer left tail, but whose mean starts to increase as we increase P_c . Indeed, one can calculate now the mean of $P(M)$. As shown in Fig. 6.5 (b) normalized by the total number of particles in the system, its behaviour is exactly the same as the averaged value we calculated in Eq. 6.4 (b). Moreover, we can now calculate the probability of finding free particles in the system, i.e. $P(1)$, as shown in Fig. 6.5 (c). We see how it follows the opposed behaviour to the mean condensate size: before the phase transition, we find free particles in the

system, with its probability lowering as we approach the critical point. Over it, all particles condensate and then $P(1) \rightarrow 0$.

Size dependent binding probability While the previous explains the dynamics of the very simple model proposed, it misses some important features observed in biological phase separated systems. For instance, it is known that this system regulate their compounds in such a way that they do not condensate above a certain size [125]. However, it is very easy to accommodate such behaviour in the model, by considering that P_c is no longer constant for every particle, but depends on the size of the condensate.

We consider here the case in which $P_c(M)$ increases linearly with the size of the condensate, until this reaches a given maximal size. From there, $P_c(M)$ decreases exponentially, preventing the formation of any bigger cluster. In Fig. 6.5 (c) we show the PDF $P(M)$ of such system. In the inset we showcase the form of $P_c(M)$. See that this new feature changes completely the distribution of condensate sizes, which present now power law tails until reaching the maximal value at which $P_c(M)$ decreases exponentially.

Similarly, the average size of condensates is also changed. However, while its behaviour changes in terms of absolute numbers, we still find that the phase transition takes place at the same point. In Fig. 6.5 (d) we see how the normalized average size, \bar{M}/N , now does not reach such big values compared to the case with constant P_c . This effect is obviously related to the exponential cut-off on the binding probability. In terms of the probability of free particles, we see now that such value never reaches zero. This means that even above the phase transition, there is a small probability of finding particles away from condensates. This has indeed a better connection to very recent experimental observations [58].

6.4 Diffusion in condensed systems

In previous sections we exposed how the growth of condensates work. However, we have not addressed how particle moves in the system. Our only consideration has been that the particles have to diffuse in such a way that they explore all the space with equal probability. This is true for all the models considered previously in this Thesis. For the sake of simplicity, we will consider now that particles move as Brownian particles. However, the results are equally valid for any diffusion model, as far as the previous consideration is fulfilled.

We are interested in understanding if variations on the diffusion due to the condensation may affect the previous discussion. In particular, we are interested in the case in which the particles in condensate may move very differently than when they are free. We will consider for instance the case in which free particles move with a diffusion coefficient D_f much larger than the one of condensed particles D_c .

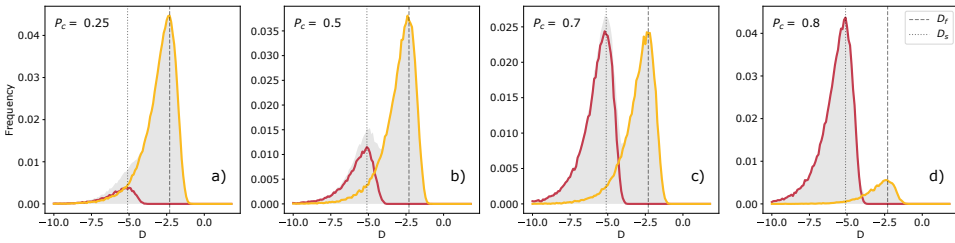


FIGURE 6.6: **Dynamic behaviour of a phase separated system:** Distribution of instantaneous diffusion coefficient for a system with $L = 1$, $N = 1$ and $r = 1$. This results are retrieved from 10^5 simulations of 100 time steps, sufficient long time for the system to reach its equilibrium. The number of particles per population correspond to the ones presented in Fig .6.5 (a) and (b).

As one may expect, the diffusion of a particle inside a condensate is heavily affected by the presence of many neighbouring particles. Moreover, one can consider the condensate as a compartment, as the ones presented in Chapter 5. As we show there, not only the diffusion coefficient, but the anomalous exponent can also be heavily affected. Such compartmentalization may occur even without the need of physical barriers, as it is the case in liquid-liquid phase separation schemes. In its most general form, the higher particle density of the condensates makes it such the the motion of the particle in it changes.

To test such behaviour, we simulate a system of Brownian particles with the previously presented features, moving in a one dimensional system. To give a closer description to any biological system, we also consider that only particles in the boundary of the condensate can escape from it. Similarly, new particles will adhere to the boundary of the formed condensates. While this was not taken into account in the theory, we will use it as a stress test to prove the generality of the model. While one may expect small quantitative variations, the final qualitative behaviour should be the same.

In Fig. 6.6 we calculate the instantaneous diffusion coefficient of the particles in the system, usual measure in experimental scenarios. As expected, we see a bimodal distribution, whose peaks correspond to D_f and D_c . We also see the appearance of heterogeneity in the coefficient distribution due to the stochastic nature of the system, and the fact that we are sampling for a finite time. The peaks of each distribution are related to the fraction of free ($P(M = 1)$) and condensed particles ($P(M > 1)$) and is in accordance to what was shown in the lower panels of Fig. 6.5.

6.5 Conclusions

In this chapter we have introduced a microscopical model able to reproduce some of the features of phase separated systems. Phase separation occurs when a previously homogeneous system separate in two distinct phases. In our case, the system is composed of particles, which interact with each other by means of a binding process. Each time two particles get closer than a give distance, they have a certain probability of binding P_c . Such probability is tunable and aims at representing biological process such as the binding of transcription factors to DNA. Importantly, the understanding of such processes and their effect of the dynamics of the system may shed light in the regulation of gene expression.

We have demonstrated that the system undergoes a phase transition from a free phase, in which particles move alone through the system, to a phase separated scenario, in which particles form condensates. Surprisingly, even for non zero binding probabilities, the particles form instantaneous condensates, which fade almost immediately. Only when the biding probability overcomes the critical point, i.e. $P_c > P_c^*$, condensates start to arise steadily. We have shown how the average condensate size grows from one, i.e. a single particle, for $P_c < P_c^*$ to an increasing value for $P_c > P_c^*$. We have shown that the critical P_c value can be exactly calculating by means of the average flux of particle of a condensate. Only when such flux is zero, the condensate reach its steady size. Then, the critical point is given by the value of P_c at which such event happens for sizes equal to two.

While the minimal model presented allows for a complete analytical study of system, some of its components show very complex and convoluted expression. However, we have seen that there exists a regime in which most of them linearised, allowing for a much simpler understanding of the phenomena. This happens when the distance at which two particles are considered to interact increases beyond the size of the system. We showed two ways of reaching such feature: either by considering long range correlations between particles or by considering enormous particles. While such case may not be well connected by any physical scenario, it's interest relies on the simplicity of the resulting equations.

Another interesting feature of the model is the distribution of condensate sizes. We have shown how this can be calculate by means of stochastic matrix theory. Interestingly, we see two very distinct behaviour, depending on the phase of the system. In the free phase, the distribution shows an Gaussian behaviour with mean zero (just as predicted by the averaged behaviour) and with variance increasing as we increase P_c . Above the critical point, the mean of the distribution increases until reaching a delta distribution at $M = N$ for $P_c = 1$. This study allows for the calculation of probability of finding a free particle in the system $P(1)$. This allows for a direct comparison to experimental observations such as the ones done by means of cartography maps.

On the other hand, we have studied how introducing heterogeneous dynamics may affect the previous results. In a biological context, condensed particles

are known to diffuse much slower, mostly due to the extreme crowding of those regions. Moreover, in terms of phase separation systems, condensates are usually formed around regions with particular biological functions, which by themselves may cause the slowing of the particles [58]. Taking this into account, we considered a system in which the particles in condensates have a much smaller diffusion coefficient than those moving freely. In order to assess the validity of the model, we proceeded with Brownian simulations of the systems, accounting for both the binding probability and the diffusion variances. We have seen how the condensate dynamics are not affected once the system reaches its steady state. In terms of the diffusion coefficients, we show that they have a bimodal distribution, peaked around the two mean values, one for the free particles and one for the ones in condensates. By tuning the binding probability, we see how the two peaks vary in size just in analogy to the distribution of free and condensed particles.

Finally, we have shown how the model may be adapted to account for different phenomena that may arise in biological systems. For instance, it has been observed in an *in vivo* system that the condensates formed in phase separated systems may only reach a maximal size [126]. To account for this, and also for other effects such as Ostwald ripening [127], we have considered that P_c increases for bigger condensates, enhancing even more their growth. However, after reaching a certain size, P_c drops exponentially to zero, accounting for the dissolution of the condensates. We have explored how this may affect the distribution of condensate sizes, showing that below the phase transition, the effect is barely noticeable. Above the phase transition, the distribution is transformed to a power law, with a cut-off, close to the exponential cut-off of P_c .

In general, we have presented a model in which phase separation occurs with only minimal considerations, hence paving the way for more complex models, accounting for the particularities of the physical systems explored.

7 Single trajectory characterization via Machine Learning

“This chapter is dedicated to the memory of Peter Witter, who show me that machine learning and physics were not so far apart.”

In this chapter we will explore how Machine Learning (ML) techniques may be used to characterize diffusion processes. Their input will be the trajectory arising from diffusion models and experiments (e.g. the ones showed in Fig. 2.1 or schematically represented in Figs. 3.1, 4.1, 5.1 and 6.1). We will show how a precise ML architecture, the Random Forest, may be used to asses two problems: the determination of the anomalous exponent and the determination of the theoretical model that better describes the trajectory.

Due to the novelty of the ML, we will first introduce the topic, covering very briefly its main features. Then, we will explore its suitability in diffusion characterization, comparing it to previously known methods. Finally, we will benchmark the method with simulated data to finally show its power by characterizing experimental datasets without any prior knowledge of their source system.

7.1 Machine learning as a scientific analysis tool

In this section, we will briefly review the main features of ML. In general, the primary goal is to create an architecture such that, after a successful training, it is able to succeed at the task it was trained for. These architectures are normally made of a huge quantity of free parameters, which are tuned in order to minimize a given loss function. The later is defined in such a way that solving the task is analogous to the minimization of the loss function.

All ML tasks can be differentiated in three families: supervised learning, unsupervised learning and semi-supervised learning. In this chapter, we will focus mostly on the first one, but will also briefly comment on the second. Semi-supervised learning mainly contains reinforcement learning [128], an algorithm

in which an agent is trained to perform a task in a certain environment by means of trial and error. Each time the agent succeeds, it is given a reward. The final goal of the agent is to get as many rewards as possible. This approach has seen a huge interest after its superhuman performances in games like go or chess [129]. While playing games may seem a unprofitable task, the algorithms presented set the basis for the use of RL in much more complex scenarios. For instance in Physics, RL has been, among others, for the generation of new quantum experiments [130], its optimal control [131], the study of the navigation of microswimmers in fluids [132] or the optimal search of ground states in Hamiltonian systems [133].

The rise of ML is mostly due to two feats: first, the increase of computational power and the improvement of the graphical processing units (GPU). While the theory of ML start to be developed in during the 80s and 90s, with studies from John Hopfield [134], Geoffrey Hinton [135] or Elizabeth Gardner [136], it is not until twenty years latter that those techniques could be implemented in real life scenarios. Second, the possibility of accessing huge amounts of data. In order to train ML architectures, it is necessary to feed the machine with as many samples of data as possible. Only since some years ago, with the start of the communication age, humans are able to extract and collect huge amounts of data, to which latter apply ML algorithms. Nevertheless, in science, such paradigm has always been present. Hence, the suitability of using ML to study complex system from which enormous amount of data arise. A large variety fields have successfully used ML techniques, such as physics [137], biology [138] or chemistry [139]. Plenty of reviews of more particular applications are available, and we have reached a point in which any field is taking advantage of such powerful techniques.

In the rest of this chapter we will introduce both supervised and unsupervised learning and show how they can be applied to the characterization of diffusion processes, as the ones we have presented throughout this Thesis. These techniques offer a very powerful tool to connect the large amount of theory developed in the last years to the experimental observations. This connection is usually difficult, due to the stochastic nature of the physical systems of study. Moreover, in a biological scenario, we are usually facing very noisy data, with samples which contain much less information that the one needed to perform an accurate characterization. The goal of the chapter is to show that ML can successfully perform such link.

7.1.1 Supervised learning

We will start our journey into ML algorithms by introducing the concept of supervised learning. In any ML, we will have access to a dataset. No matter what this dataset contains, we consider that is possible to transform each sample of data in a vector (or tensor) X of arbitrary dimension. The dataset is then the set

$\vec{X} = \{X_i\}_{i \in \mathcal{T}}$, where \mathcal{T} refers to the number of samples in the dataset. As an example, one can consider that the dataset is a collection of images, of $N \times N$ pixels, which in the case of RGB images defines a tensor of dimension $3 \times N \times N$.

Once given the dataset, we have to define the task that we would like to achieve for the machine to proceed with. Let us continue with the example of the images, and consider that each of them shows a hand-written digit. This dataset is the renowned MNIST dataset [140] and is shown in Fig. 7.1. Let us define here the task as the classification of each image by the number shown. To further simplify, let us consider only the images showing zeros or ones. This means that we have 2 different classes. In supervised learning, the machine has access not only to the images, but also to the result of the task for every sample of the dataset. This means that for each image, it is also given a *label* referring to its class.

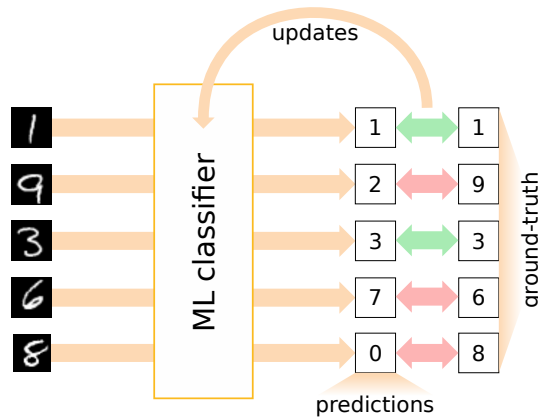
The loss function is then defined by comparing the predicted class of the machine for every image, Y_{pred} to the ground-truth value, Y_{true} . Various loss functions can be defined for such classifications problems. The most simple one is just to consider the accuracy, defined here as the number of correct predictions over the number of total predictions.

Note that until now, we have not entered into any discussion about the nature of the machine. We have only considered that such entity has a number of free parameters θ that we can tune at will in order to minimize the cost function. The most used architecture are the neural networks, a set of neurons distributed in layers and connected by weights. Its input are the samples of the dataset and its output is, in the current classification scheme, the class of the input sample. A different architecture used for the same purposes are the Random Forests. We will further comment on those in Section 7.2.1, as it is the architecture we will consider for the trajectory characterization problem. For more details on the training of neural networks, Ref. [141] offers a very practical introduction to the topic, while Ref. [142] is particularly directed to physicists.

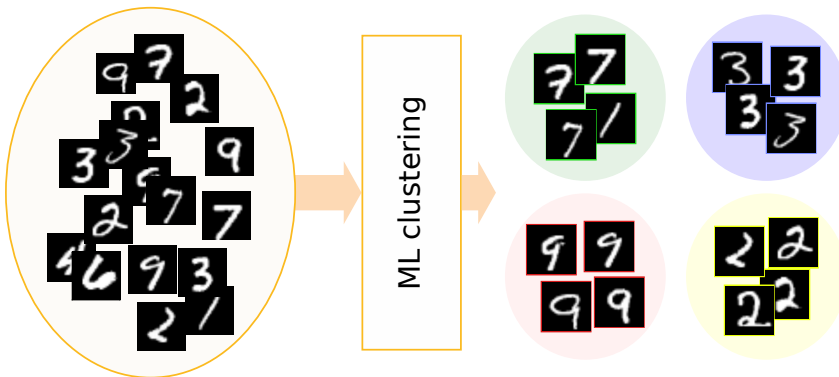
7.1.2 Unsupervised learning

In unsupervised learning, a similar framework is set. However, in this case the machine has only access to the samples, and not to their labels. In such setup, the machines can be used for various applications. The most common is clustering, where the machine tries to find patterns in the dataset and separate in clusters samples with common features. Note that these features may be completely different from the ones we expect. For instance, in the case of a dataset containing images of dogs of various breeds, the machine could cluster them by their coat's colour, and not their breed. For instance, such methods have been used to detect phase transitions [143]. Interestingly, the authors also found that the machine was clustering samples not only by their phase, but also by other experimentally relevant parameters.

(a) Supervised learning



(b) Unsupervised learning



(c) Generative models

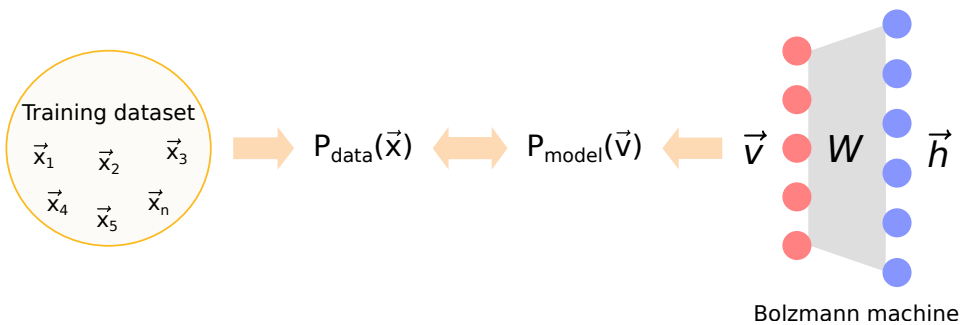


FIGURE 7.1: **Machine learning methods summary** (a) Supervised learning: the machine is trained by comparing its predictions to the given, ground truth labels. (b) Unsupervised learning: the machine is trained by minimizing some distance metric, in order to separate and/or cluster the input data. (c) The machine, in this case a Boltzmann machine, is trained in order to approximate the probability distribution of the training set images.

Another application is anomaly detection, where the machine learns to differentiate pathological samples which have very little in common with the rest of the dataset [144]. In physics, such approach has been used to find new physics beyond the standard model [145] or explore the phase space of unknown Hamiltonian systems [146]. While both clustering and anomaly detection have gained a lot of attention in various fields of physics, they have not yet been explored in terms of anomalous diffusion characterization. We will further on their feasibility in following sections.

Machine learning with physical models

One of the most promising applications, but also the hardest, is the creation of generative models. In such problem, a machine is given a dataset, with an associated probability distribution $P(X)$. The goal of the machine is to mimic such probability distribution and generate new samples according to it. In plain words, given a dataset, the machine tries to create samples resemblant to the ones it has already seen. The state-of-the-art in such problems are the generative adversarial networks (GAN) [147]. However, in the first stages of the field, Restricted Boltzmann machines (RBM) [148] captured the attention of both computer scientist and physicist. For the former, RBM supposed one of the first trainable ML architectures that could deal with generative models. For the latter, its construction is analogous to the one of a spin model and with so, they both share similar features.

In general, the training of an RBM is not very distinct to the problem of solving an Ising system, such as the one we presented in Chapter 4. The RBM consists of two layers of neurons, with inter-layer connections. This means that a visible neuron v_i is connected to all the hidden neurons h_j , but not to the rest of visible. In the spin analogous, one considers that the neurons are spins. The system evolves by means of a Hamiltonian H , in which the inter-layer connections are now the couplings between spins. By defining H , using the usual statistical physics, we can define the probability of finding a certain spin configuration given the current set of weights. The goal of the training is to tune the weights of the couplings in such a way that the probability of finding a certain visible configuration $P_{\text{rbm}}(v)$ is equal to $P(x)$.

One of the main drawbacks of RBM and of any energy based model, is that the sampling of $P_{\text{rbm}}(v)$ is very hard, and in general an NP-hard problem. This difficulty comes from the original definition of the machine as a Hamiltonian, or more precisely, Ising model. Sampling from an Ising model requires the use of Monte Carlo techniques, which are usually stuck in local minima. Specially in the so-called spin glass phase, such sampling becomes prohibitively expensive. While many techniques have been developed to train efficiently RBM, none have dealt with the problem of the sampling difficulty [149, 150, 151, 152].

Recently, we have proposed that the spin-glass phase is an unnecessary bottleneck for the training of energy based models [60]. In its usual realizations RBM are initialized with random weights, giving rise to an spin-glass Ising model where the sampling is difficult. It has been shown how restricting the value of the weights in order to avoid such phase increases in orders of magnitude the training of RBM. While RBM were one of the most used ML architecture for generative purposes, due to the hardness of their training, they have been taken away by GAN. Our recent work, presented in Ref. [60], sets the pace for a considerable improvement of its training, but also the possibility of training deep Boltzmann networks, shown analytically to be universal approximators of any distribution function.

7.2 Single trajectory characterization as machine learning problem

Once introduced the basic concepts of ML, we will explore how these can be used to characterize the motion of particles at the single trajectory level. In previous chapters we have widely studied the trajectories arising from various diffusion models. Their main characteristic is their stochastic behaviour. This means that to faithfully characterize such trajectories one needs to proceed with statistical approaches, mainly in the form of averages. As widely commented in previous chapters, the most used feature to study diffusion is the mean squared displacement (MSD), Eq. (2.5). As we have seen, to recover such metric from a set of trajectories one needs to proceed either with an ensemble averaged MSD (eMSD), Eq.(2.7), or a time averaged MSD (tMSD), Eq.(2.6).

While in theoretical studies both techniques are completely valid, taking obvious care of the use of tMSD in non-ergodic systems, in experimental scenarios such analysis is not so easy. In particular, the usual single particle tracking (SPT) experiments, where diffusion models are mostly applied, give rise to very short and noisy trajectories. In terms of the ensemble, it is usually experimentally challenging to get a big set of representative samples, while the presence of heterogeneities in the system can strongly affect its analysis. These two features makes it such that the averages approach may fail without proper considerations.

Nevertheless, there has been in past years a huge effort to create algorithms to correctly characterize trajectories by from their tMSD. For instance, in Refs. [153, 154, 155] the authors present methods for correctly fitting the tMSD, even in the presence of noisy data. Many other works try to characterize various properties of the trajectories by means of it, such as the anomalous scaling exponent [156] or the change of diffusion modes [157]. Nevertheless, all these works mainly focus on the fractional Brownian motion, i.e. an ergodic diffusion model for which the tMSD gives significant information. In the presence of ergodicity breaking, it is an

open question how many of these methods are indeed valid. In a similar fashion, other works such as the ones based on Power Spectral Density [158] rely on the possibility of being able to theoretically construct such feature, while methods relying on Bayesian approaches [159, 82] need prior information on the system to correctly assess its characteristics.

Considering the previous challenges, we have seen in the past year a huge effort in the use of ML techniques to characterize diffusion models. Such techniques offer mostly two advantages: the ML algorithm should be model independent and should have no need of previous information of the system where the trajectories are collected from; It should be applied at the single trajectory level, where the effects of ergodicity breaking will not affect its correct characterization. The latter is of high importance, as it is still an open question if ML algorithms may perform better in systems in which tMSD techniques are suitable. Indeed, there is currently a common effort to assess which methods are better for trajectory characterization and under which circumstances [61].

The first approach of trajectory characterization by means of ML methods was done in Ref. [160], where the authors used a neural network to classify trajectories by its diffusion model: Brownian, confined and directed motion. A similar study was done in Ref. [161], in which the authors also show that ML based methods were superior than feature-based predictions. Other works have focused in determining the anomalous exponent of the input trajectories, either with convolutional neural networks [162] or long short term memory neural networks [163]. Moreover, in the latter, the authors address the problem of the change point, i.e. finding the point in which a trajectory switches from one exponent to another. Nevertheless, all previous approaches focused their studies on FBM trajectories, hence leaving as an open question the suitability of ML methods in non-ergodic data.

In the following sections we will present the method proposed in Ref. [59], which was developed to solve two problems: first, extracting the anomalous exponent of the input trajectories; second, classify them by their diffusion model. We will show how the ML methods are indeed capable of dealing with non-ergodicity, while maintaining state-of-the-art predictions for ergodic trajectories.

7.2.1 Machine learning method

We will now present the different pieces of the ML method, sketched in Fig 7.2. We will focus first in the ML architecture of use, the Random Forest. We will then comment on the dataset used to train such model and we will finally present a method to preprocess the data in order to correctly normalize the data, no matter from which system it is arising.

Random Forest

Random forest is an architecture based on Decision Trees. A decision tree is an efficient non-parametric method widely used for classification and regression problems [164]. The basic idea consists in producing recursive binary splits of the input space, so that the samples with the same label are grouped together. The criterion to produce the splits is based on a homogeneity measure (usually, the information entropy) of the target variable within each of the obtained groups. In regression problems, a commonly used criterion is to select the split that minimizes the Mean Squared Error (MSE); this recursive process continues until some stopping rule is satisfied, e.g., a common one is to consider that a tree node can be split if it contains more than a given number of samples; therefore, the minimum number of samples required to split a tree node should be adjusted in order to control the size of the tree, thus preventing overfitting. Once a decision tree is obtained, the output for unseen samples is computed just passing them through the nodes of the tree, where a decision is made with respect to which direction to take. Finally, a terminal tree node is reached, where the output is obtained.

A RF is a tree-based ensemble method, which builds several decision tree models independently and then computes a final prediction by combining the outputs of the different individual trees [165]. In particular, the ensemble is produced with single trees built from samples drawn randomly with replacement (bootstrap) from the training set. An additional randomness is added when splitting a tree node because the split is chosen among a random subset of the input variables, selected in this case without replacement, instead of the greedy approach of considering all the input variables. Due to this randomization, the bias of the ensemble is slightly higher than that of a single tree, but the variance is decreased and the model is more robust to variations in the dataset.

RF is a very powerful, state-of-the-art technique for both regression and classification problems, usually outperforming not only single decision trees but also sophisticated models, as shown in a thorough comparison study [166].

Training and test datasets

The training dataset is built out of numerical simulations of trajectories from various kinds of theoretical models. As a natural choice, we included three of the best-known and used models that can give rise to anomalous diffusion: CTRW [20], FBM [19] and Lévy walks (LW) [106]. Moreover, we included trajectories from the annealed transient time model (ATTM) [74], which has been lately associated with various experimental observations. Each of these models was presented in Section 2.3, where more details can be found. Building a good dataset is key in ML techniques. For instance, one needs to create them in such a way that they represent as faithfully as possible the problem as a whole. ML dataset have then to be

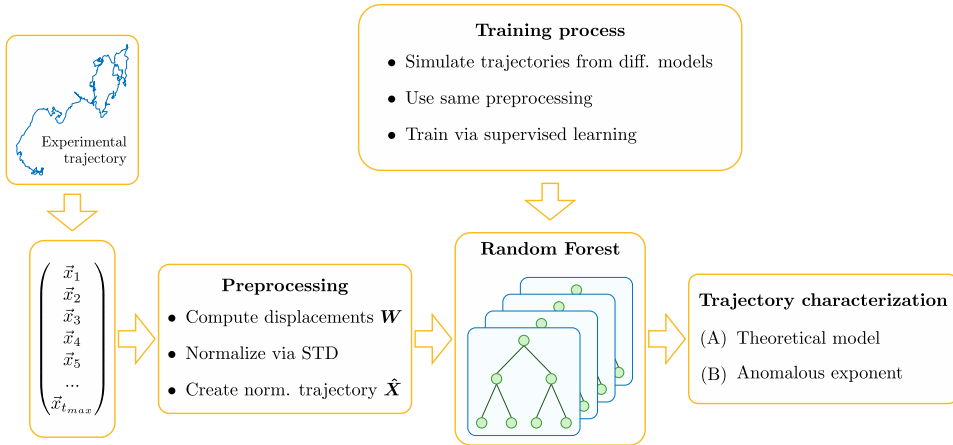


FIGURE 7.2: **Schematic of the method.** An experimental trajectory is first transformed into a time series and preprocesses according to the procedure described in Section 7.1. The trajectory is fed to the algorithm for its characterization through a RF, previously trained on simulated data. We show RF capability to extract two characteristics of the trajectory: (A) the most likely theoretical model among the ones contained in the training dataset and (B) the anomalous exponent α .

balanced (i.e. each class has to be equally represented). Then, for each ML architecture considered, the trajectories need to show similar features, so that one can correctly compare the results. To standardize the creation of anomalous diffusion trajectories, we have developed the python package *andi*, accessible in Ref. [167]. This accessible tool allows us to create datasets of trajectories from different models and exponents, helping us to correctly characterize the results of the ML algorithm.

Preprocessing

Our aim is to design a method that can be used to accurately characterize heterogeneous trajectories without having to calculate other parameters or using a priori knowledge. In order to be able to analyse data coming from any possible spatio-temporal scale, we designed a preprocessing procedure that properly rescale the data. In Ref. [59], the following procedure was implemented:

1. We use one of the models above to simulate the trajectory of a particle during t_{max} time steps. The result is a vector of positions, $\mathbf{X} = (\mathbf{x}_1, \mathbf{x}_2, \dots, \mathbf{x}_{t_{max}})$.
2. This vector is transformed into a vector of distances travelled in an interval of time T_{lag} , i.e., $\mathbf{W} = (\Delta \mathbf{x}_1, \Delta \mathbf{x}_2, \dots, \Delta \mathbf{x}_{J-1})$, where $J = t_{max}/T_{lag}$. We

define $\Delta \mathbf{x}_i$ as

$$\Delta \mathbf{x}_i = \left| \mathbf{x}_{iT_{\text{lag}}} - \mathbf{x}_{(i+1)T_{\text{lag}}} \right|. \quad (7.1)$$

3. To normalize the data, we divide \mathbf{W} by its standard deviation (STD) to get a new vector $\hat{\mathbf{W}}$.
4. Then, we do a cumulative sum of $\hat{\mathbf{W}}$ to construct a normalized trajectory $\hat{\mathbf{X}}$.

Summarizing, the previous procedure generates a new trajectory which is constructed via the normalized displacements of the original trajectory. While this normalization showed great results, it did mostly in big enough trajectories. Note that as one increases T_{lag} , the length of the resulting vector $\hat{\mathbf{X}}$ decreases. Moreover, considering big time windows erases the microscopical details of the trajectories. We will see later how this affect the accuracy of the machine. Nevertheless, different normalizations have been proposed lately, showing great success. An example would be to create trajectories following

$$\hat{\mathbf{X}} = \frac{\mathbf{X} - \langle \mathbf{X} \rangle}{\langle \mathbf{X}^2 \rangle}. \quad (7.2)$$

In the following sections we will focus in the first procedure, as it gives insights on the importance of the microscopical dynamics for the correct trajectory characterization. Note that both procedures make that the magnitudes of the resulting trajectories are comparable, no matter what were their original values. Moreover, while the RF could be trained using $\hat{\mathbf{W}}$, our results show that training with $\hat{\mathbf{X}}$ gives indeed much better results. The same preprocessing is applied to both the simulated and experimental trajectories used in Sections 7.2.2 and 7.3.

7.2.2 Benchmarking the model with simulated data

We will use our method to characterize single trajectories according to two different schemes: (A) discrimination among diffusion models; (B) prediction of the anomalous exponent α , that inherently implies classification as normal or anomalous diffusion. For each of these problems, we created a dataset of $1.2 \cdot 10^5$ trajectories with $t_{\text{max}} = 10^3$, divided into a training and test set with ratio 0.8/0.2, respectively. The results presented in all the figures and the values of the accuracy discussed in the text correspond to the ones measured in the test set, ensuring that the RF does not present overfitting in any of the problems considered. The different classes considered in each problem have an equal number of trajectories, hence allowing us to use the accuracy as a measure of the goodness of the RF. For technical details and a practical example of the implementation, we refer the reader to the repository in Ref. [62].

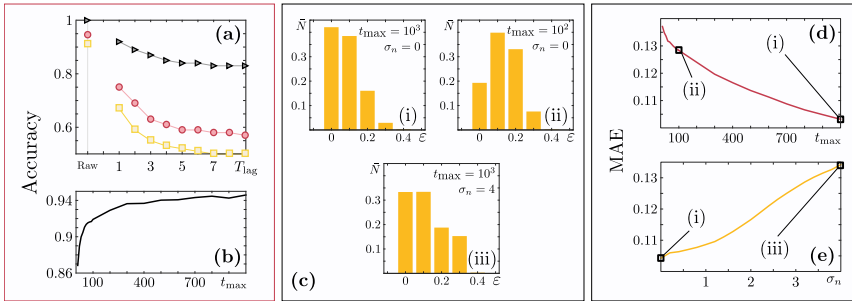


FIGURE 7.3: **Benchmarking the RF algorithm:** (a) Accuracy of the RF when discriminating among models as a function of the preprocessing parameter T_{lag} . Black triangles = CTRW *vs* FBM, Red circles= CTRW, LW, FBM, ATTM, and Yellow squares= CTRW *vs* ATTM. (b) Accuracy of the model discrimination as a function of the length of the trajectories t_{max} . (c) Histograms of the error in the prediction of the anomalous exponent for different values of the length trajectory t_{max} and noise variance σ_n . Y-axis is percentage of trajectories \bar{N} with given error ϵ when predicting the value of α . (d) MAE of the anomalous exponent prediction as a function of the length of the trajectories t_{max} . (e) MAE in anomalous exponent prediction as a function of the variance of the normal noise variance.

Discrimination among diffusion models

In order to predict the diffusion model underlying a certain trajectory, we construct a RF whose input is the normalized trajectory $\hat{\mathbf{X}}$, and the output is a number between 0 and $N - 1$ corresponding to the different models, with N the total number of models used in the training. Figure 7.3 (a) shows the accuracy of the RF. Each line corresponds to a training dataset made up of different models. In the absence of data preprocessing (point marked as 'Raw' in the x-axis), the RF shows large accuracy. The accuracy drops significantly as T_{lag} increases, likely as a consequence of the removal of microscopical properties of the model, such as short-time correlations, hence preventing the RF from learning important features of them. This might lead to the conclusion that the filtering introduced by the preprocessing steps only limits the time resolution. This is obviously true for simulated data, obtained at the same scale, for which preprocessing is unnecessary. However, when dealing with experimental data of unknown spatio-temporal scale, such a preprocessing is of fundamental importance to be able to apply the same architecture and training dataset, in spite of the little loss of performance.

In addition, the accuracy heavily depends on similarities among the models to be discriminated. For example, the accuracy obtained with a RF trained only with trajectories reproducing conceptually different models such as FBM and CTRW (triangular markers in Fig. 7.3 (a)) is higher than the one obtained when including in the training models with similar characteristics, such as CTRW and ATTM,

independently of T_{lag} (red circles and yellow squares in Fig. 7.3 (a)).

Anomalous exponent estimation

A first approximation toward the characterization of the anomalous exponent can be based on a regression problem, in which the output of the RF is the value of the anomalous exponent α . The nature of the regression algorithm makes that the output of the RF is the continuous value which better satisfies the constraints learned during training.

To characterize the performance of the method, we calculate the prediction error ε of a trajectory as the absolute distance between the predicted exponent and the ground truth value. The percentage of trajectories $\tilde{N}(\varepsilon)$ with a given error ε is represented in the bar plots of Fig. 7.3 (c) for three different cases and a subdiffusive dataset including trajectories obtained from FBM, CTRW and ATTM. The case (i) considers trajectories with $t_{\text{max}} = 10^3$ without noise, while the case (ii) and (iii) show results for shorter and noisy trajectories (see discussion below). For case (i) the calculated mean absolute error (MAE) of the prediction of the anomalous exponent gives a value of 0.11. Moreover, the histogram showed in Fig. 7.3 (c)(i) shows that for $\sim 80\%$ of the trajectories, the output exponent lies within 0.1 from the true value.

7.2.3 Experimental scenario: short and noisy trajectories

A remarkable feature of the method is the possibility to correctly characterize very short trajectories. In Fig 7.3 (b) and (d), we show the ability of the RF to characterize short trajectories. In Fig 7.3 (b), we plot the accuracy in model discrimination as a function of the length of the trajectories, t_{max} . In Fig 7.3(d), a similar study is done, now tracking the MAE of the RF trained to predict α . Although we observe an expected decrease of performance for short trajectories, both plots show that the RF is able to characterize trajectories as short as only 10 points. Quantitatively, when comparing trajectories of 10 points with larger ones, of 1000 points, the model discrimination accuracy only decreases by a factor of 8.2%, while the MAE decreases by a factor of 18%. Panel (ii) in Fig 7.3(e) shows the error distribution when predicting α for $t_{\text{max}} = 100$.

Importantly, one has also to take into account that the experimental trajectories have a limited localization precision, that results into Gaussian noise. Therefore, it is necessary to test the robustness to noise of the RF. To this end, we trained the RF with trajectories simulated as described before and then we try to predict the anomalous exponent of trajectories belonging to the same dataset, but whose positions \mathbf{X} were perturbed with noise to obtain the dataset $\mathbf{X}^{(n)}$

$$\mathbf{x}_i^{(n)} = \mathbf{x}_i + \mu_i(\mu, \sigma_n), \quad (7.3)$$

where $\mu_i(\mu, \sigma_n)$ is a random number retrieved from a Normal distribution with mean $\mu = 0$ and variance σ_n . The results obtained for training with FBM, CTRW and ATTMs are presented in Fig. 7.3(d). The RF shows a great robustness against noise. For $\sigma_n < 1$, the MAE appears almost unaffected. When increasing σ_n , we see that the MAE increases, as expected, but even for large σ_n the MAE is still reasonable.

7.3 Transfer learning in simulated and experimental data

To further show the advantages of our Machine Learning algorithm, we applied it to three sets of trajectories different from those included in the training/test dataset. This is often referred as transfer learning, as certain architecture is trained in one setting and then applied to a different one. For this, we will consider three datasets:

- (i) Simulated data coming from a recently presented model presented in Chapter 5, describing the movement of a diffuser in a network of compartments of random size and random permeability, both drawn from universal distributions. This model shares the same subordination as the quenched trap model, i.e. a CTRW with power-law distributed trapping times and recapitulates the complexity and heterogeneity found in some biological environments. This choice allows to test the algorithm over a conceptually different model with respect to the training dataset, while having the advantage of tuning the value of anomalous exponents.
- (ii) Experiment 1, reporting the motion of individual mRNA molecules inside live bacterial cells [168]. The tMSD shows anomalous diffusion with $\alpha \sim 0.7$; this behaviour has been associated to FBM [81, 169].
- (iii) Experiment 2, corresponding to a set of trajectories obtained for the diffusion of a membrane receptor in living cells [77]. Although the time-averaged MSD shows a nearly linear behaviour, the data present features of ergodicity breaking due to changes of diffusivity [170] and have been associated to the ATTM model.

Following the scheme presented in Fig. 7.2, first we train the RF with simulated trajectories obtained with different theoretical frameworks. It should be noted that for this section, since we deal with trajectories that do not show superdiffusive behaviour, we do not include the Lévy walks process in the training dataset.

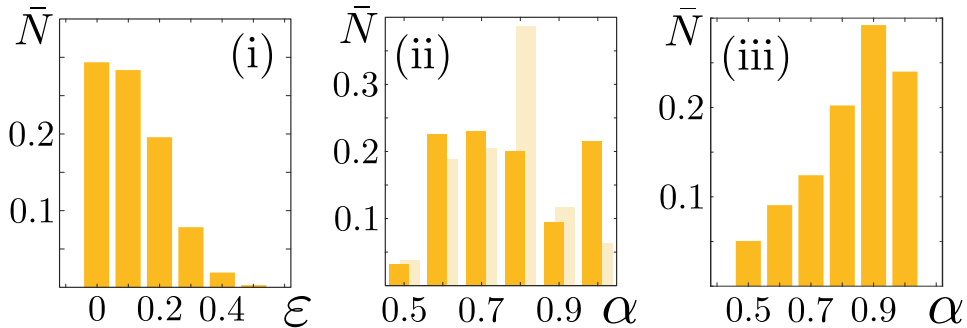


FIGURE 7.4: **Transfer learning: predicting the anomalous exponent for experimental trajectories.** Labels (i),(ii) and (iii) refer to the datasets discussed in Section 7.3. For dataset (i), we plot the percentage of trajectories \bar{N} where the predicted value of α has an absolute error ϵ . As it is a simulated dataset, exponents from 0.2 to 1 are considered. The input to the RF were the raw trajectories, with no preprocessing. For datasets (ii) and (iii), we present the percentage of trajectories predicted to have an anomalous exponent α . The trajectories were preprocessed with $T_{\text{lag}} = 1$. For dataset (ii), we present results two training datasets: dark yellow for a mixed dataset and light yellow for a FBM dataset.

7.3.1 Results

Following the same structure of the previous section, we start by discriminating the diffusion model that can be associated to datasets (i)-(iii). The results are reported in Table 7.1, showing a high rate of correct classification for the dataset (i). For the experimental data in datasets (ii) and (iii), we do not dispose of ground truth values, thus we compare our results with those of previous analysis, performed with alternative methods. For the trajectories of Experiment 1, we found that the algorithm largely assign them to the FBM, in strong agreement with previously reported results based on the concept of variation [81]. The data of Experiment 2 are mainly assigned to the ATTM model. This model was shown to reproduce features observed in these data, such as subdiffusion and weak ergodicity breaking [77]. Moreover, a little fraction of trajectories are classified as CTRW. As previously mentioned, CTRW and ATTM share similar features (such as time subordination), increasing the difficulty in discriminating between them. This appears to be the main source of error in the results.

To obtain further insights on the study of the diffusion, we used the RF to extract the anomalous exponents. For the first dataset (i), based on simulations, we generated trajectories having a broad range of subdiffusive trajectories, namely $\alpha \in [0.2, 1]$. Then, we used the trained RF to predict the value of the anomalous exponent and evaluated the error as the absolute value of the difference between

TABLE 7.1: Process discrimination for the datasets considered in section 7.3. Shown is the percentage of trajectories classified as associated to each model. The results for (i) were done with $T_{\text{lag}} = 0$ and for datasets (ii) and (iii) with $T_{\text{lag}} = 1$.

Dataset	Predicted Model		
	CTRW	FBM	ATTM
(i) Compartments model	89.2%	0	10.7%
(ii) Experiment 1	4.5%	86.6%	8.9%
(iii) Experiment 2	16.4%	33.2%	50.4%

the actual and predicted α . The results are reported in the histogram of Fig. 7.4 (i) and display a distribution similar to the one obtained for the training/testing data. Thus, we run the same procedure on the experimental data. For the two datasets, in Fig. 7.4 (ii)-(iii) we report the values obtained for the anomalous exponent α . The histogram of the α obtained for the trajectories of Experiment 1 (dark yellow) shows mainly subdiffusive values, peaked in the range $0.6 - 0.8$. This is in good agreement with the original paper [168], where α was estimated by means of two different approaches as 0.7 and 0.77. However, the method also classifies a percentage of the trajectories as having $\alpha = 1$. Importantly, the performance of the method can be further improved by taking advantage of the results of the model discrimination discussed above and shown in Table 7.1. In fact, when the latter classification indicates that most of the trajectories follow a specific diffusive model, one can train the algorithm with a dataset composed only of trajectories simulated with that model. This kind of training produces exponent values in the same range, but largely reduce the fraction of those associated to $\alpha = 1$, as shown in Fig. 7.4 (ii) (light yellow).

Last, in Fig. 7.4 (iii) we plot the distribution of exponents obtained for the Experiment 2. The subdiffusive values show a large number of occurrences in the $0.8 - 0.9$ range, compatible with the exponent 0.84 calculated in previous studies [77]. Noteworthy, due to the non-ergodic nature of the data, in the original paper α could only be calculated from the ensemble-averaged MSD, whereas the RF is able to determine this exponent from single trajectories.

7.4 Conclusions

During this Thesis, we have widely commented on the stochastic nature of anomalous diffusion and used various statistical approaches to study its features. From a theoretical point of view, it is usually possible to either find them analytically or simulate the system in order to do so. However, in an experimental scenario, we face many problems: the arising of noise coming from the experimental techniques, the difficulty of tracking certain particles for long enough times,... Recently, various

approaches have been proposed to solve this problem. In this chapter we have proposed how one may use machine learning (ML) techniques with such aim.

More precisely, we have presented a machine learning method, based on a Random Forest architecture, which is capable to analyse a single trajectory and to determine the theoretical model that describes it at best. Moreover the same method is used for predicting its anomalous exponent with high accuracy, and thus classify the motion as normal or anomalous. The method does not need any prior information over the nature of the system from which the trajectory is obtained. It acts as a blackbox, which we train with a dataset of simulated trajectories, and then it is used to characterize the trajectory of interest. In particular, its spatial scale is not of any relevance, as we devised a preprocessing strategy which rescales trajectories to obtain comparable estimators from very different systems. The method requires a minimal amount of information. First, because it performs extremely well even with surprisingly short trajectories. Second, because it is robust with respect to the presence of a large amount of thermal noise, and can thus be applied even with low localization precision.

In order to test the validity of the method, we have first created a series of benchmark tests, all performed by means of simulated data. For instance, we have studied how the appearance of noise or the shortening of the input trajectories affects both problems. While we observe a decrease in the accuracy, we have shown how the RF may still robustly characterize trajectories of only ten points. Most importantly, the method is able to characterize trajectories even for non-ergodic models, for which no previous methods existed besides from numerical fittings. Note that in the case of ergodicity breaking, an ensemble average over multiple samples is needed to faithfully retrieve the anomalous exponent. We have shown how the RF overcomes such problem with surprising accuracy.

Finally, we showcased the suitability of our method by applying it to two experimental datasets by means of transfer learning. In both cases, even if the two datasets show very distinct behaviour, the RF is able to correctly assess both the theoretical prediction of the model and the anomalous exponent. Of our interest, one of the datasets contains non ergodic trajectories, hence giving another proof of the suitability of ML for single trajectory characterization.

While the results presented in this Thesis show that it is possible to study some features of diffusion by means of ML, it also paves the way for even more important questions. In terms of the anomalous exponent prediction, we believe that an increase in the accuracy is for sure possible by means of more complex ML architectures. In this direction, an important step would be to create a method which is non size dependent, i.e. that we can train with trajectories of certain size but then can use for any other input size. Methods such as the one of natural language processing (NLP), where sentences of various sizes are analysed by means of recurrent neural networks, may be of great use in this scenario.

Another even more important question is related to the classification of the

theoretical model. For instance, what happens when we try to characterize a trajectory from a model that was not previously known? We showed in the case of transfer learning with the trajectories of Chapter 5, the method usually assigns the trajectories to the closest model of the training dataset. However, this may not always be true. There exists different ways of tackling this problem, as e.g. solving an $N + 1$ problem, where N models are considered and an extra label is assigned to 'Not known model'.

Following the trend of recent advances in ML applied to physics, one could instead work in an unsupervised scenario and more generally in the interpretability of the trained methods. This will lead to various advantages. For example, one could investigate which features are more important for the machine while learning to predict the anomalous exponent. In the case of model prediction, this problem is even more relevant, as we know from their theoretical framework than most of the model share features. It would be interesting to understand until which extend the information used by the machine is related to the actual parameters and metrics used in diffusion problems and even discover new properties that were hidden to previous statistical methods.

8 Conclusions

The concept of diffusion plays a key role in the understanding of our surrounding, specially in those systems in which the motion of particles cannot be completely described by a determinist theory. For a long time, most stochastic processes were associated to a Brownian (or normal)-like behaviour. However, in recent years, we have seen how many of the systems of study diverge from it. In order to explain such divergence, physicist have proposed a plethora of models that currently form what we now know as the anomalous diffusion theory. Inspired and closely related to Brownian motion, these contain crucial features, as e.g. crowding, correlations, ageing,... which help us understand the phenomena arising in different experimental observations.

There exist nowadays various ways of observing the departure from normal to anomalous diffusion. In practical terms, the easiest is related to the mean squared displacement (MSD) of a moving particle, as given in Eq. (2.5). For Brownian motion, the MSD is linear with time. When such linear dependence is broken, we consider the particles to be anomaly diffusing. In this case, the MSD is proportional to time up to a certain exponent, defined as the anomalous exponent. We differentiate then two regimes: when the exponent is smaller than one, we say that particles subdiffuse, while they superdiffuse for exponents bigger than one. The anomalous exponent is currently the main feature used to study anomalous diffusion in experimental scenarios, as it very easily calculated by means of the MSD of sampled trajectories. In practical terms, one proceeds either to perform an ensemble averaged MSD (eMSD), Eq. (2.7), over a set of trajectories coming from the same experiment, or by performing a time averaged MSD (tMSD), Eq. (2.6), over a single, usually long trajectory.

An important feature appearing in anomalous diffusion cases is the concept of weak ergodicity breaking. In non-ergodic systems, a single trajectory is not able to explore the whole phase space (see e.g. Fig. 2.4). Then, the approach of using the tMSD to characterize diffusion fails, as it will depend on which part of the phase space the particle has 'visited'. In statistical terms, we know now that in non-ergodic systems the tMSD is a random variable usually with linear dependence with time. Lately, the study on the fluctuations of the tMSD has been shown to be a powerful tool to study anomalous diffusion, as e.g. with the use of the ergodicity breaking parameter [71].

If one studies Brownian motion directly from the Einstein-Smoluchowski diffusion equation, Eq. (2.1), it is easy to see that the probability distribution function (PDF) of such process is a Gaussian with zero mean and variance directly related to the diffusion coefficient. Another widely studied departure from the normal diffusion occurs when such PDF is no longer Gaussian. This may or may not be followed by the MSD diverging from its linear behaviour [66]. A good measure of this behaviour is given by the non-Gaussianity parameter, i.e. the comparison between the second and fourth moment of the PDF of the particle, just as we showed in Sec. 3.1.4.

All the previous measures show that anomalous diffusion is currently well understood macroscopically. However, there is still a lot to be understood microscopically. This means the exploration of which particular interactions between the particles and its surrounding lead to anomalous behaviour. Such study often leads to microscopical models, i.e. a model in which the focus relies on the particular behaviour of each component of a system, in contrast to its macroscopic behaviour. These are usually motivated by experimental observations, as the goal is to understand the specific patterns particles or any stochastic process follow when anomaly diffusing. More importantly, one may use such ideas in the completely opposite direction: once the microscopic model is understood, we can study it just by studying the diffusion of the particles and relate its properties to the actual microscopical behaviour of the system.

With the previous context, the work presented in this Thesis has focused in two main directions. The first one, related to Chapters 3, 4, 5 and 6, aims at proposing new microscopical models, inspired by recent experiments, giving rise to many of the anomalous diffusion features and other complex behaviour such as phase separation. The second direction, presented in Chapter 7, focuses at proposing new techniques for the characterization of anomalous diffusion without the need of neither ensemble and time averages and any prior information on the system of study. We briefly review now the main conclusions of each of the chapters, summarizing what was presented at the end of each of them.

Heterogeneous interactions as source of non-ergodic subdiffusion In Chapter 3, we proposed a model in which a particle moves in a crowded environment. While moving freely, the particle performs a CTRW with exponential waiting time distribution, hence analogous to Brownian diffusion. However, when encountering one of its neighbouring particles, the motion of the particle is affected in such a way that its diffusion coefficient is altered. We argued how such changes in diffusion coefficients may be seen as the introduction of a disorder parameter in the waiting time distribution of the particle. Moreover, we showed how the precise distribution of the disorder, considered in this case as a power-law distribution, could change the diffusion of the particle drastically, switching from normal to

anomalous. Once derived the analytical relation between the disorder distribution and the resulting anomalous exponent, we focused in other features of the diffusion. For instance, we showed how the motion of the particle showed weak ergodicity breaking, similarly to what is expected in a power-law CTRW. Moreover, we also proved the non-Gaussianity of the model.

In terms of the microscopical model, we showed how the system could present two different disorder realizations, i.e. annealed or quenched disorder. While conceptually different, we showed how they converge to the same behaviour at certain regimes, for instance, when the density of surrounding particles is big enough. At low densities they have both significant difference in terms of absolute values, but show nevertheless the same scaling. In general, we have seen how the density of the system affects the motion of the particle. Even if the asymptotic limit is equal in all cases, the time the particle takes to reach the subdiffusive behaviour is highly dependent on the density, as we show both numerical and analytically. The previous result opens the door for the direct calculations of microscopic parameters of the system under investigation. For instance, one may use the offset in subdiffusion to study the crowding of the system. As a whole, the model proposed is able to show very interesting anomalous diffusion features, while also offering an interesting playground for the understanding of their microscopical source.

Subdiffusion in critical environments In Chapter 4, explored a very different microscopical model, in this case it was closely related to the critical properties of the widely known Ising model. We considered the motion of a particle, performing a discrete CTRW through a regular lattice, just as in Chapter 3. At each of the vertex of such lattice we considered to be a spin. The collection of spins forming the system followed Ising dynamics. Importantly, these spins could point in two directions, up or down. When neighbouring spins point all in the same direction, they form a domain. The size distribution of such domains is related to the temperature of the Ising environment. For temperatures below the critical one, the environment tends to form a single infinite domain. Above the critical temperature, no domains are usually formed, as the spins point in random directions, with any correlation with their neighbours. Interestingly, at criticality the distribution of domain sizes follows a power-law distribution.

Returning to the motion of the particle, we considered that its disorder emerges from the environment itself, rather than the interaction with other particles. With this, the model mimics the spatio-temporal heterogeneities known to be the source of anomalous diffusion in a plethora of experimental observations. More precisely, we proposed that the waiting time distribution of the particle is heavily affected by a disorder parameter, directly connected to the size of the domain the particle is visiting. Another important factor affecting the diffusion of the particle

is the interplay between the time scales of the particle's motion and the environment's dynamics. We showed how the system could be explained thanks to two limiting regimes: 1) when the environment dynamics are much faster than the time scale of the particle, which effectively means that the particle sees a new environment at each step (analogous to a annealed system); 2) the opposite case, in which the particle effectively perceives the environment as static.

Thanks to these two limiting cases we were able to find the exact relation between the anomalous exponent and the various features of the environment. Let us first review the results for a critical environment. In this case, the particle subdiffuses with an exponent related to the ratio between the two timescales. We have seen that in quasi static environments the particle is not able to completely explore the domain size distribution. Moreover, it has a non-zero probability of entering an infinite cluster a remaining there forever. This shows that the slower the environment dynamics, the smaller the anomalous exponent. This happens until reaching a certain value at which the dynamics are so slow that the particle recovers normal diffusion.

The environment has two ways of departing from criticality. The most trivial is when the system is no longer at critical temperature. We showed how this affected the domain size distribution, inserting an exponential cut-off. Effectively, this produces that the probability of finding infinite domain goes exponentially to zero. The environment can also depart from criticality due to its finite size. Both cases lead to the similar behaviour: for a transient time, temperature and size dependant, the particle subdiffuses. After this time, the particle recovers normal diffusion. To summarize, the model presented aims at understanding which kind of spatial heterogeneities may lead to anomalous subdiffusion, specially inspired by the recent observations of critical biological systems [96, 95].

Anomalous diffusion through porous compartments The work presented in Chapter 5 was directly motivated by the findings of the previous chapter. We set there a relation between the disorder parameter and the size of the domains, but the actual source of such connection was not explicitly explored. Our goal in this chapter was to understand if anomalous diffusion may be directly related to the heterogeneities of the environment, without the need of an explicit connection. In this case, the environment is made of compartments, just as the previously mentioned domains. As a particularity, this compartments have porous boundaries, i.e. the particle has a certain probability of transmitting to the next compartment or being reflected back to the initial one. Our first contribution is related to the actual method for studying diffusion in such systems. Usually, the microscopical walk studies how each of the interactions between the particle and the boundaries affects its behaviour. In our case, we consider a much bigger scale, in which we only track the particle when exiting a certain compartment.

We showed how this approach, completely analogous to the real microscopical behaviour of the particle, leads to a much simpler model of the system. This allows for a complete analytical description of the walk, given in this case by a Lévy walk (LW) with rests. Even if close to previous descriptions of this walk, we extended the theory to consider the particularities of this model, as for instance the fact that rests and walks have now complementary probabilities. With this new framework, we studied how heterogeneous distributions of compartment sizes and boundary transmittances affect the diffusion of the particle. For instance, in the case of equally long compartments but with stochastic transmittances, the walk reduces to a subdiffusive CTRW. Interestingly, when the compartments have also stochastic sizes, the motion of the particle can be reverted to normal diffusion. In general, we have studied how the interplay between the probability distribution functions of compartment sizes and boundary transmittances play a key in the emerging anomalous diffusion of the particle, all thanks to a novel analytical description of the system.

Phase separation in diffusing interacting systems Contrary to what was done in all previous chapters, in Chapter 6 our focus was not in the emergence of anomalous diffusion but of another crucial phenomena: phase separation. Lately, this process has been associated to the efficient transport of various components in cellular environments. The model presented aims at finding the actual microscopical interactions leading to a phase separated system, with a focus on simplicity and modularity. We consider a system of particles that have a certain probability of binding P_c to each other if they get closer than a distance r . The system then undergoes a phase transition from a phase in which particles move freely to a phase separated scenario, in which particles form condensates of varying size. We have analytically shown at which critical binding probability the phase transition takes place, showing its dependence of the distance r and the density of the system.

Interestingly, even in the presence of a non zero binding probability, but below the critical point, the particles do not form steady condensates. This was shown by calculating the average flux of particles per condensate size. Below the critical P_c , the flux shows how in average more particles escape than get absorbed by the minimal condensate, i.e. the one with only two particles. Only above the phase transition, the flux is positive, hence arising as a perfect tool to study the behaviour of the system. The difference between the two phases can also be studied by means of the distribution of condensate sizes. In the free phase, the distribution is Gaussian, with mean one, as was also predicted by the flux's study. The variance increases as we increase P_c . Above the phase transition, the mean starts to increase, but the Gaussian form is maintained. Trivially, at $P_c = 1$, all particles merge at a single condensate, hence the distribution being a delta function.

For the previous study, only few assumptions need to be taken related to the actual motion of the particles, being one of the advantages of the model. To test

the suitability of the model to describe actual physical systems, we consider that the particles may see changes in the diffusion coefficient, related to whether they are or not in a condensate. By studying the distribution of diffusion coefficient in actual dynamic simulations, we see the arising of a bimodal distribution, whose peaks correspond to the average value of the diffusion coefficient of the condensed and free particles. The latter gives us a powerful tool to compare the theoretical model with actual experimental observations, and thus the understanding of phase separation by means of microscopical interactions.

Diffusion characterization with Machine Learning In order to understand how anomalous diffusion arises in physical systems, two aspects are needed: first, having the appropriate theoretical framework, as the ones proposed in the previous parts of this Thesis. Second, and even more importantly, we need tools with which correctly characterize experimental trajectories. Without the correct extraction of the various parameters considered, having a perfect theory is useless, as its fitting to wrong data will lead to the incorrect understanding of the phenomena. Due to its stochastic nature, anomalous diffusion processes have always been hard to study, and one often relies on averages. However, this may not always be possible, either because one cannot gather enough samples to perform a correct ensemble average, or because of the presence of weak ergodicity breaking, for which time averages failed to correctly characterize trajectories.

In Chapter 7 we proposed a novel approach for the correct characterization of diffusion trajectories based on Machine Learning (ML) techniques. In last years, ML has proven as a powerful tool to study systems in which theoretical or statistical techniques have failed. More precisely, we have focused in two problems. First, in the prediction of the anomalous exponent of single trajectories. See that, for instance, in non-ergodic system this has never been assessed, as we always relied on ensemble averages. We have shown that ML can produce accurate results for such parameter in the presence of noise, short trajectories and even non ergodic processes. Similarly, we have also studied the problem of model classification. This is, given a pool of known theoretical models, the machine has to classify an input trajectory to the one that better describes it. This novel approach paves the way for the systematic characterization of trajectories even without prior knowledge of the system from which the trajectories arise.

Nevertheless, much work is still needed to understand until which extend this techniques may help to increase even more our understanding of stochastic processes. One of the big open question is about interpretability: what information is the machine using to make predictions? Is it related to our current knowledge of anomalous diffusion? Can this lead to new theoretical features that we did not know before? On the other hand, in terms of model classification, another important question: what happens when the input trajectory comes from a model that has no relation with the ones in the training set? By the same interpretability

techniques, can we assess which features the machine is using to differentiate between models? Can this help to discover never-seen models from experimental data? As shown by all these open problems, ML paves the way to a much better understanding of stochastic physical processes, where the amount of data is never a problem, as one can often easily simulate these systems, but the complexity of the system does not allow for their analytical understanding.

Bibliography

- [1] Albert Einstein. "On the movement of small particles suspended in stationary liquids required by the molecular-kinetic theory of heat". In: *Annalen der physik* 322.8 (1905), pp. 549–560.
- [2] Marian Von Smoluchowski. "Zur kinetischen theorie der brownschen molekularbewegung und der suspensionen". In: *Annalen der physik* 326.14 (1906), pp. 756–780.
- [3] Jarosław Piasecki. "Centenary of Maria Smoluchowski's theory of Brownian motion." In: *Acta Physica Polonica B* 38.5 (2007).
- [4] Robert Brown. "A brief account of microscopical observations made in the months of June, July and August 1827, on the particles contained in the pollen of plants; and on the general existence of active molecules in organic and inorganic bodies". In: *The Philosophical Magazine* 4.21 (1828), pp. 161–173.
- [5] Johannes Ingen-Housz. *Nouvelles expériences et observations sur divers objets de physique*. chez Théophile Barrois le jeune, 1785.
- [6] Chr Wiener. "Erklärung des atomistischen Wesens des tropfbar-flüssigen Körperzustandes, und Bestätigung desselben durch die sogenannten Molekularbewegungen". In: *Annalen der Physik* 194.1 (1863), pp. 79–94.
- [7] William Ramsay. "On the volumes of liquids at their boiling points, obtainable from unit-volumes of their gases". In: *Journal of the Chemical Society, Transactions* 35 (1879), pp. 463–474.
- [8] Thorvald Nicolai Thiele. *Om Anvendelse af mindste Kvadraters Methode i nogle Tilfælde, hvor en Komplikation af visse Slags uensartede tilfældige Fejlkilder giver Fejlene en "systematisk" Karakter, af TN Thiele*. B. Lunos Kgl. Hof.-Bogtrykkeri, 1880.
- [9] Louis Bachelier. *Louis Bachelier's theory of speculation: the origins of modern finance*. Princeton University Press, 2011.
- [10] Peter Achinstein. *Evidence, explanation, and realism: Essays in philosophy of science*. Oxford University Press, 2010.

- [11] William Sutherland. "A dynamical theory of diffusion for non-electrolytes and the molecular mass of albumin". In: *The London, Edinburgh, and Dublin Philosophical Magazine and Journal of Science* 9.54 (1905), pp. 781–785.
- [12] Jean Perrin. "Movement brownien et realite molec". In: *Ann. de Chim. et de Phys.* 18 (1909), pp. 1–114.
- [13] I Nordlund. "A new determination of Avogadro's number from Brownian motion of small mercury spherules". In: *Z. Phys. Chem* 87 (1914), pp. 40–62.
- [14] Eugen Kappler. "Versuche zur Messung der Avogadro-Loschmidtschen Zahl aus der Brownschen Bewegung einer Drehwaage". In: *Annalen der Physik* 403.2 (1931), pp. 233–256.
- [15] Karl Pearson. "The problem of the random walk". In: *Nature* 72.1867 (1905), pp. 342–342.
- [16] Lewis Fry Richardson. "Atmospheric diffusion shown on a distance-neighbour graph". In: *Proceedings of the Royal Society of London. Series A, Containing Papers of a Mathematical and Physical Character* 110.756 (1926), pp. 709–737.
- [17] Steve A Thorpe. *The turbulent ocean*. Cambridge University Press, 2005.
- [18] Andrei Nikolaevitch Kolmogorov. "Curves in Hilbert space which are invariant with respect to a one-parameter group of motions". In: *Dokl. Akad. Nauk SSSR* 26.1 (1940), pp. 6–9.
- [19] Benoit B Mandelbrot and John W Van Ness. "Fractional Brownian motions, fractional noises and applications". In: *SIAM review* 10.4 (1968), pp. 422–437.
- [20] Harvey Scher and Elliott W Montroll. "Anomalous transit-time dispersion in amorphous solids". In: *Physical Review B* 12.6 (1975), p. 2455.
- [21] Benoit B Mandelbrot. "The Fractal Geometry of". In: *Nature* (1982), pp. 394–397.
- [22] Joseph Klafter and Igor M Sokolov. *First steps in random walks: from tools to applications*. Oxford University Press, 2011.
- [23] Ralf Metzler et al. "Anomalous diffusion models and their properties: non-stationarity, non-ergodicity, and ageing at the centenary of single particle tracking". In: *Physical Chemistry Chemical Physics* 16.44 (2014), pp. 24128–24164.
- [24] Ralf Metzler. "Brownian motion and beyond: first-passage, power spectrum, non-Gaussianity, and anomalous diffusion". In: *Journal of Statistical Mechanics: Theory and Experiment* 2019.11 (2019), p. 114003.
- [25] Yasmine Meroz and Igor M Sokolov. "A toolbox for determining subdiffusive mechanisms". In: *Physics Reports* 573 (2015), pp. 1–29.

- [26] Felix Höfling and Thomas Franosch. "Anomalous transport in the crowded world of biological cells". In: *Reports on Progress in Physics* 76.4 (2013), p. 046602.
- [27] Eric Betzig, Stefan W Hell, and William E Moerner. "The nobel prize in chemistry 2014". In: *Nobel Media AB* (2014).
- [28] Carlo Manzo and Maria F Garcia-Parajo. "A review of progress in single particle tracking: from methods to biophysical insights". In: *Reports on progress in physics* 78.12 (2015), p. 124601.
- [29] Hao Shen et al. "Single particle tracking: from theory to biophysical applications". In: *Chemical reviews* 117.11 (2017), pp. 7331–7376.
- [30] Lothar Schermelleh et al. "Super-resolution microscopy demystified". In: *Nature cell biology* 21.1 (2019), pp. 72–84.
- [31] Frederic Bartumeus et al. "Animal search strategies: a quantitative random-walk analysis". In: *Ecology* 86.11 (2005), pp. 3078–3087.
- [32] Gandhimohan M Viswanathan et al. *The physics of foraging: an introduction to random searches and biological encounters*. Cambridge University Press, 2011.
- [33] Mevin B Hooten et al. *Animal movement: statistical models for telemetry data*. CRC press, 2017.
- [34] Toby A Patterson et al. "Statistical modelling of individual animal movement: an overview of key methods and a discussion of practical challenges". In: *AStA Advances in Statistical Analysis* 101.4 (2017), pp. 399–438.
- [35] David A Raichlen et al. "Evidence of Lévy walk foraging patterns in human hunter–gatherers". In: *Proceedings of the National Academy of Sciences* 111.2 (2014), pp. 728–733.
- [36] Andy Reynolds. "Liberating Lévy walk research from the shackles of optimal foraging". In: *Physics of life reviews* 14 (2015), pp. 59–83.
- [37] Valérie C Reijers et al. "A Lévy expansion strategy optimizes early dune building by beach grasses". In: *Nature communications* 10.1 (2019), pp. 1–9.
- [38] Graham H Pyke. "Understanding movements of organisms: it's time to abandon the Lévy foraging hypothesis". In: *Methods in Ecology and Evolution* 6.1 (2015), pp. 1–16.
- [39] Vasiliki Plerou et al. "Economic fluctuations and anomalous diffusion". In: *Physical Review E* 62.3 (2000), R3023.
- [40] Rosario N Mantegna and H Eugene Stanley. *Introduction to econophysics: correlations and complexity in finance*. Cambridge university press, 1999.
- [41] Mark M Meerschaert and Enrico Scalas. "Coupled continuous time random walks in finance". In: *Physica A: Statistical Mechanics and its Applications* 370.1 (2006), pp. 114–118.

- [42] Enrico Scalas. “The application of continuous-time random walks in finance and economics”. In: *Physica A: Statistical Mechanics and its Applications* 362.2 (2006), pp. 225–239.
- [43] Rosario Nunzio Mantegna. “Lévy walks and enhanced diffusion in Milan stock exchange”. In: *Physica A: Statistical Mechanics and its Applications* 179.2 (1991), pp. 232–242.
- [44] Erik Van der Straeten and Christian Beck. “Superstatistical fluctuations in time series: Applications to share-price dynamics and turbulence”. In: *Physical Review E* 80.3 (2009), p. 036108.
- [45] Injong Rhee et al. “On the levy-walk nature of human mobility”. In: *IEEE/ACM transactions on networking* 19.3 (2011), pp. 630–643.
- [46] Kyunghan Lee et al. “Slaw: A new mobility model for human walks”. In: *IEEE INFOCOM 2009*. IEEE, 2009, pp. 855–863.
- [47] Dirk Helbing. “Traffic and related self-driven many-particle systems”. In: *Reviews of modern physics* 73.4 (2001), p. 1067.
- [48] Heinz-Peter Breuer, Francesco Petruccione, et al. *The theory of open quantum systems*. Oxford University Press on Demand, 2002.
- [49] Aniello Lampo, Miguel Ángel García March, and Maciej Lewenstein. *Quantum Brownian motion revisited: extensions and applications*. Springer, 2019.
- [50] Christos Charalambous et al. “Control of anomalous diffusion of a Bose polaron”. In: *Quantum* 4 (Feb. 2020), p. 232. ISSN: 2521-327X.
- [51] Giovanni Modugno. “Anderson localization in Bose–Einstein condensates”. In: *Reports on progress in physics* 73.10 (2010), p. 102401.
- [52] E Lucioni et al. “Observation of subdiffusion in a disordered interacting system”. In: *Physical review letters* 106.23 (2011), p. 230403.
- [53] Salvador Elías Venegas-Andraca. “Quantum walks: a comprehensive review”. In: *Quantum Information Processing* 11.5 (2012), pp. 1015–1106.
- [54] Q Liu et al. “Quantum walks: the first detected transition time”. In: *arXiv preprint arXiv:2001.00231* (2020).
- [55] C Charalambous et al. “Nonergodic subdiffusion from transient interactions with heterogeneous partners”. In: *Physical Review E* 95.3 (2017), p. 032403.
- [56] G Muñoz-Gil et al. “Transient subdiffusion from an Ising environment”. In: *Physical Review E* 96.5 (2017), p. 052140.
- [57] Gorka Muñoz-Gil et al. “Diffusion through a network of compartments separated by partially-transmitting boundaries”. In: *Frontiers in Physics* 7 (2019), p. 31.

- [58] Gorka Muñoz Gil et al. "Phase separation of tunable biomolecular condensates predicted by an interacting particle model". In: <https://doi.org/10.1101/2020.09.09.28987> (2020).
- [59] Gorka Muñoz-Gil et al. "Single trajectory characterization via machine learning". In: *New Journal of Physics* 22.1 (2020), p. 013010.
- [60] Alejandro Pozas-Kerstjens et al. "Efficient training of energy-based models via spin-glass control". In: *arXiv preprint arXiv:1910.01592* (2019).
- [61] Gorka Muñoz-Gil et al. "AnDi: The Anomalous Diffusion Challenge". In: *arXiv preprint arXiv:2003.12036* (2020).
- [62] *Random Forest for Single trajectory characterization*. <https://github.com/gorkamunoz/RF-Single-Trajectory-Characterization>. doi:10.5281/zenodo.2581267.
- [63] Igor M Sokolov and Joseph Klafter. "From diffusion to anomalous diffusion: a century after Einstein's Brownian motion". In: *Chaos: An Interdisciplinary Journal of Nonlinear Science* 15.2 (2005), p. 026103.
- [64] Albert Einstein. "Zur theorie der brownschen bewegung". In: *Annalen der physik* 324.2 (1906), pp. 371–381.
- [65] Paul Langevin. *On the theory of Brownian motion*. 146. 1908, pp. 530–533.
- [66] Aleksei V Chechkin et al. "Brownian yet non-Gaussian diffusion: from superstatistics to subordination of diffusing diffusivities". In: *Physical Review X* 7.2 (2017), p. 021002.
- [67] Ryszard Kutner and Jaume Masoliver. "The continuous time random walk, still trendy: fifty-year history, state of art and outlook". In: *The European Physical Journal B* 90.3 (2017), p. 50.
- [68] Alfred Tauber. "Ein Satz aus der Theorie der unendlichen Reihen". In: *Monatshefte für Mathematik und Physik* 8.1 (1897), pp. 273–277.
- [69] Ludwig Boltzmann. *Vorlesungen über Gastheorie: Th. Theorie van der Waals'; Gase mit zusammengesetzten Molekülen; Gasdissociation; Schlussbemerkungen*. Vol. 2. JA Barth, 1898.
- [70] Jean-Philippe Bouchaud. "Weak ergodicity breaking and aging in disordered systems". In: *Journal de Physique I* 2.9 (1992), pp. 1705–1713.
- [71] Y He et al. "Random time-scale invariant diffusion and transport coefficients". In: *Physical Review Letters* 101.5 (2008), p. 058101.
- [72] V Ziburdaev, S Denisov, and J Klafter. "Lévy walks". In: *Reviews of Modern Physics* 87.2 (2015), p. 483.
- [73] Mykyta V Chubynsky and Gary W Slater. "Diffusing diffusivity: a model for anomalous, yet Brownian, diffusion". In: *Physical review letters* 113.9 (2014), p. 098302.

- [74] P Massignan et al. "Nonergodic subdiffusion from Brownian motion in an inhomogeneous medium". In: *Physical review letters* 112.15 (2014), p. 150603.
- [75] Bo Wang et al. "Anomalous yet brownian". In: *Proceedings of the National Academy of Sciences* 106.36 (2009), pp. 15160–15164.
- [76] Bo Wang et al. "When Brownian diffusion is not Gaussian". In: *Nature materials* 11.6 (2012), pp. 481–485.
- [77] Carlo Manzo et al. "Weak ergodicity breaking of receptor motion in living cells stemming from random diffusivity". In: *Physical Review X* 5.1 (2015), p. 011021.
- [78] Weichun Pan et al. "Viscoelasticity in homogeneous protein solutions". In: *Physical review letters* 102.5 (2009), p. 058101.
- [79] Julia F Reverej et al. "Superdiffusion dominates intracellular particle motion in the supercrowded cytoplasm of pathogenic *Acanthamoeba castellanii*". In: *Scientific reports* 5.1 (2015), pp. 1–14.
- [80] T Guggenberger et al. "Fractional Brownian motion in a finite interval: correlations effect depletion or accretion zones of particles near boundaries". In: *New Journal of Physics* 21.2 (2019), p. 022002.
- [81] Marcin Magdziarz et al. "Fractional Brownian motion versus the continuous-time random walk: A simple test for subdiffusive dynamics". In: *Physical review letters* 103.18 (2009), p. 180602.
- [82] Samudrajit Thapa et al. "Bayesian analysis of single-particle tracking data using the nested-sampling algorithm: maximum-likelihood model selection applied to stochastic-diffusivity data". In: *Physical Chemistry Chemical Physics* 20.46 (2018), pp. 29018–29037.
- [83] Samudrajit Thapa et al. "Leveraging large-deviation statistics to decipher the stochastic properties of measured trajectories". In: *arXiv preprint arXiv:2005.02099* (2020).
- [84] Aneesur Rahman. "Correlations in the motion of atoms in liquid argon". In: *Physical review* 136.2A (1964), A405.
- [85] Michael J Saxton. "Single-particle tracking: the distribution of diffusion coefficients." In: *Biophysical journal* 72.4 (1997), p. 1744.
- [86] Christian Beck, Ezechiel GD Cohen, and Harry L Swinney. "From time series to superstatistics". In: *Physical Review E* 72.5 (2005), p. 056133.
- [87] Juan A Torreno-Pina, Carlo Manzo, and Maria F Garcia-Parajo. "Uncovering homo-and hetero-interactions on the cell membrane using single particle tracking approaches". In: *Journal of Physics D: Applied Physics* 49.10 (2016), p. 104002.

- [88] Shalini T Low-Nam et al. "ErbB1 dimerization is promoted by domain co-confinement and stabilized by ligand binding". In: *Nature structural & molecular biology* 18.11 (2011), p. 1244.
- [89] Kenichi GN Suzuki et al. "Transient GPI-anchored protein homodimers are units for raft organization and function". In: *Nature chemical biology* 8.9 (2012), p. 774.
- [90] Zemaoyang et al. "Mapping of quantitative trait loci underlying cold tolerance in rice seedlings via high-throughput sequencing of pooled extremes". In: *Plos one* 8.7 (2013).
- [91] Jean-Baptiste Masson et al. "Mapping the energy and diffusion landscapes of membrane proteins at the cell surface using high-density single-molecule imaging and Bayesian inference: application to the multiscale dynamics of glycine receptors in the neuronal membrane". In: *Biophysical journal* 106.1 (2014), pp. 74–83.
- [92] Carmine Di Rienzo et al. "Diffusion tensor analysis by two-dimensional pair correlation of fluorescence fluctuations in cells". In: *Biophysical journal* 111.4 (2016), pp. 841–851.
- [93] Francisco Balzarotti et al. "Nanometer resolution imaging and tracking of fluorescent molecules with minimal photon fluxes". In: *Science* 355.6325 (2017), pp. 606–612.
- [94] Barry M McCoy and Tai Tsun Wu. *The two-dimensional Ising model*. Courier Corporation, 2014.
- [95] Benjamin B Machta et al. "Minimal model of plasma membrane heterogeneity requires coupling cortical actin to criticality". In: *Biophysical journal* 100.7 (2011), pp. 1668–1677.
- [96] Alf Honigsmann et al. "Scanning STED-FCS reveals spatiotemporal heterogeneity of lipid interaction in the plasma membrane of living cells". In: *Nature communications* 5.1 (2014), pp. 1–12.
- [97] Michael E Fisher. "The theory of condensation and the critical point". In: *Physics Physique Fizika* 3.5 (1967), p. 255.
- [98] Dietrich Stauffer and Amnon Aharony. *Introduction to percolation theory*. CRC press, 2018.
- [99] Pierre C Hohenberg and Bertrand I Halperin. "Theory of dynamic critical phenomena". In: *Reviews of Modern Physics* 49.3 (1977), p. 435.
- [100] Shang-Keng Ma. *Modern theory of critical phenomena*. Routledge, 2018.
- [101] MP Nightingale and HWJ Blöte. "Dynamic exponent of the two-dimensional Ising model and Monte Carlo computation of the subdominant eigenvalue of the stochastic matrix". In: *Physical review letters* 76.24 (1996), p. 4548.

- [102] Y Lin and F Wang. "Linear relaxation in large two-dimensional Ising models". In: *Physical Review E* 93.2 (2016), p. 022113.
- [103] David Cirauqui García et al. "Quantum Random Number Generators: Benchmarking and Challenges". In: *In preparation* (2020).
- [104] Sanaz Sadegh et al. "Plasma membrane is compartmentalized by a self-similar cortical actin meshwork". In: *Physical Review X* 7.1 (2017), p. 011031.
- [105] Gabrielle de Wit et al. "Revealing Compartmentalized Diffusion in Living Cells with Interferometric Scattering Microscopy". In: *Biophysical Journal* 114.12 (2018), pp. 2945–2950.
- [106] J Klafter and G Zumofen. "Lévy statistics in a Hamiltonian system". In: *Physical Review E* 49.6 (1994), p. 4873.
- [107] V Yu Zaboruaev and KV Chukbar. "Enhanced superdiffusion and finite velocity of Levy flights". In: *Journal of experimental and theoretical physics* 94.2 (2002), pp. 252–259.
- [108] V Zaboruaev, S Denisov, and J Klafter. "Lévy walks". In: *Reviews of Modern Physics* 87.2 (2015), p. 483.
- [109] G Lehner. "One dimensional random walk with a partially reflecting barrier". In: *The Annals of Mathematical Statistics* (1963), pp. 405–412.
- [110] Jean-Philippe Bouchaud and Antoine Georges. "Anomalous diffusion in disordered media: statistical mechanisms, models and physical applications". In: *Physics reports* 195.4-5 (1990), pp. 127–293.
- [111] Vasily Yu Zaboruaev. "Random walk model with waiting times depending on the preceding jump length". In: *Journal of statistical physics* 123.4 (2006), pp. 871–881.
- [112] M Khantha and V Balakrishnan. "First passage time distributions for finite one-dimensional random walks". In: *Pramana* 21.2 (1983), pp. 111–122.
- [113] Bartłomiej Dybiec, Ewa Gudowska-Nowak, and Peter Hänggi. "Lévy-Brownian motion on finite intervals: Mean first passage time analysis". In: *Physical Review E* 73.4 (2006), p. 046104.
- [114] Gerald John Lapeyre Jr. "Anomalous diffusion from Brownian motion with random confinement". In: *arXiv preprint arXiv:1504.07158* (2015).
- [115] William S Trimble and Sergio Grinstein. "Barriers to the free diffusion of proteins and lipids in the plasma membrane". In: *J Cell Biol* 208.3 (2015), pp. 259–271.
- [116] GH Weiss and S Havlin. "Some properties of a random walk on a comb structure". In: *Physica A* 134.2 (1986), pp. 474–482.
- [117] E Baskin and A Iomin. "Superdiffusion on a Comb Structure". In: *Physical Review Letters* 93.12 (2004), p. 120603.

- [118] Anthony A Hyman, Christoph A Weber, and Frank Jülicher. "Liquid-liquid phase separation in biology". In: *Annual review of cell and developmental biology* 30 (2014), pp. 39–58.
- [119] Salman F Banani et al. "Biomolecular condensates: organizers of cellular biochemistry". In: *Nature reviews Molecular cell biology* 18.5 (2017), pp. 285–298.
- [120] John W Cahn. "Phase separation by spinodal decomposition in isotropic systems". In: *The Journal of Chemical Physics* 42.1 (1965), pp. 93–99.
- [121] Richard P Sear. "Nucleation: theory and applications to protein solutions and colloidal suspensions". In: *Journal of Physics: Condensed Matter* 19.3 (2007), p. 033101.
- [122] Paul J Flory. "Thermodynamics of high polymer solutions". In: *The Journal of chemical physics* 10.1 (1942), pp. 51–61.
- [123] Rodrigo Soto and Ramin Golestanian. "Run-and-tumble dynamics in a crowded environment: Persistent exclusion process for swimmers". In: *Physical Review E* 89.1 (2014), p. 012706.
- [124] Christian Vanhille Campos et al. "Collective motion of run-and-tumble particles drives aggregation in one-dimensional systems". In: *arXiv* (2019), arXiv-1912.
- [125] Stephanie C Weber and Clifford P Brangwynne. "Inverse size scaling of the nucleolus by a concentration-dependent phase transition". In: *Current Biology* 25.5 (2015), pp. 641–646.
- [126] Joel Berry et al. "RNA transcription modulates phase transition-driven nuclear body assembly". In: *Proceedings of the National Academy of Sciences* 112.38 (2015), E5237–E5245.
- [127] Peter W Voorhees. "The theory of Ostwald ripening". In: *Journal of Statistical Physics* 38.1-2 (1985), pp. 231–252.
- [128] Richard S Sutton and Andrew G Barto. *Reinforcement learning: An introduction*. MIT press, 2018.
- [129] David Silver et al. "A general reinforcement learning algorithm that masters chess, shogi, and Go through self-play". In: *Science* 362.6419 (2018), pp. 1140–1144.
- [130] Alexey A Melnikov et al. "Active learning machine learns to create new quantum experiments". In: *Proceedings of the National Academy of Sciences* 115.6 (2018), pp. 1221–1226.
- [131] Marin Bukov et al. "Reinforcement learning in different phases of quantum control". In: *Physical Review X* 8.3 (2018), p. 031086.
- [132] Simona Colabrese et al. "Flow navigation by smart microswimmers via reinforcement learning". In: *Physical review letters* 118.15 (2017), p. 158004.

- [133] Borja Requena et al. "Approximating ground states via reinforcement learning". In: *In preparation* (2020).
- [134] John J Hopfield. "Neural networks and physical systems with emergent collective computational abilities". In: *Proceedings of the national academy of sciences* 79.8 (1982), pp. 2554–2558.
- [135] David E Rumelhart, Geoffrey E Hinton, and Ronald J Williams. *Learning internal representations by error propagation*. Tech. rep. California Univ San Diego La Jolla Inst for Cognitive Science, 1985.
- [136] Elizabeth Gardner. "The space of interactions in neural network models". In: *Journal of physics A: Mathematical and general* 21.1 (1988), p. 257.
- [137] Giuseppe Carleo et al. "Machine learning and the physical sciences". In: *Reviews of Modern Physics* 91.4 (2019), p. 045002.
- [138] Adi L Tarca et al. "Machine learning and its applications to biology". In: *PLoS computational biology* 3.6 (2007).
- [139] Keith T Butler et al. "Machine learning for molecular and materials science". In: *Nature* 559.7715 (2018), pp. 547–555.
- [140] Yann LeCun. "The MNIST database of handwritten digits". In: <http://yann.lecun.com/exdb/mnist/> (1998).
- [141] Michael A Nielsen. *Neural networks and deep learning*. Vol. 2018. Determination press San Francisco, CA, USA: 2015.
- [142] Pankaj Mehta et al. "A high-bias, low-variance introduction to machine learning for physicists". In: *Physics reports* (2019).
- [143] Benno S Rem et al. "Identifying quantum phase transitions using artificial neural networks on experimental data". In: *Nature Physics* 15.9 (2019), pp. 917–920.
- [144] Varun Chandola, Arindam Banerjee, and Vipin Kumar. "Anomaly detection: A survey". In: *ACM computing surveys (CSUR)* 41.3 (2009), pp. 1–58.
- [145] Jack Collins, Kiel Howe, and Benjamin Nachman. "Anomaly detection for resonant new physics with machine learning". In: *Physical review letters* 121.24 (2018), p. 241803.
- [146] Korbinian Kottmann et al. "Unsupervised phase discovery with deep anomaly detection". In: *arXiv preprint arXiv:2003.09905* (2020).
- [147] Ian Goodfellow et al. "Generative adversarial nets". In: *Advances in neural information processing systems*. 2014, pp. 2672–2680.
- [148] Geoffrey E Hinton and Terrence J Sejnowski. "Optimal perceptual inference". In: *Proceedings of the IEEE conference on Computer Vision and Pattern Recognition*. Vol. 448. Citeseer. 1983.

- [149] E. Marinari and G. Parisi. “Simulated Tempering: A New Monte Carlo Scheme”. In: *EPL* 19.6 (1992), pp. 451–458. DOI: [10 . 1209 / 0295 - 5075 / 19/6/002](https://doi.org/10.1209/0295-5075/19/6/002). URL: <https://iopscience.iop.org/article/10.1209/0295-5075/19/6/002>.
- [150] M. Mézard. “Mean-field message-passing equations in the Hopfield model and its generalizations”. In: *Phys. Rev. E* 95 (2 2017), p. 022117. DOI: [10 . 1103/PhysRevE.95.022117](https://doi.org/10.1103/PhysRevE.95.022117). URL: <https://link.aps.org/doi/10.1103/PhysRevE.95.022117>.
- [151] Y. Du and I. Mordatch. “Implicit Generation and Modeling with Energy-Based Models”. In: *arXiv:1903.08689* (2019). eprint: [1903.08689](https://arxiv.org/abs/1903.08689). URL: <http://arxiv.org/abs/1903.08689>.
- [152] T. Tieleman. “Training Restricted Boltzmann Machines Using Approximations to the Likelihood Gradient”. In: *Proceedings of the 25th International Conference on Machine Learning*. Helsinki, Finland, 2008, pp. 1064–1071. ISBN: 978-1-60558-205-4. DOI: [10 . 1145 / 1390156 . 1390290](https://doi.org/10.1145/1390156.1390290). URL: <http://doi.acm.org/10.1145/1390156.1390290>.
- [153] Krzysztof Burnecki et al. “Estimating the anomalous diffusion exponent for single particle tracking data with measurement errors—An alternative approach”. In: *Scientific reports* 5.1 (2015), pp. 1–11.
- [154] Eldad Kepten et al. “Guidelines for the fitting of anomalous diffusion mean square displacement graphs from single particle tracking experiments”. In: *PLoS One* 10.2 (2015).
- [155] Yann Lanoiselée et al. “Optimal parameters for anomalous-diffusion-exponent estimation from noisy data”. In: *Physical Review E* 98.6 (2018), p. 062139.
- [156] Grzegorz Sikora et al. “Statistical properties of the anomalous scaling exponent estimator based on time-averaged mean-square displacement”. In: *Physical Review E* 96.2 (2017), p. 022132.
- [157] Denis S Grebenkov. “Time-averaged mean square displacement for switching diffusion”. In: *Physical Review E* 99.3 (2019), p. 032133.
- [158] Diego Krapf et al. “Power spectral density of a single Brownian trajectory: what one can and cannot learn from it”. In: *New Journal of Physics* 20.2 (2018), p. 023029.
- [159] Konrad Hinsén and Gerald R Kneller. *Communication: A multiscale Bayesian inference approach to analyzing subdiffusion in particle trajectories*. 2016.
- [160] Patrice Dosset et al. “Automatic detection of diffusion modes within biological membranes using back-propagation neural network”. In: *BMC bioinformatics* 17.1 (2016), p. 197.
- [161] Patrycja Kowalek, Hanna Loch-Olszewska, and Janusz Szwabiński. “Classification of diffusion modes in single-particle tracking data: Feature-based versus deep-learning approach”. In: *Physical Review E* 100.3 (2019), p. 032410.

- [162] Naor Granik et al. "Single-Particle Diffusion Characterization by Deep Learning". In: *Biophysical journal* 117.2 (2019), pp. 185–192.
- [163] Stefano Bo et al. "Measurement of anomalous diffusion using recurrent neural networks". In: *Physical Review E* 100.1 (2019), p. 010102.
- [164] Leo Breiman et al. *Classification and regression trees*. CRC press, 1984.
- [165] Leo Breiman. "Random forests". In: *Machine learning* 45.1 (2001), pp. 5–32.
- [166] Manuel Fernández-Delgado et al. "Do we need hundreds of classifiers to solve real world classification problems?" In: *The journal of machine learning research* 15.1 (2014), pp. 3133–3181.
- [167] *The Anomalous Diffusion Challenge datasets*. https://github.com/AnDiChallenge/ANDI_datasets. doi:10.5281/zenodo.3707702.
- [168] Ido Golding and Edward C Cox. "Physical nature of bacterial cytoplasm". In: *Physical review letters* 96.9 (2006), p. 098102.
- [169] Daniel Molina-García et al. "Fractional kinetics emerging from ergodicity breaking in random media". In: *Physical Review E* 94.5 (2016), p. 052147.
- [170] Michał Balcerek et al. "Inhomogeneous membrane receptor diffusion explained by a fractional heteroscedastic time series model". In: *Physical Chemistry Chemical Physics* 21.6 (2019), pp. 3114–3121.